Quantitative Magnetic Resonance Imaging to evaluate patients with liver cirrhosis

by

Robert Archie Dobson Scott

Thesis submitted to

The University of Nottingham

for the degree of

Doctor of Philosophy

October 2019

Contents

Abstract

Introduction

The incidence and mortality of liver disease is increasing. Most morbidity and mortality in patients with liver cirrhosis results from the development and progression of portal hypertension, characterised by increased intrahepatic resistance and splanchnic vasodilatation. Transjugular hepatic venous pressure gradient (HVPG) is the only validated technique for the assessment of portal pressure to stratify an individual's risk and changes following therapeutic interventions. However, HVPG measurements are expensive, invasive and only available in specialist centres which precludes the use of HVPG in routine clinical practice.

Magnetic Resonance Imaging (MRI) technologies provide unique methods for imaging the whole liver and abdomen. As a result, several favourable characteristics required to stratify chronic liver diseases are obtained. These methodologies are non-invasive, provide objective measurements, are organ-specific and do not use ionising radiation. They measure multiple parameters in a single scan session. Uniquely amongst imaging modalities, it is possible to concordantly assess several different measures in the same scan session.

Methodology

All three prospective studies compared non-invasive quantitative MRI measures to current gold-standard measures.

In the first part of the thesis, I investigated the effect of field strength on surrogate MR measures of portal pressure. A prospective cross-sectional study of patients undergoing transjugular liver biopsies across two sites recruited participants to attend for a single study visit within 12 weeks. Patients underwent transient elastography, blood tests and a single non-invasive MRI scan at a field strength of 3 Tesla. All measures were compared to HVPG.

In the second part of the thesis, I investigated the effects of Direct Acting Antiviral therapy given to patients with advanced liver disease caused by Hepatitis C virus. Patients eligible for treatment were invited to take part in a prospective observational study. Participants underwent an MRI scan before and after treatment completion (within 12 weeks of last tablet swallowed). Patients followed standard management protocols for therapy and monitoring. Routine clinical information including medical history, clinical examination and laboratory values were recorded for each participant and compared to the MRI measures.

In the third part of the thesis, I aimed to develop a novel quantitative MRI tool to evaluate increased small bowel permeability in a double-blind, placebo-controlled, healthy volunteer study. Development of bacterial translocation is believed to be a key prognostic event precipitating decompensation and life-threatening complications in patients with advanced chronic liver disease. The best available tools to evaluate gut permeability were compared with a newly developed MRI assessment of the small bowel. Provocation with enteral Indomethacin administration, an accepted positive control for experimental medicine studies, was used to compare the MRI measures to bowel permeability assessed by the Lactulose/Mannitol urinary excretion ratio (LMR).

Results

In the first prospective cross-sectional study, 39 patients were recruited who had MRI data for comparison to HVPG. At 3 Tesla, HVPG significantly correlated with: iron corrected liver longitudinal relaxation time (T_1: R=0.60, p<0.001), Spleen T_1 (R=0.599, p<0.001), SMA velocity (R=0.45, p=0.008) and Splenic artery flow (R=0.456, p=0.017). There was a significant correlation of cardiac index and Splenic artery flow as well as a clear correlation of differing azygous vein flow in the presence or absence of varices. Combining this data with the original derivation data at 1.5 Tesla (n=40) showed a field strength dependent ceiling effect of structural measures and a reduction in SMA and splenic artery velocity >15 mmHg.

In the second prospective observational study of patients undergoing new treatments for chronic Hepatitis C infection, multiparametric MRI, in a time window of 3-6 months between pre- and post-treatment scans, demonstrated changes in hepatic composition in 17 patients. Liver longitudinal relaxation time (T_1, 35±4 ms), transverse relaxation time (T_2, 2.5±0.8 ms; T_2*, 3.0±0.7 ms) and liver perfusion (28.1±19.7ml/100g/min) all significantly reduced. These measures are likely linked to reduced pro-inflammatory milieu, including interstitial oedema, within the liver. By chance, seven patients were diagnosed with hepatocellular carcinoma after starting treatment in whom pre-treatment MRI lesions could be identified on the research scans.

In the double-blind placebo-controlled study of 22 healthy volunteers, only a newly developed measure of small bowel T_2 significantly increased (70 ± 36 ms vs 115 ± 63ms, p=0.017) and correlated (R=0.68, p<0.01) with increased LMR following indomethacin administration (0.019 (IQR 0.016-0.026) to 0.025 (IQR 0.021-0.039), p=0.002).

Conclusions

This thesis provides data that suggests a non-contrast MRI scan may uniquely be able to simultaneously evaluate multiple measures of prognostic importance in patients with chronic liver disease including liver fibrosis, portal pressure, the development of a hyperdynamic circulation, small bowel permeability and hepatocellular carcinoma surveillance. These findings need to be validated, optimised and shown to evaluate efficacy of interventions in order to lead to clinical adoption. MRI has the potential to be a key non-invasive tool to evaluate the efficacy of interventions in chronic liver disease and stratify patients according to the potential clinical outcomes.

Acknowledgements

I am grateful to the National Institute for Health Research (NIHR) and the Nottingham Biomedical Research Centre (BRC) in GI & liver disease who funded my Academic Clinical Fellowship. This post provided training in research methods and the time to perform pilot studies that have evolved into the research chapters of this PhD. The NIHR Nottingham Biomedical Research Centre funded this PhD with some additional resources from the Medical Research Council (MRC) and Nottingham Hospitals Charity.

I would like to express my sincere thanks for the generous support, guidance and patience of my supervisors Guruprasad Aithal, Neil Guha, Penny Gowland and Sue Francis who gave me the freedom to explore novel avenues of interest whilst keeping me focused to complete this thesis.

This work would not have been possible without the tireless support from all the staff at the Nottingham Biomedical Research Centre and Sir Peter Mansfield Imaging Centre to whom I am extremely grateful. Special thanks in particular to Dr Caroline Hoad who patiently guided a clinician to understand the physics and analysis methods behind the black box of MRI. Christopher Bradley who single handedly scanned and analysed all the liver patients with me and Hannah Williams who painstakingly developed the novel analysis methods of small bowel wall T_2.

To all the members of the “liver lobule” – Dave Harman, Naaventhan Palaniyappan, Rebecca Harris, Jane Chalmers, Prarthana Thiagarajan and Jane Grove – thank you. They have supplied endless coffee, companionship and support with great humour that has spurred me along to completion

Finally I would like to thank my wife Esther for enabling me to follow my dreams and our children Emilia and Harriet who make everything worthwhile.

Abbreviations

2D-SWE	Two dimensional real-time shear wave elastography
AASLD	American association for the study of liver diseases
ACLF	Acute on chronic liver failure
Alc Hep	Alcoholic hepatitis
ALD	Alcoholic liver disease
ALP	Alkaline phosphatase
ALT	Alanine transaminase
ARFI	Acoustic radiation force impulse
ASL	Arterial spin labelling
AST	Aspartate transaminase
AUROC	Area under receiver operating curve
bFFE	Balanced fast field echo
BMI	Body mass index
BRC	Nottingham Biomedical Research Centre
BSG	British society of gastroenterology
bTFE	Balanced turbo field echo
cACLD	Compensated advanced liver disease
CI	Confidence intervals
CoV	Coefficient of variation
CPA	Collagen proportionate area

CPRD	UK Clinical Practice Research Datalink
CSPH	Clinically significant portal hypertension
CT	Computed tomography
CTP	Child-Turcotte-Pugh
DAA	Direct Acting Antiviral
DWI	Diffusion weighted imaging
EASL	European association for the study of the liver
ECF	Extracellular fluid (ECF)
ELF	Enhanced liver fibrosis
ELISA	Enzyme-linked immunosorbent assay
EndoCAb	Endotoxin core antibodies
EPI	Echo planar imaging
ET	Echo times
FAIR	Flow alternating inversion recovery
FHWM	Full width half maximum
FHVP	Free hepatic venous pressure
GCP	Good clinical practice
GGT	Gamma-glutamyl transferase
HA	Hyaluronic acid
HBV	Hepatitis B virus
HCC	Hepatocellular carcinoma
HCV	Hepatitis C virus

HIC	Hepatic iron concentration
HR	Hazard ratio
HRV	High risk varices
HSC	Hepatic stellate cells
HVPG	Hepatic venous pressure gradient
ICG	Indocyanine green
i-FABP	Intestinal fatty acid binding proteins
IQR	Interquartile range
IR SE-EPI	Inversion-recovery spin-echo echo planar imaging
IVC	Inferior vena cava
kPa	kiloPascals
LASSO	Least absolute shrinkage and selection operator
LBP	Lipopolysaccharide Binding Protein
LMR	Lactulose/Mannitol urinary excretion ratio
LSM	Liver stiffness measurement
LSPS	Liver stiffness measurement spleen diameter to platelet ratio score
MAP	Mean arterial pressure
MELD	Modified for End-Stage Liver Disease
MRC	Medical Research Council
MRE	Magnetic resonance elastography
MRI	Magnetic resonance imaging
MT	Magnetization transfer

NAFLD	Non-alcoholic fatty liver disease
NASH	Non-alcoholic steatohepatitis
NIHR	National Institute for Health Research
NNT	Number needed to treat
NO	Nitric oxide
NPV	Negative predictive value
NSBB	Non-selective beta blocker
OGD	Oesophagogastroduodenoscopy
OR	Odds ratio
OV	Oesophageal varices
P3NP	Aminoterminal peptide of procollagen III
PC-MRI	Phase-contrast magnetic resonance imaging
PPI	Patient and Public Involvement
PPV	Positive predictive value
Pro-C5	Procollagen type V
pSWE	Point shear wave elastography
PV	Portal vein
PVP	Portal venous pressure
RCT	Randomised clinical trial
RF	Radiofrequency
ROI	Region of interest
RR	Relative risk

RRDR	Robust Data Decomposition Registration
SA	Splenic artery
SBP	Spontaneous bacterial peritonitis
sCD163	soluble CD163
SD	Standard deviation
SE-EPI	Spin-echo echo planar imaging
SHAPE	Subharmonic aided pressure estimation
shMOLLI	Shortened Modified Look Locker Inversion recovery sequence
SMA	Superior mesenteric artery
SNR	Signal-to-noise ratio
SPMIC	Sir Peter Mansfield Imaging Centre
SRTFL	Segmented saturation-recovery turboFLASH pulse sequence
SSI	Supersonic shear imaging
SVR	Sustained virological response
TE	Transient elastography
TIMP1	Tissue inhibitor of matrix metalloproteinase 1
TIPSS	Transjugular intrahepatic portosystemic shunt
US	Ultrasound
VEGF	Vascular endothelial growth factor
V_{enc}	Encoding sensitivity velocity
VH	Variceal haemorrhage
vWF-Ag	von Willebrand factor antigen

WHVP	Wedged hepatic venous pressures

1 Introduction

1.1 Abstract

This chapter provides an overview of liver disease and current understanding behind the pathophysiology of portal hypertension. Included is the evidence behind available prognostic tests, including portal pressure measurement. The proven and speculated risk/benefits of treatment of portal hypertension/primary prevention of oesophageal varices with beta-blockers are summarised. There is a lack of objective measures to define the proposed treatment window for beta-blockers and therefore there is a desperate unmet need to guide clinicians in tailoring treatment for an individual patient. Magnetic Resonance Imaging (MRI) has many attractive qualities and may provide a solution to this clinical need. MRI has been shown to perform well in cross-sectional descriptive studies. The aim of this thesis is to start to evaluate MRI's clinical utility in defining an individual's risk of clinical outcomes and developing MRI measures that can evaluate the effect of interventions.

1.2 Liver disease

Liver disease stands out as the only chronic disease in which the incidence and mortality continues to increase in the UK [1]. This is predominantly driven by increasing alcohol consumption and obesity [2]. In the UK, three-quarters of deaths from liver disease are the result of excess alcohol consumption, but deaths caused by other lifestyle risk factors of obesity and viral hepatitis are increasing. Twenty-five percent of adults are now categorised as obese, and 80-90% of obese individuals have non-alcoholic fatty liver disease, with 10-15% having ongoing inflammation and scarring that has a potential to lead to cirrhosis [3]. The incidence of cirrhosis has increased by 40% from 2002 to 2012 in England and Wales; the increase of incidence rates is higher than that of the top four cancers in the United Kingdom [4, 5]. Most patients die within working age (18-65), and liver disease now constitutes the third biggest cause of premature mortality with 62,000 years of working life lost each year [1, 6]. Correspondingly, there has been a 20% rise in mortality from chronic liver disease and cirrhosis in the under 65s in England, making it the fifth leading cause of death [7]. In England and Wales there are

600,000 patients with liver disease, of whom 60,000 have cirrhosis. In 2012, there were 57,682 hospital admissions and 10,948 deaths due to liver disease [5].

There is an absence of symptoms during the early stages of liver disease and therefore the majority of people with liver disease are unaware at the time of their diagnosis. A recent study, using data from the UK Clinical Practice Research Datalink (CPRD), suggested that 50% of cases of cirrhosis have their initial diagnosis only after their first presentation with overt liver failure (decompensation). A hospital admission at diagnosis or subsequently for liver disease substantially impaired prognosis independent of stage of cirrhosis (hazard ratio, HR = 2.78, 95% confidence intervals, CI: 2.53 - 3.06) [4]. Tests to diagnose chronic liver disease in its asymptomatic phase, predict its prognosis, stratify patients for treatment and evaluate efficacy of interventions are desperately required in liver disease to meet this growing clinical burden.

1.3 Natural history

1.3.1 Fibrosis

Fibrosis is part of the innate wound healing response, which occurs in injured tissues; a common pathway thus exists in the different aetiologies of chronic liver disease. As a result of continued liver injury, liver fibrosis is characterised by progressive deposition of extracellular matrix. Cirrhosis is defined histologically as a diffuse process in which the normal anatomical lobules are replaced by regenerative nodules separated by fibrous tissue.

1.3.2 Increased Intrahepatic Resistance

The sinusoidal structure in the liver becomes distorted (fibrosis, vascular remodelling, vascular occlusion, nodule formation) and increases the resistance to the portal blood flow. The increased intra-hepatic resistance caused by these hepatic architectural changes denominate the “static” component of portal hypertension.

In addition, “dynamic” components of intrahepatic vasoconstriction contributes between 10-30% of the increase in portal resistance in portal hypertension [8]. Hepatic stellate cells, portal myofibroblasts

and vascular smooth muscle cells comprise cells with paracrine and autocrine effects that can increase intrahepatic resistance. In cirrhosis, there is a net decrease in vasodilators (such as nitric oxide, NO) and an increase in vasoconstrictors (such as endothelin, norepinephrine, angiotensin II, vasopressin, leukotrienes and thromboxane A_2)[9].

1.3.3 Sinusoidal Remodelling and Angiogenesis

In advanced liver fibrosis fibrous vascularised septa form, linking portal tracts and central veins. Intrahepatic shunts develop, with anastomoses between the afferent (hepatic arteries and portal veins) and efferent (central veins) vessels in the liver. This shunting of blood alters the fluid dynamics in the liver, further increases the intrahepatic resistance, and leaves a proportion of the liver parenchyma hypo-perfused [10].

Sinusoidal vascular remodelling involves a complex interplay of hepatic cells (hepatic stellate cells, portal myofibroblasts and vascular smooth muscle cells) and appears to contribute to increased intrahepatic resistance [11]. Angiogenesis, the formation of new blood vessels from pre-existing vascular beds, occurs in two distinctive manners both of which are growth-factor dependent processes. Sprouting from existing vasculature involves interaction between numerous signalling pathways, including Notch, vascular endothelial growth factor (VEGF), semanorphins and netrins [12]. Intussusceptive angiogenesis is less studied but involves Notch, Tek/Tie-2, mTOR, ephrins and Eph receptors [13]. Both forms of angiogenesis increase intrahepatic resistance and result in the formation of an extensive network of portosystemic collateral vessels in the splanchnic circulation.

1.3.4 Portosystemic collateral circulation

Increased pressure within the portal venous system leads to the compensatory development of porto-systemic collateral circulation. This results in the formation of engorged veins and anastomoses (varices) that may occur in the gastro-oesophageal, rectal, para-umbilical, retroperitoneal or any other region. Varices are the cause of significant morbidity and mortality in patients with liver cirrhosis, particularly with the formation of varices along the gastro-intestinal tract.

1.3.5 Splanchnic circulation

The modified “peripheral arterial vasodilation hypothesis” combines arterial underfilling with an increase in hepatosplanchnic capillary pressure and filtration with increased lymph formation [14]. Arteriolar splanchnic vasodilatation is seen in liver cirrhosis with a number of potential vasodilators suggested to be involved (including NO) [15]. In cirrhosis, there is continued systemic vasodilation despite intense activation of vasoconstrictor mechanisms for reasons that remain poorly understood. In the systemic circulation, splanchnic vasodilatation leads to decreased mean arterial pressure (MAP) and physiological effective hypovolemia. This activates the sympathetic nervous system, the renin-angiotensin-aldosterone system and non-osmotic release of vasopressin resulting in renal sodium and water retention [16, 17]. Vasodilation increases plasma volume and cardiac output increases leading to a hyperdynamic circulation (Figure 1:1).

Recently, a modified version of the arterial vasodilatation hypothesis has been proposed to explain the transition to decompensated cirrhosis in the “systemic inflammation hypothesis” [17]. This hypothesis suggests bacterial translocation is associated with increased systemic inflammation exacerbating the hyperdynamic circulation leading to decompensation, hepato-renal syndrome and acute on chronic liver failure.

1.3.6 Hyperdynamic circulation and multi-organ involvement

The hyperdynamic circulation is characterised by increased cardiac output and a decreased systemic vascular resistance with low arterial blood pressure (Figure 1:1). This in turn leads to increased splanchnic and portal venous inflow into the liver thereby maintaining and perpetuating portal pressure [18].

The hyperdynamic state results in a hyperdynamic multi-organ syndrome. Cirrhotic cardiomyopathy is characterised by increased cardiac output with a sub-optimal ventricular response to stress, and structural and electrophysiological abnormalities [19]. This is seldom symptomatic but may become overt with the stress of interventions such as liver transplantation or with insertion of a transjugular intrahepatic portosystemic shunt (TIPSS) [20, 21]. Renal vasoconstriction, related to splanchnic vasolidation and activation of compensatory neurohormonal systems, is a precursor for the development of hepatorenal syndrome [22-24] . Vasodilatation in the pulmonary circulation and the development of arterio-venous shunting results in ventilation perfusion mismatch in some with liver cirrhosis, termed hepatopulmonary syndrome [25].

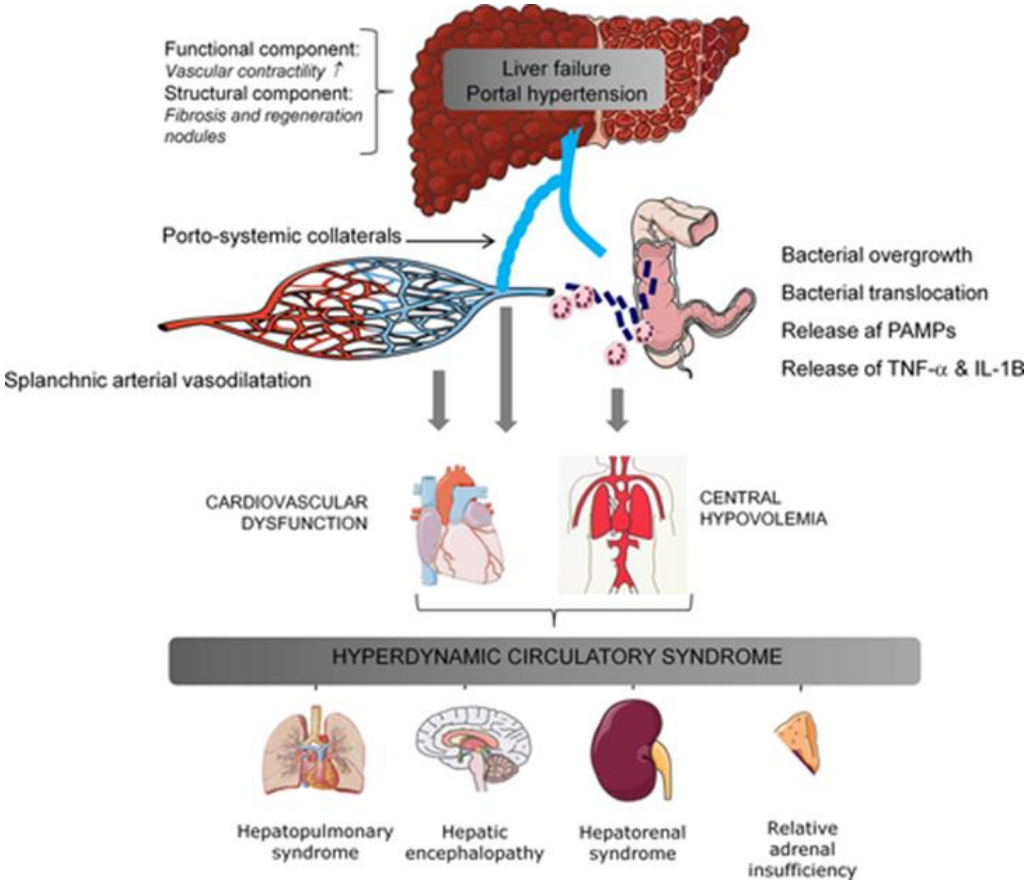

Figure 1:1: Overview of the development of portal hypertension, splanchnic vasodilation and the hyperdynamic circulation in cirrhosis by Moller et al. 2018 [15].

1.4 Clinical Outcomes

Historically, the description of a liver as "cirrhotic" was sufficient to describe the pathology, prognosis and clinical status of a patient with advanced liver disease. Cirrhosis is the end-stage of every chronic liver disease. Its natural history is characterised by an asymptomatic phase, termed "compensated" cirrhosis, followed by a rapidly progressive phase marked by the development of complications of portal hypertension and/or liver dysfunction, termed "decompensated cirrhosis". This has led to the evolution of cirrhosis defined by stages mapped to clinical outcomes.

Cirrhosis is now distinguished between compensated and decompensated stages, with different features, prognoses and predictors of death [26]. Compared to the general population, individuals with compensated cirrhosis have a 5 fold increase, whereas patients with decompensated disease have a 10 fold increase in mortality [27]. Overall survival is lower at 1 year (75% vs. 87%) and five years

(45% vs. 67%) for persons with decompensated cirrhosis as compared to compensated cirrhosis. The probability of transitioning from a compensated to decompensated state varies from 4% to 12% per year [28, 29]. Given that a majority of deaths in patients with compensated cirrhosis are due to progression to a decompensated state and the development of its ensuing complications, the ability to predict decompensation is important.

Portal hypertension is the earliest and most important consequence of cirrhosis which underlies most of the clinical complications of the disease. In the compensated phase, portal pressure may be normal or below the threshold level identified for the development of varices or ascites [5]. As the disease progresses, portal pressure increases and liver function decreases, resulting in the development of complications such as ascites, portal hypertensive bleeding, encephalopathy and jaundice. Within the compensated stage, two subpopulations have been identified based upon the absence or presence of varices, each of which confers a distinct prognosis.

The development of any of these complications marks the transition from a compensated to a decompensated phase. Progression may be accelerated by the development of other complications such as (re)bleeding, renal impairment (refractory ascites, hepato-renal syndrome), hepato-pulmonary syndrome and sepsis (e.g. spontaneous bacterial peritonitis). The decompensated stage can be sub-classified further into a more severe stage defined by the development of recurrent variceal haemorrhage, refractory ascites, hyponatremia and/or hepato-renal syndrome [26]. The development of hepatocellular carcinoma (HCC) may accelerate the course of the disease at any stage. Understanding the natural history of liver disease progression allows planning of management and development of effective strategies to prevent complications.

By defining populations, we can stratify risk, focus resources and concentrate interventions to improve outcomes. The first attempt at creating a disease progression model was performed in a systematic review of the natural history and prognostic indicators of survival in cirrhosis [29]. For the first time, the authors suggested one-year outcome probabilities for cirrhosis according to the clinical stages of cirrhosis agreed at the Baveno IV consensus conference (Figure 1:2). The study included 118

publications, and reported a wide range of retrospective estimates of survival and factors that predicted death from secondary care.

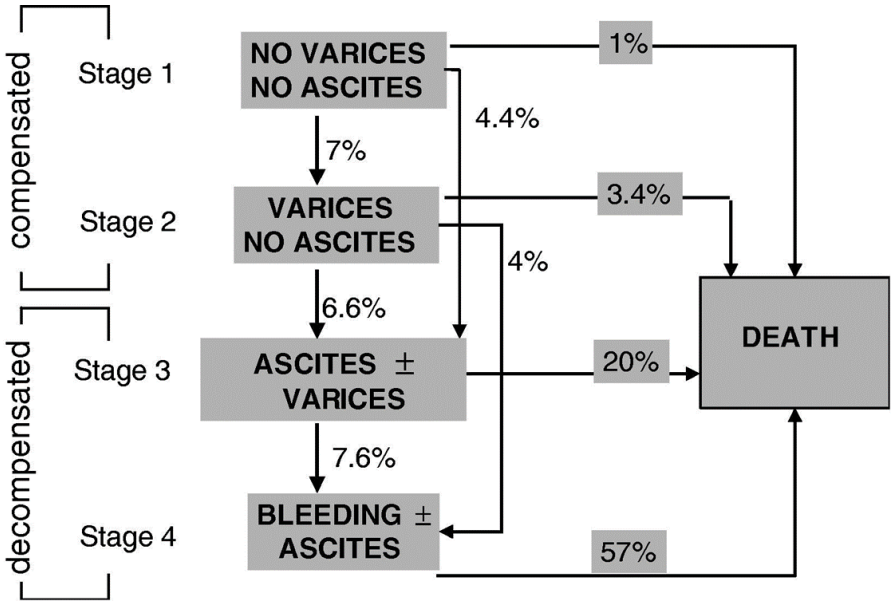

Figure 1:2: Clinical course of cirrhosis: 1-year outcomes probabilities according to clinical stages from secondary care data [29].

A more recent study, also based upon the Baveno IV stage of disease criteria, presented prospectively recorded electronic primary care data from the UK to determine the rate of decompensation and the progression of disease in patients with cirrhosis [28]. The authors found a similar clear demarcation of risk of death between compensated and decompensated disease, although with higher rates of death (Figure 1*:3*). The non-linear increase in mortality across the stages likely reflects methodological differences, misclassification due to coding and differing aetiologies between studies.

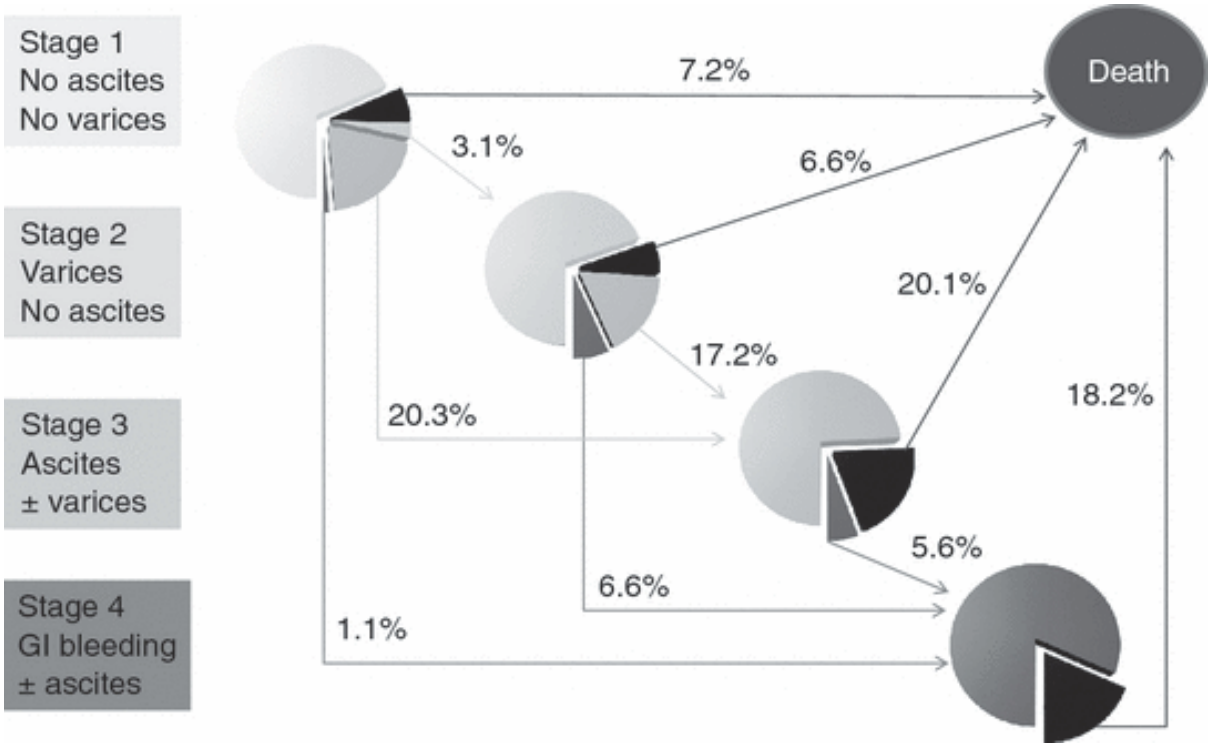

Figure 1:3: Probabilities for progression within 1 year of all patients with cirrhosis from primary care data [28].

Given the evidence that these proposed stages of cirrhosis correlate to clinical outcomes, the next question to address is how do we reliably differentiate these stages and stratify high risk individuals before events occur?

1.5 Stratifying risk

If a test could accurately predict prognosis, it could be used to identify those at risk and provide valuable information for optimising the management of patients with chronic liver disease. For example, providing longitudinal assessment of the impact of interventions such as lifestyle modifications and treatment. The ideal reference standard to evaluate the performance of such a diagnostic test would be clinical outcomes. The vast majority of cases of chronic liver disease are asymptomatic until the disease has progressed to cirrhosis, when portal hypertension and/or hepatocellular failure develop. These liver-related outcomes present as one or more of bleeding oesophageal varices, ascites, encephalopathy or jaundice all of which may take decades to develop.

Consequently, it is difficult to identify cases of advanced liver disease before symptoms herald decompensated disease, and so prediction of future morbidity and mortality is problematic.

A number of tests correlate with mortality and liver-related clinical outcomes in patients with chronic liver disease (summarised in *Table 1:1*). The Child-Turcotte-Pugh (CTP) classification was the first attempt to predict peri-operative risk in patients undergoing surgical portosystemic shunt [30]. It was found to be generally useful to assess prognosis in patients with cirrhosis [31]. It has never been validated for the purpose of predicting non-operative survival or clinical outcomes. Two major criticisms of the classification are the subjective nature and ceiling effect of constituent parts. The Modified for End-Stage Liver Disease (MELD) was originally designed to predict the short-term survival of patients undergoing a transjugular intrahepatic portosystemic shunt [32]. It is based exclusively on objective measures and its primary role is now to predict 90-day mortality of patients awaiting liver transplantation. There is a poor correlation between MELD score and the development of late complications of cirrhosis, such as ascites and hepatic encephalopathy [33, 34].

Subsequent alternative objective measures have attempted to overcome these shortcomings to predict prognosis. Broadly, they split into two themes;

i. serum markers such as Enhanced Liver Fibrosis (ELF), FibroTest and others that attempt to objectively quantify parameters either directly or indirectly related to liver fibrosis
ii. assessment of the liver structure with liver biopsy, ultrasound based transient elastography (TE), magnetic resonance imaging (MRI) or magnetic resonance elastography (MRE)

Study	Disease	N	Years Follow-up median (range)	% (n) outcomes	Test	Performance
Christensen et al. (1984)[31]	Mixed	231	6.4 years (0 - 16)	82% (189)	Child-Turcotte-Pugh (CTP)	None reported
Kamath et al. (2001)[35]	Mixed	282	1.4 years (0 - 5.6)	46% (129)		AUROC, 3m survival
					MELD	0.87 (95% CI 0.82-0.92)
					CTP	0.84 (95% CI 0.78-0.90)
Ekstedt et al. (2015) [36]	NAFLD	229	26.4 years (6 - 33)	42% (96)	Biopsy	Fibrosis ≥2; HR 3.28 (95% CI 2.27-4.76)
Ripoll et al. (2007) [37]	Mixed	213	4.3 years (IQR 2.75 – 6.42)	29% (62)		AUROC for decompensation
					HVPG	0.71 (95% CI 0.64-0.78)
					MELD	0.64 (95% CI 0.55-0.72)
					CTP	0.61 (95% CI 0.52-0.71)
Parkes et al. (2010)[38]	Mixed	457	6.9 years (0 - 9.0)	13% (61)		AUROC, 6y survival
					ELF	0.87 (0.81 to 0.92)
					Biopsy	0.81 (0.76 to 0.89)
					MELD	0.74 (CI not reported)
Naveau et al. (2009) [39]	ALD	218	8.2 years (0 - 11.8)	19% (42)		AUROC, 5 and 10 years
					FibroTest	0.79 (95% CI 0.68-0.86)
					Biopsy	0.77 (95% CI 0.70-0.83)
					CTP	0.69 (95% CI 0.58-0.77)

Vergniol et al. (2011) [40]	HCV	1457	5 years	6% (93)		AUROC, 5y survival
					Biopsy	0.76 (95% CI 0.64-0.84)
					TE	0.82 (95% CI 0.68-0.90)
					FibroTest	0.80 (95% CI 0.69-0.87)
Robic et al. (2011) [41]	Mixed	100	2 years	41% (41)		AUROC, 2y survival
					HVPG	0.82 (95% CI 0.73-0.90)
					TE	0.84 (95% CI 0.75-0.92)
Angulo et al. (2013) [42]	NAFLD	320	8.73 years (0.25 – 26.4)	13% (41)		AUROC for liver outcomes,
					NAFLD-FS	0.70 ± 0.04 (95% CI 0.62-0.78)
					APRI	0.63 ± 0.05 (95% CI 0.53-0.72)
					BARD	0.66 ± 0.04 (95% CI 0.58-0.74)
					Fib-4	0.67 ± 0.05 (95% CI 0.58-0.76)
Asrani et al. (2014) [43]	Mixed	167	2.3 years (0 - 5.5)	7% (12)		Decompensation,
					MRE	HR 4.96 (95% CI 1.4–17.0)
Pavlides et al. (2016) [44]	Mixed	112	2.3 years (IQR 1.3 - 2.6)	14% (16)	MRI Liver	Liver outcomes,
					MultiScan	HR 75.7 (95% CI 7.6–752)
Bradley et al. (2018) [45]	Mixed	67	2.74 years (0.2 – 6.3)	18% (11)		Liver outcomes,
					MRI	Not reported

Table 1:1: Derivation studies for prognostic markers in chronic liver disease associated with mortality and clinical outcomes. 95% CI confidence intervals. NAFLD non-alcoholic fatty liver disease. ALD alcoholic liver disease. HCV Hepatitis C virus. IQR inter-quartile range. MELD model for end-stage liver disease. HVPG wedged hepatic venous portal gradient. ELF enhanced liver fibrosis score. TE transient elastography. APRI AST to Platelet Ratio Index. MRE magnetic resonance elastography. AUROC area under the receiver operating characteristic curve. HR hazards ratio. m months, y years.

As yet, it is unclear whether any test can stratify compensated patients at risk of clinical decompensation [46] or reliably evaluate response to interventions [47]. Both approaches have limitations. Serum markers are not liver-specific and outside strict selection criteria of trials become influenced by other causes of inflammation and fibrosis. They are able to categorise liver disease into risk groups but whether they can stratify risk in terms of clinical outcomes along a continuous disease progression model and/or track dynamic changes with interventions remains to be evidenced.

Quantitative markers of liver structure are equally constrained. They often require costly new hardware, are prone to sampling error and variability. To date, these measures cannot directly or reliably quantify the complex haemodynamic changes thought to be critical to the development of portal hypertension-related complications of liver disease once cirrhosis is established. This again creates a ceiling effect at the point of developing portal hypertension as current tools are unable to dissect the crucial interplay between changing intra-hepatic resistance and portal inflow.

Overall, despite recent advances in non-invasive liver assessment, the drawbacks of the currently available techniques mean that they are not widely available and have not been validated for use as surrogate endpoints in clinical trials. Several professional and regulatory bodies recognise the need to develop better stratification tools to use in future clinical trials [1, 48].

The ideal measurement of a continuous variable would provide a means for assessing the prognosis and treatment response. Longitudinal validation studies of the association between a quantitative surrogate biomarker and clinical outcomes such as death or hepatic decompensation require significant investment. Objective tests that predict the risk of transition to a decompensated state are lacking.

1.6 Hepatic Venous Pressure Gradient (HVPG)

The first portal pressure measurement with mesenteric vein catheterisation connected to a water manomoeter was performed on a dog in 1896 [49]. The direct measurement of portal venous pressure is invasive and impractical for clinical practice. In 1951, the measurement of wedged hepatic venous pressure (WHVP) was first described as an indirect measure of portal pressure [50]. In a healthy liver, the sinusoidal pressure is slightly lower than the portal pressure due to pressure equilibration, but this difference is insignificant. In cirrhosis the sinusoidal architecture is disrupted, hence occlusion of the hepatic vein causes a static column of blood reflecting the pressure at the hepatic sinusoids. WHVP is therefore used as a surrogate measure of portal pressure.

The free hepatic vein pressure (FHVP) is measured in the lumen of the hepatic vein and closely positioned (no more than 2-3 cm) to the junction with the inferior vena cava [51]. The hepatic venous pressure gradient (HVPG) is the difference between the WHVP and the FHVP. Thus, hepatic venous pressure gradient (HVPG), as an indirect measure of portal pressure across the liver, is a potential marker of this transition.

1.7 Outcomes associated with HVPG

HVPG ≤5 mmHg is normal with higher pressures signifying portal hypertension [52]. Published studies linking HVPG to clinical outcomes are summarised in Table 1:2 and Figure 1:4.

Study	Population	Study design	n	FU period	Outcome	%(n) outcomes	HVPG Cut-off	Risk (95% CI)
Garcia-Tsao et al. (1985) [53]	ALD admissions	Single centre case series	93	N/A	Bleeding OVs OVs present	52.7% (49) 82.8% (72)	≥12 ≥12	
Gluud et al. (1988) [54]	ALD cirrhosis & HVPG	Single centre case series	58	31 months	Death	29% (17)	≥15	RR 1.13 (1.02-1.26)
Merkel et al. (1992) [55]	Mixed admissions	Single centre case series	129	45 months	Death	41.9% (54)	>16	
Moitinho et al. (1999) [56]	VH in ALD & NAFLD	Single centre case series	65	1 year	Adverse outcomes	35.4% (23)	≥20	N/A
Merkel et al. (2000) [57]	VH & HVPG	Single centre case series	49	2 years	Death	22.4% (11)	≥16	N/A
Villanueva et al. (2001) [58]	VH	Blinded single centre RCT	40	5 days	Treatment failure	25% (10)	≥20	OR 4.5 (0.8-29)
Monescillo et al. (2004) [59]	VH & HVPG ≤24 hours	Prospective two centre open-label TIPSS trial	116	1 year	Treatment failure Death	20.7% (24)	≥20 ≥19	OR 1.25 (1.08-1.43) HR 1.36 (1.21-1.48)
Ripoll et al. (2005) [52]	HVPG	Single centre case series	393	1 year	Survival	56.0% (220)	>5	HR 1.02 (1-1.04)
Groszmann et al. (2005) [60]	CSPH & no varices	Prospective RCT at four sites	213	54.9 months	Developing varices	39.4% (84)	≥10	N/A

Ripoll et al. (2007)[37]	Nested study in a trial [60]	Prospective RCT at four sites	213	51.1 months	Decompensation	29.1% (62)	≥10	HR 1.15 (1.08-1.23)
Rincon et al. (2007) [61]	Severe AAH	Single centre case series	60	Admission	Death	38.3% (23)	≥22	OR 6.7 (1.1-39.9)
Abraldes et al. (2008) [62]	VH & HVPG ≤48hours	Case series at four centres	117	5 days	Treatment failure	15.4% (18)	≥20	OR 4.52 (1.52–13.46)
Ripoll et al. (2009) [63]	Nested study in trial [60]	Prospective RCT at four sites	213	58 months	HCC	12.2% (26)	≥10	HR 6.1 (1.8-20.1)
Berzigotti et al. (2011) [64]	Cirrhosis and CSPH	Single centre case series	86	28 months	Decompensation Death	25.3% (16) 11.6% (10)	≥16 ≥16	OR 1.22 (1.05-1.4) OR 1.08 (1.01-1.26)
Zipprich et al. (2012) [65]	Any patient with HVPG	Single centre case series	443	1 year	Death	58.5% (259)	≥10	HR 2.2 (1.09-4.4)
Silva-Junior et al. (2015) [51]	Any patient with HVPG	Single centre case series	380	43 months	Transplant-free survival	39.7% (151)	≥16	HR 1.70 (1.14-2.54)

Table 1:2: Summary of prognostic HVPG correlated with clinical outcomes published studies. ALD alcoholic liver disease, NAFLD non-alcoholic liver disease, Severe AAH severe acute alcoholic hepatitis. VH variceal haemorrhage, OV oesophageal varices, HCC hepatocellular carcinoma. HVPG wedged hepatic venous pressure gradient. CSPH clinically significant portal hypertension (HVPG ≥10mmHg). TIPSS transjugular intrahepatic portosystemic shunt. RCT randomised clinical trial. RR relative risk. OR odds ratio. HR hazard ratio.

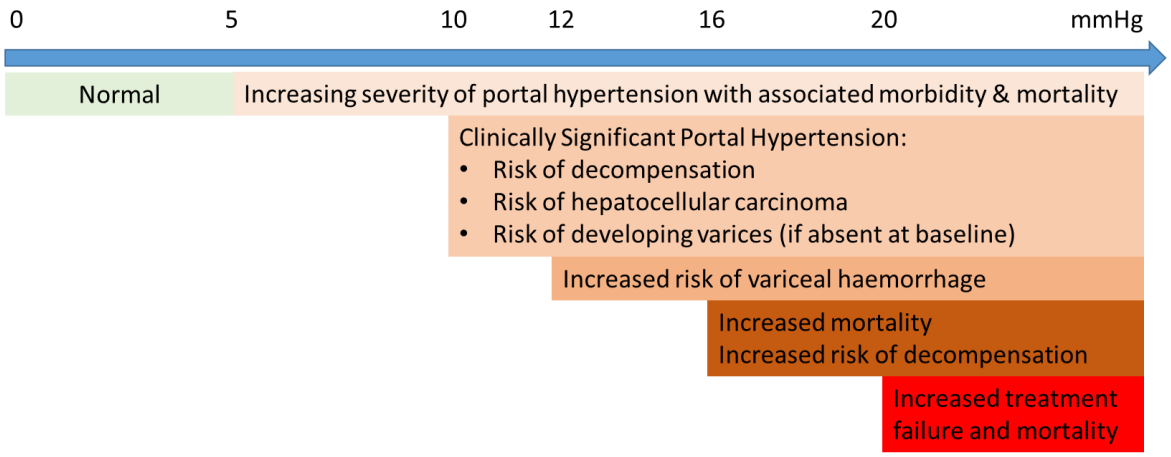

Figure 1:4: Summary of published clinical outcomes from portal hypertension relating to HVPG values in mmHg (Table 1:2).

It is important to highlight some of the limitations of this data. All the published literature originates from a handful of expert specialist centres. The patients within these studies are therefore skewed towards large transplant centres with a disproportionate number of patients with potentially treatable HCC or potential liver transplantation candidates. Nearly all the data are from retrospective case series with the exception of three studies [58-60], one of which had several sub-analyses performed on a highly selected cohort of patients without varices at baseline [60]. The measurement of HVPG is invasive, expensive, subject to operator variability and not readily available in clinical practice.

1.8 Clinical management of portal hypertension

1.8.1 Identification

Current clinical practice follows national [66, 67] and international [68, 69] guidelines summarised in Table 1:3. Oesophageal varices are present in almost half of patients with cirrhosis at the time of diagnosis [70]. Development of varices occurs at a rate of 7% per year [71]. Variceal haemorrhage is associated with a six week mortality of 20% [72]. Patients with cirrhosis undergo regular surveillance with gastroscopy to determine the presence and size of varices [68, 69, 73].

Guideline	Identifying cirrhosis	Gastroscopy surveillance interval	Patients who require primary prophylaxis	Primary prophylaxis suggested
NICE [66, 67] (2016)	TE ELF >10.51 ARFI Liver biopsy	3 years	Medium to large varices	Banding ligation
BSG (2015) [73]	Unspecified	3 years (1 year if small varices)	Medium to large varices or any high risk features	NSBBs (band ligation if contra-indicated)
EASL (2015) [68]	TE >15 kPa Liver biopsy HVPG >5 mmHg	1-3 years depending on risk	Medium to large varices or any high risk features	NSBBs or band ligation
AASLD (2016) [69]	TE>20 kPa Liver biopsy HVPG >5mmHg	1-3 years depending on risk	Compensated cirrhosis: Medium to large varices or any high risk features Decompensated cirrhosis: any varices	NSBBs or band ligation

Table 1:3: Summary of guidelines for primary prophylaxis of portal hypertension in patients with liver cirrhosis. NICE National Institute for health and care excellence. BSG British society of gastroenterology. EASL European association for the study of the liver. AASLD American association for the study of liver diseases. TE transient elastography. ELF enhanced liver fibrosis score. ARFI acoustic radiation force impulse. HVPG hepatic venous pressure gradient. NSBBs non selective beta blockers.

1.8.2 Compensated Advanced Liver Disease (cACLD)

Liver biopsy is recognised as an imperfect gold standard to measure fibrosis and vascular remodelling in chronic liver disease. The introduction of TE in clinical practice has allowed the early identification of patients with advanced chronic liver disease at risk of developing clinically significant portal hypertension (CSPH), without the need to undergo a liver biopsy. The Baveno VI guidelines proposed a new alternative term "compensated advanced chronic liver disease (cACLD)" to better encapsulate the spectrum of severe fibrosis and cirrhosis as a continuum in asymptomatic patients, particularly given distinguishing between the two is often not possible on clinical grounds [68].

1.8.2.1 Criteria to suspect cACLD [68]

- TE is sufficient to suspect cACLD in asymptomatic subjects with known causes of chronic liver disease
- TE often has false-positive results; hence, two measurements on different days are recommended in fasting conditions
- TE <10 kPa in the absence of other known clinical signs rule out cACLD; values between 10-15 kPa are suggestive of cACLD but need further test for confirmation; values >15 kPa are highly suggestive of cACLD

1.8.2.2 Criteria to Confirm cACLD [68]

- Invasive methods are employed in referral centers in a stepwise approach when the diagnosis is in doubt or as confirmatory tests.
- Methods and findings that confirm the diagnosis of cACLD are:
    - Liver biopsy showing severe fibrosis or established cirrhosis
    - Collagen proportionate area (CPA) measurement on histology provides quantitative data on the amount of fibrosis and holds prognostic value
    - Gastroscopy showing gastroesophageal varices
    - HVPG measurement; values >5 mmHg indicate sinusoidal portal hypertension

Of note, two international guidelines now advocate it is safe to rule out the need for surveillance gastroscopy in patients with a liver stiffness <20kPa and a platelet count > 150,000/mm^3 [68, 69]. The first guideline with this advice had no supporting published evidence at the time of publication [68]. A summary of the evidence behind these recommendations is in Table 1:4. All the published studies are retrospective audit data and predominantly in patients with viral hepatitis before starting treatment. Patient data from two earlier studies [74, 75] were included in one of the subsequent validation studies [76]. This data was subsequently merged with another study [77] and one additional cohort in a subsequent paper trying to expand the original criteria [78].

There was a flurry of publications after the adoption of Baveno VI criteria to the international guidelines (overview of fully published papers in Table 1:4). These were combined with 11 abstracts in a meta-analysis of the Baveno criteria [79] which showed a very low chance of varices requiring treatment being missed (0.3%) in patients with cACLD caused by alcohol, NAFLD, and chronic viral hepatitis. Baveno VI criteria were found to reduce the number of surveillance endoscopies by 32.8% [79]. Although the negative predict value is excellent, there are still a large number of screening endoscopies needlessly performed. One paper improved the reduction in endoscopy surveillance to 43.8% by combing the Baveno VI criteria with spleen stiffness measurements (with a cut-off of ≤ 46kPa) [80] with a continued <5% risk of missed varices requiring treatment [68]. However, there remains a 15-20% unsuccessful rate of spleen stiffness measurements meaning the clinical utility of this model remains in question [81].

Paper	Aetiology	N (total)	No. with varices	Best model	Model used	Performance
Kim et al. (2010) [82]	HBV	253	184 (72.7%)	TE × spleen diameter / platelet count.	LSPS <3.5 >5.5	Any varices: NPV=94.7% PPV=93.3%
Berzigotti et al. (2013) [74]	HCV 71.6% HBV 8.7% HCC 36.4%	173	70 (40.5%)	TE × spleen diameter / platelet count	LSPS ≥3.21	Any varices: NPV=90.8% PPV=73.2%
Augustin et al. (2014) [75]	HCV 84%	49	10 (20.4%)	TE	>25	Any varices: NPV=93% PPV=42%
Perazzo et al. (2015) [83]	Not stated	97	54 (55.7%)	TE & Platelets	>20 & >150,000	Any varices: PPV=63% NPV=71%
Maurice et al. (2016) [77]	HCV 55% HBV 8% ALD 13%	310	57	TE & Platelets	<20 & >150,000	High risk varices (HRV) PPV=6% NPV=98%
Abraldes et al. (2016) [76]	Viral 70% ALD 14% HCC 15%	518	223 (43.1%)	TE & Platelets	<20 & >150,000	HRV: NPV=95%
Jangouk et al. (2017) [84]	Viral 70.6% ALD 12.6%	262	108 (41.2%)	Baveno VI	<20 &	HRV: NPV=100%

	NASH 7.6%				>150,000	
Augustin et al. (2017) [78]	HCV 62.8%	925	322 (34.8%)	TE & Platelets	<25 & >110,000	HRV: NPV=98.4%
Llop et al. (2017) [85]	HCV 85.1% HBV 3.7% NASH 3.7%	161	25 (15.5%)	Baveno VI	<20 & >150,000	HRV NPV=94.4% PPV=20.6%
Silva et al. (2017) [86]	HCV 78.4% ALD 8.2% HBV 3.1%	97	14 (14.4%)	Baveno VI	<20 & >150,000	HRV NPV=100% PPV=16.3%
Sousa et al. (2017) [87]	HCV 82% ALD 12% HBV 4%	104	9 (9%)	Baveno VI	<20 & >150,000	HRV: NPV=100% PPV=16.1%
Bae et al. (2018) [88]	HBV 60.6% HCV 12.0% ALD 13.1%	1035	100 (9.7%)	Baveno VI	<20 & >150,000	HRV: NPV=96% PPV=25%
Bellan et al. (2018) [89]	HCV	160	18 (11%)	Baveno VI	<20 & >150,000	HRV: NPV=94% PPV=21%

Colecchia et al. (2018) [80]	HCV 70.6% HBV 5.8% ALD 8.8% NASH 3.1%	613	117 (19%)	Baveno VI Spleen TE Combined	<20 & >150,000 ≤46 kPa	HRV: NPV=99.1% PPV=23.2% NPV=98.8% NPV=98.1%
Matsui et al. (2018) [90]	NAFLD 39% HCV 39% ALD 9%	384	11 (2.9%)	Baveno VI MRE	<4.2kPa	HRV: NPV=99% PPV=1% NPV=98%
Petta et al. (2018) [91]	NAFLD	639	71 (11%)	Baveno VI	<20 & >150,000	HRV: NPV=97.4% PPV=16.5%
Stanislas et al. (2018) [92]	HBV	60	20 (33.3%)	Baveno VI	<20 & >150,000	HRV: NPV=100% PPV=41.7%
Lee et al. (2019) [93]	HBV 39.7% HCV 12.1% ALD 29.2%	1218	249 (20.4%)	Baveno VI Combined to spleen diameter	<20 & >150,000	HRV: NPV=98.1% PPV=26.9% AUROC=0.78

Moctezuma-Velazquez et al. (2019) [94]	PBC 64.8% PSC 35.2%	227	30 (13.2%)	Baveno VI	<20 & >150,000	HRV: NPV=100% PPV=20.7%
Thabut et al. (2019) [95]	HCV 81% HBV 16.6%	891	72 (8.1%)	Baveno VI	<20 & >150,000	HRV: NPV=99% PPV=10.3%
Tosetti et al. (2019) [96]	HCV 69% HBV 10% NASH 15%	442	31 (7%)	Baveno VI	<20 & >150,000	HRV: NPV=100% PPV=8.7%

Table 1:4: Summary of published evidence to support guidelines in using non-invasive biomarkers to exclude the need for gastroscopy for varices surveillance in patients with cirrhosis. HBV hepatitis B virus. HCV hepatitis C virus. HCC hepatocellular carcinoma. ALD alcoholic liver disease. NASH non-alcoholic steatohepatitis. TE transient elastography. NPV negative predictive value. PPV positive predictive value. LSPS liver stiffness measurement spleen diameter to platelet ratio score.

1.8.3 Primary prophylaxis

Once high risk varices are identified at screening gastroscopy, treatment is initiated termed primary prophylaxis. Non-selective beta-blockers (NSBBs) or endoscopic variceal ligation can be used for the primary prophylaxis against bleeding in patients with varices [68, 69, 73]. A meta-analysis showed equivalent efficacy with no differences in survival [97].

NSBBs such as propranolol act in two main ways to reduce portal pressure; β-1 receptor blockade results in reduced cardiac output and splanchnic blood flow, and β-2 blockade results in splanchnic vasoconstriction via unopposed effect of α-1 receptors. Carvedilol is a NSBB with additional vasodilating actions through α-1 receptor blockade, which reduces portocollateral and intrahepatic resistance [98].

1.8.4 Stratifying based on treatment response

HVPG is the only validated tool to stratify the changes in portal pressure and therefore the risk of variceal haemorrhage and liver related outcomes. A reduction in HVPG to less than 12 mmHg virtually abolishes the risk of variceal haemorrhage [53]. A reduction by ≥20% reduces the risk of bleeding irrespective of the final HVPG value [99]. A systematic review showed HVPG reduction of ≥20% or to <12 mmHg significantly reduces the risk of bleeding [29, 99]. Patients achieving these targets with treatment are termed '*haemodynamic responders*.' Long term follow-up of patients presenting with variceal haemorrhage (median 48 months) demonstrated worse outcomes in patients who lost or who did not achieve this haemodynamic response, usually associated with progressive liver disease [100].

1.8.5 Beyond portal pressure

A large proportion of patients experience a protective effect from NSBBs regardless of haemodynamic response, suggesting there is another unknown mechanism of benefit [101], possibly related to bowel permeability [102]. Reducing portal pressure with NSBBs has a significant protective effective against infections (such as spontaneous bacterial peritonitis) in a meta-analysis [103]. Both experimental [104] and clinical [102] studies suggest that NSBB treatment is associated with decreased bacterial

translocation. This suggests a possible second mechanism of efficacy for NSBBs that remains untested [101].

NSBBs appear to improve survival in patients with acute on chronic liver injury (OR= 0.596; 95% CI 0.361 – 0.985, p = 0.0436) and may exert additional anti-inflammatory effects in patients with cirrhosis [40]. In a Danish registry with 2 year follow-up, propranolol, a NSBB, reduced mortality in mildly (HR=0.7; 95% CI 0.6 – 0.9) and severely (HR=0.6; 95% CI 0.4 – 0.9) decompensated cirrhosis. NSBBs also reduced the likelihood of developing spontaneous bacterial peritonitis (HR=0.4; 95% CI 0.2 – 0.9) and the mortality in those who had it previously (HR=0.5; 95% CI 0.3 – 0.8) [105].

The PREDESCI trial demonstrated that in patients with compensated cirrhosis and HVPG ≥10 mmHg (mostly due to untreated Hepatitis C), NSBBs significantly decreased the incidence of hepatic decompensation or death (HR=0·51; 95% CI 0·26 - 0·97, p=0·041) after a median follow-up of 37 months [106]. The was mostly driven by a reduction in the incidence of ascites (HR=0·44; 95% CI 0·20 - 0·97, p=0·0297). Currently in each patient, the clinician is asked to judge the benefits against possible harms of starting NSBB treatment (Figure 1:5) with no way of routinely objectively quantifying it.

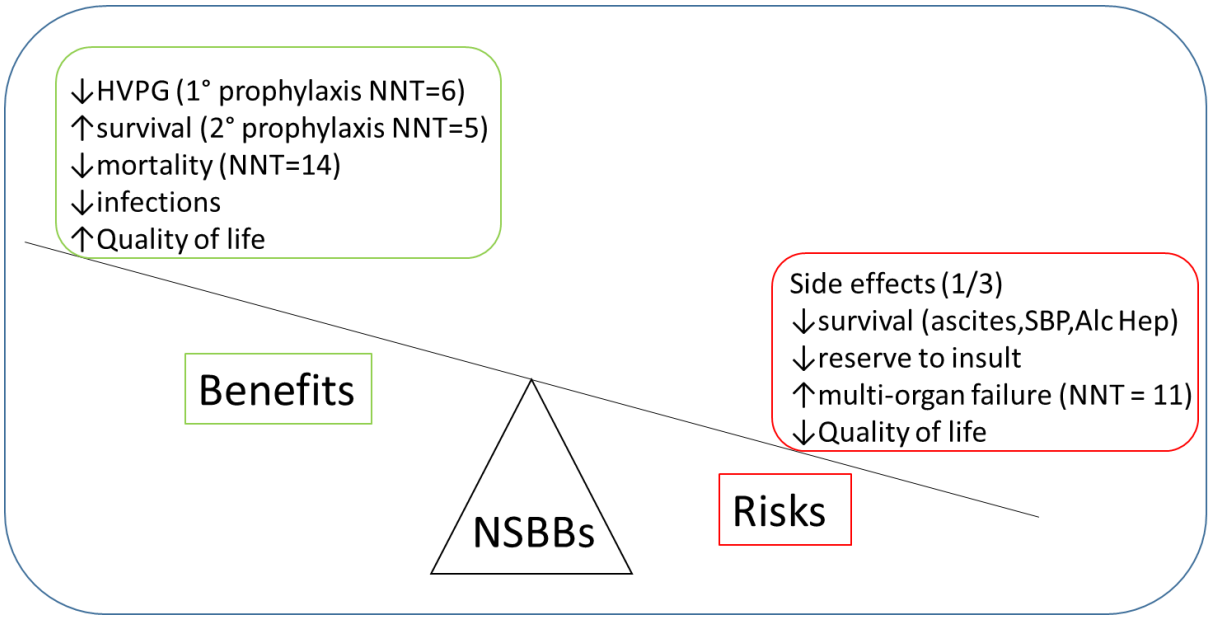

Figure 1:5: Summary of the clinical judgement clinicians make for an individual patient with cirrhosis without routinely available measures before commencing treatment with

NSBBs. NNT number needed to treat. SBP spontaneous bacterial peritonitis. Alc Hep alcoholic hepatitis.

1.8.6 Harms and the window hypothesis

Carvedilol reduces HVPG significantly more than propranolol and is thought to be the most effective NSBB to reduce portal pressure [107]. Even so, at best NSBBs like Carvedilol are effective at adequately reducing portal pressure in only 50% of patients meaning half the patients started on treatment remain at significant risk of a life-threatening bleed [107]. In contrast, NSBBs are associated with significant rates of adverse events (fatigue and shortness of breath) that preclude treatment or require discontinuation in 15-20% of patients.

In addition, NSBBs may attenuate the hyperdynamic circulatory state and further lower the arterial blood pressure [98, 108]. Low arterial blood pressure is associated with increased mortality and with the development of ascites [109]. There is also a suggestion that NSBBs increase mortality in patients who have decompensated cirrhosis with ascites [110, 111], spontaneous bacterial peritonitis [112] and alcoholic hepatitis [113]. Combined, this emphasises the use of NSBBs may be harmful in some patients with advanced fluid retention and renal dysfunction, leading to the concept of a physiological therapeutic window hypothesis for the use of NSBBs in treating portal hypertension [114]. The evidence for NSBB efficacy to prevent variceal bleeding comes from trials that excluded patients with ascites or renal dysfunction. Clear evidence is lacking and so the uncertainty of how to identify the therapeutic window remains a focus for research [115] .

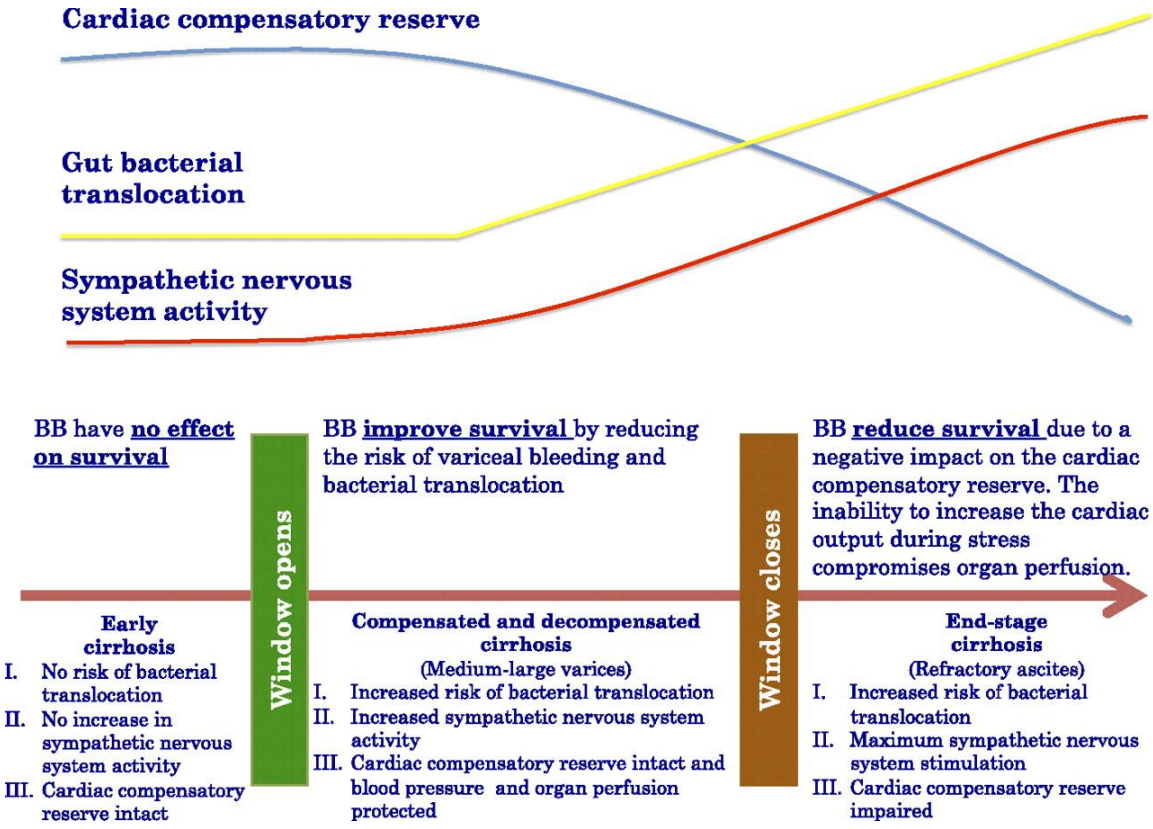

Figure 1:6: The therapeutic window hypothesis for use of NSBBs in patients with cirrhosis proposed by Krag et al. [114]

1.8.7 Personalised medicine

The ideal for an individual would be tailored treatment depending on haemodynamic response to NSBBs to justify the risks of ongoing treatment. A meta-analysis found the relative risk of bleeding in hemodynamic responders compared with non-responders was 0.13 (95% CI 0.06 – 0.29) [116]. A subsequent randomised controlled clinical trial demonstrated improved outcomes after a median of 24 months in those who received HVPG-guided therapy compared to blind treatment [117]. Mortality was lower in the HVPG-guided therapy group than in the control group (HR=0.59; 95% CI 0.35 - 0.99). There was less rebleeding (HR=0.53; 95% CI 0.29-0.98), and further decompensation reduced (HR=0.68; 95% CI 0.46 - 0.99). The survival probability was higher with HVPG-guided therapy than in controls, both in acute (HR=0.59; 95% CI 0.32 - 1.08) and chronic non-responders (HR=0.48; 95% CI 0.23 - 0.99). There is some emerging data that early NSBBs may also reduce the incidence of ascites, decompensation and death (HR=0·51; 95% CI 0·26–0·97) in those with compensated cirrhosis and

CSPH in those with a haemodynamic response (defined as a ≥10% decrease in HVPG or to <10 mmHg)[106].

HVPG measurements are invasive and available only in specialised hepatology units, precluding the use of HVPG in routine clinical practice. Hospitals across the NHS therefore follow a pragmatic approach as set out in National, European and American guidelines [68, 69, 73]. Specifically, unless there is a contra-indication, all patients with cirrhosis with oesophageal varices that require primary prophylaxis receive NSBBs. Treatment success is evaluated by absence of clinical outcomes over time and annual surveillance endoscopy. There is tacit acceptance of treatment associated side effects and risk of haemodynamic non-response. NSBBs are cheap and do not require expertise to administer. Endoscopic variceal ligation can be performed at the time of screening endoscopy and its side effects are less frequent. However, specific expertise is necessary and there is a small, but significant, potential for lethal haemorrhage from post-procedure ulcers [70]. There is a desperate need for a non-invasive measure to stratify portal pressure changes to assess the efficacy of therapeutic interventions so that the risk:benefit ratio of any treatment (eg NSBBs) is optimised.

1.9 Non-invasive measures of HVPG

Clinical practice guidelines advocate portal pressure measurement is important for prognosis and pivotal for clinical management [68, 69, 73]. In addition, treatment efficacy is established by pre and post therapy HVPG measurement. The have been a plethora of surrogate markers proposed to non-invasively assess portal pressure with high heterogeneity across published studies in terms of methods used and underlying causes of liver disease (overview of techniques shown in Figure 1:7 [118], studies outlined in Table 1:5).

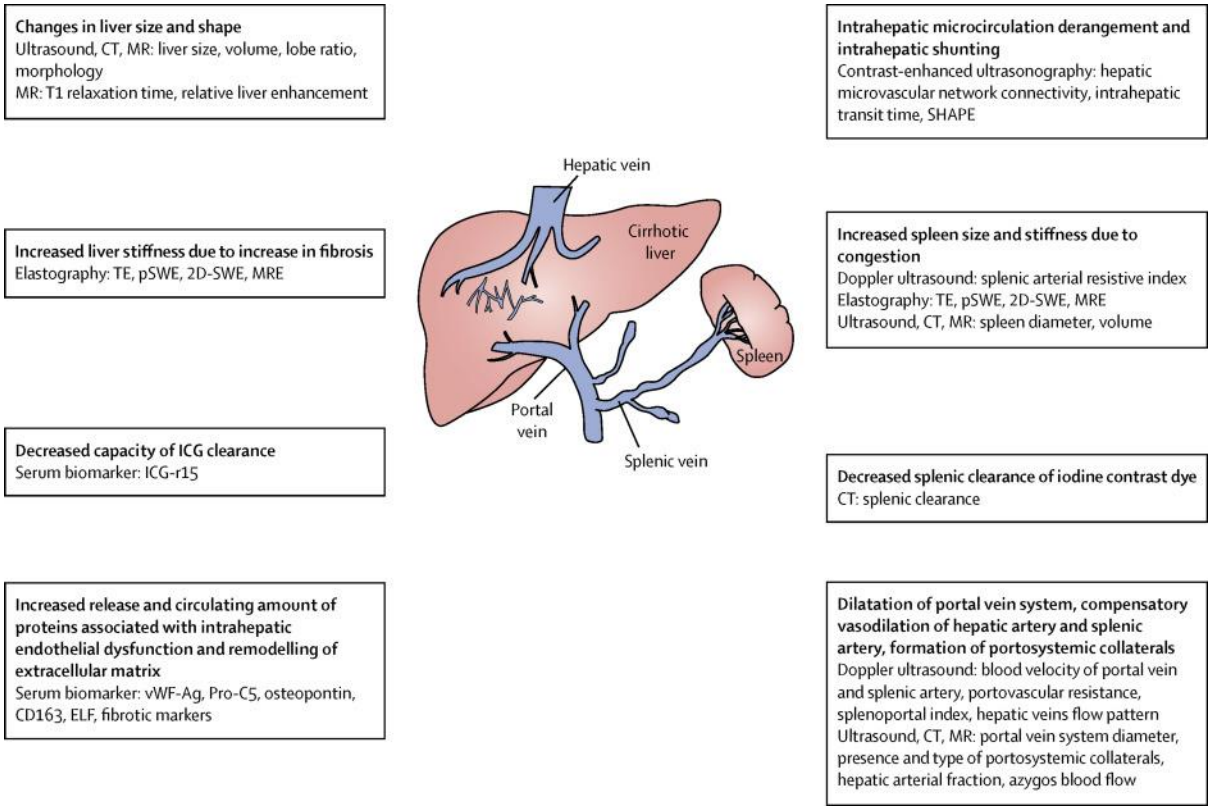

Figure 1:7:Overview summary of non-invasive approaches for diagnosis and monitoring of portal hypertension [118]. Methods aim to detect changes in the development of cirrhosis and portal hypertension (in liver, spleen, intra-hepatic and extra-hepatic vessels), properties of the liver and spleen parenchyma (stiffness, indocyanine green [ICG] and dye clearance) or circulating proteins associated with fibrogenesis and portal hypertension. 2D-SWE=two dimensional real-time shear wave elastography. ELF=enhanced liver fibrosis. ICG-r15-indocyanine green 15 min retention test. MRE=magnetic resonance elastography. pSWE=point shear wave elastography. Pro-C5=procollagen type V. SHAPE=subharmonic aided pressure estimation. TE=transient elastography. vWF-Ag=von Willebrand factor antigen.

Test	Measured component(s)	How is it measured?	Aim	Performance
VITRO score [119]	vWF-Ag platelet count	VWF-Ag / platelet ratio	Dichotomise HVPG ≥10	AUROC=0.86
CD163-fibrosis score [120]	sCD163 ELF score	Algorithm based on sCD163 and ELF score	Dichotomise HVPG ≥10	AUROC=0.90
ICG-r15 test [121]	Indocyanine green	Infusion and retention of ICG after 15minutes	Dichotomise HVPG ≥10	AUROC=0.832 (CP-A)
Pro-C5 [122]	Pro-C5	Plasma Pro-C5: (a)Cutoff of 330 ng/mL (b)Cutoff of 346 ng/mL	Dichotomise (a)HVPG≥10 (b)HVPG≥16	 AUROC=0.73 AUROC=0.68
Osteopontin [123]	Osteopontin	Plasma osteopontin Cutoff 80 ng/mL	Dichotomise HVPG ≥10	AUROC=0.763
Damping Index [124]	Hepatic vein doppler	min/max velocity Cutoff 0.6	Dichotomise HVPG>12	AUROC=0.860
Splenic arterial resistance index [125]	Splenic artery & Portal vein doppler	Algorithm based on splenic pulsatility index & portal blood flow	Dichotomise HVPG ≥10	AUROC=0.87 [126]
SHAPE [127]	SHAPE gradient	Portal & hepatic vein doppler with microbubble contrast	Dichotomise HVPG≥12	AUROC=0.94
ARFI [128]	Spleen stiffness	acoustic radiation force impulse	Dichotomise HVPG≥10	AUROC=0.97
SSI [129]	Liver stiffness	Supersonic shear imaging	Dichotomise HVPG ≥10	AUROC=0.84

2D-SWE [130]	Liver stiffness	Shear wave elastography Cutoff 15.4kPa	Dichotomise HVPG ≥10	AUROC=0.939
Virtual HVPG with CTA [131]	CT angiography with contrast	Computational fluid dynamic analysis	Dichotomise HVPG ≥10	AUROC=0.88
Radiomics HVPG [132]	Contrast enhanced CT	Radiomics feature extraction & LASSO	Dichotomise HVPG ≥10	AUROC=0.849
Azygous flow [133]	PC MRI	Cutoff 4.4 mL/s	Dichotomise HVPG ≥16	AUROC=0.96
predicted HVPG [134]	MR and PC MRI	SE EPI Liver T1 & splenic artery velocity	Continuous measure	R=0.90
Caval subtraction [135]	PC MRI	Caval subtraction and portal vein inflow	Continuous measure	R=0.780
MRE	Liver Stiffness	Shear wave velocity	Continuous measure	R=0.377

Table 1:5: Examples of published studies of emerging non-invasive approaches for markers of HVPG and performance characteristics. vWF-Ag=von Willebrand factor antigen. AUROC=area under the receiver operating characteristic. sCD163=soluble CD163. ELF=enhanced liver fibrosis score. ICG-r15=indocyanine green 15 minute retention test. SHAPE=subharmonic aided pressure estimation. ARFI= acoustic radiation force impulse. SSI= supersonic shear imaging. 2D-SWE=two-dimensional real-time shear wave elastography. CTA=computed tomography angiography. LASSO=least absolute shrinkage and selection operator. PC MRI=phase contract magnetic resonance imaging. MRE=magnetic resonance elastography.

Technical challenges to apply these measures to patients with obesity and/or multiple co-morbidities remain. None of the alternative measures have yet proven sufficient accuracy nor shown an ability to reliably evaluate the efficacy of interventions along the continuous variable of HVPG rather than dichotomise into groups with and without clinically significant portal hypertension in a cross-sectional snapshot.

1.10 MRI

Magnetic Resonance Imaging (MRI) technologies provide unique methods for imaging the whole liver and abdomen. As a result, several favourable characteristics required to stratify chronic liver diseases are obtained. These methodologies are non-invasive, provide objective measurements, are organ-specific and do not use ionising radiation. They measure multiple parameters in a single scan session. Uniquely amongst imaging modalities, it is possible to concordantly assess several different measures within the same session. Non-invasive and contrast agent free, quantitative MRI provides the opportunity to acquire information on liver composition (volume, fibrosis and inflammation) and haemodynamics (liver tissue perfusion and blood flow) in a single scan session (<40 minutes).

MRI measures correlate with cross-sectional invasive measures of both liver structure and portal pressure. Longitudinal relaxation time (T_1) of liver tissue is validated against inflammation/fibrosis on liver biopsy [136, 137]. MRI measurements also closely correlate with invasive HVPG measurement [134]. Inflammation and fibrosis lengthen transverse relaxation time (T_2) [138, 139]. More recently specific MR liver biomarkers, including Liver T_1 and liver perfusion, have been shown to predict clinical outcomes by separate research groups [44, 45].

1.11 Aims

The aims of this thesis is to explore the utility of newly developed MR tools to stratify patients with cirrhosis;

1. To investigate the effect of field strength on surrogate MR measures of portal pressure
2. To investigate the effects of Direct Acting Antiviral therapy given to patients with advanced liver disease caused by Hepatitis C virus
3. To develop a novel MR tool to evaluate increased small bowel permeability

2 Methods

2.1 Abstract

In this chapter, there is a brief description of the methods used in all three studies within the thesis. This includes a description of public and patient involvement, blood samples, and transient elastography. The principles behind measuring portal pressure, the evidence behind balloon catheters and the variability of the measure of HVPG are discussed. Finally, the underlying principles of MRI are outlined together with how these techniques have been applied to patients with liver disease.

2.2 Patient and Public Involvement (PPI)

Each study within this thesis was designed with integrated patient and public involvement. I prepared a lay overview of the background, rationale and proposed study design. With the assistance of the NIHR Nottingham Biomedical Research Centre's PPI engagement facilitator (Andy Wragg), I advertised to recruit members from the Nottingham Digestive Diseases Patient Advisory Group. I recruited a PPI focus group (some of whom have liver disease) for each of the three studies. Their input significantly influenced the study design. In addition to writing the content for all study-specific patient materials (such as the participant information sheets, posters and consent forms), they also suggested practical measures to maximise the feasibility of the study, facilitate recruitment and retention.

Examples include:

- Closely align study visits to clinical care appointments
- Detailed transport arrangements and reimbursement
- Free Wi-Fi at study visits
- Regular study updates through the centre's website, social media outlets and newsletter to interested parties

- A generic lunch voucher: - enable participants to have the ability to choose food to address particular dietary requirements which the standard hospital snack lunch does not permit eg low fat content, appealing vegetarian food etc.

2.3 Serum markers

2.3.1 Sample collection

Blood was collected into 4.0ml ethylenediaminetetraacetic acid (EDTA) K2E vacutainer tubes, 6.0ml SSTII vacutainer tubes and 2.7ml sodium citrate vacutainer tubes (Becton Dickinson Ltd, Oxford, UK). To obtain the serum samples, the plain blood collection tubes were allowed to coagulate for 60 minutes at ambient temperature (18-22^{o}C). The samples were then centrifuged at 2000g for 10 minutes. The serum was carefully aspirated and separated into 500 µl aliquots. The aliquots were frozen immediately on liquid nitrogen and stored at -70^{o}C. The processing of all blood samples was performed by Melanie Lingaya and Yirga Falcone (NIHR Nottingham Biomedical Research Centre).

2.3.2 Routine clinical tests

Analysis of full blood count (FBC) and coagulation profile is performed by the department of haematology in both hospitals (Nottingham University Hospitals NHS Trust and Derby Teaching Hospitals NHS Foundation Trust). Analysis of renal profile and liver function tests (LFTs) is by the department of clinical chemistry.

2.3.3 MELD

The Modified for End-Stage Liver Disease (MELD) consists of a freely available published score based upon serum bilirubin, creatinine levels and International Normalized Ratio (INR) [35].

2.3.4 Enzyme-linked immunosorbent assays (ELISAs)

Under the supervision of Jane Grove, I performed all three ELISAs detailed in the small bowel permeability chapter in the Nottingham NIHR BRC with commercial kits as per the manufacturer's instructions.

2.4 Transient Elastography

Transient Elastography is an ultrasound-based non-invasive method of quantifying liver stiffness measurement using FibroScan® (Echosens, Paris, France) [140, 141]. Measurements are performed on the right lobe of the liver through intercostal spaces with the patient lying in the dorsal decubitus position with the right arm in maximal abduction. This is repeated until ten successful acquisitions are recorded. The median value represents the liver elastic modulus. Only cases with 10 successful acquisitions are evaluated. The liver stiffness is expressed in kiloPascals (kPa). The success rate is calculated as the number of successful measurements divided by the total number of measurements.

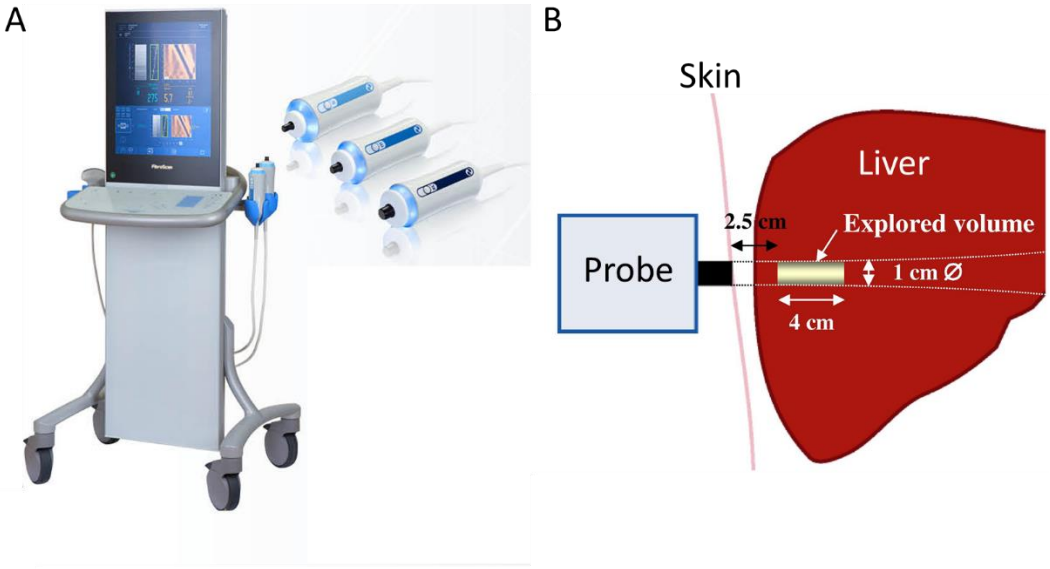

Figure 2.1: (A) Fibroscan™ machine that measures transient elastography (B) Position of probe between ribs and explored volume of liver **[142]**

2.5 HVPG

In both Nottingham University Hospital NHS Trust and Derby Teaching Hospitals NHS Foundation Trust, the hepatic venous pressure gradient (HVPG) measurement is performed by interventional radiologists. I learnt to perform HVPG measurements at Derby prior to starting the work within this thesis. All HVPG measurements included here were performed by interventional radiologists at the respective centres, some of which I attended to ensure compliance with published methods (see

below). The majority are outpatient day case procedures routinely performed prior to a transjugular liver biopsy in all patients as standard clinical care. There are no absolute contraindications for HVPG measurement. The procedure is generally safe with rare complications. Transjugular liver biopsy is offered to patients deemed high risk for percutaneous liver biopsy such as those with suspected cirrhosis, low platelets, and/or prolonged prothrombin time. Almost all transjugular liver biopsies irrespective of specific indications were combined with HVPG measurements. Allergy to contrast medium and previous cardiac arrhythmias are equally relative contraindications to the procedure. The complications are mostly related to local access vessel injury, which are greatly reduced with the use of ultrasonographic guidance in the hands of experienced vascular radiologists.

2.5.1 Measuring HVPG

HVPG is measured according to established standards in the morning following an overnight fast (of minimum 6 hours) [143]. The procedure is performed with continuous non-invasive vital signs monitoring and no sedation (although low doses of intravenous midazolam may be used if required). Under ultrasonographic guidance, the right internal jugular vein is cannulated and a 9-French vascular sheath placed by the modified Seldinger technique. Under fluoroscopic guidance, a 6-French compliant balloon-tipped catheter (Berenstein occlusion catheter, Boston Scientific, UK) is placed through the right atrium and inferior vena cava (IVC) into the right hepatic vein.

Free hepatic vein pressure (FHVP) is measured by maintaining the catheter tip ‘free’ in the hepatic vein at 2–4 cm from its opening into the IVC [51]. The difference between the FHVP and IVC pressure should not exceed 2 mmHg; if this occurs it is likely due to the catheter being inaccurately placed. The balloon catheter is inflated and the wedged hepatic venous pressure (WHVP) is measured (*Figure 2.2*). After recording WHVP total occlusion of the hepatic vein is checked with slow injection of contrast. This should demonstrate a typical wedged pattern without reflux of the contrast or washout via connections with other hepatic veins. If there is inadequate occlusion caused by shunts or insufficient balloon inflation, then measurements are repeated with altered catheter position. The WHVP readings

are taken before the slow injection of dye to avoid falsely elevated pressures (contrast medium does not transmit pressure well). The venous pressure stabilises (up to 60 seconds) before readings are recorded. Triplicate readings of FHWP and WHVP are obtained. The balloon catheter is flushed between each reading. If any of the two pressure readings differ by more than 1 mmHg, all 3 sets are repeated. The pressures in the IVC and right atrium are also measured. The pressure tracings are recorded using a Philips IntelliVue MP50 patient monitor (Philips Healthcare).

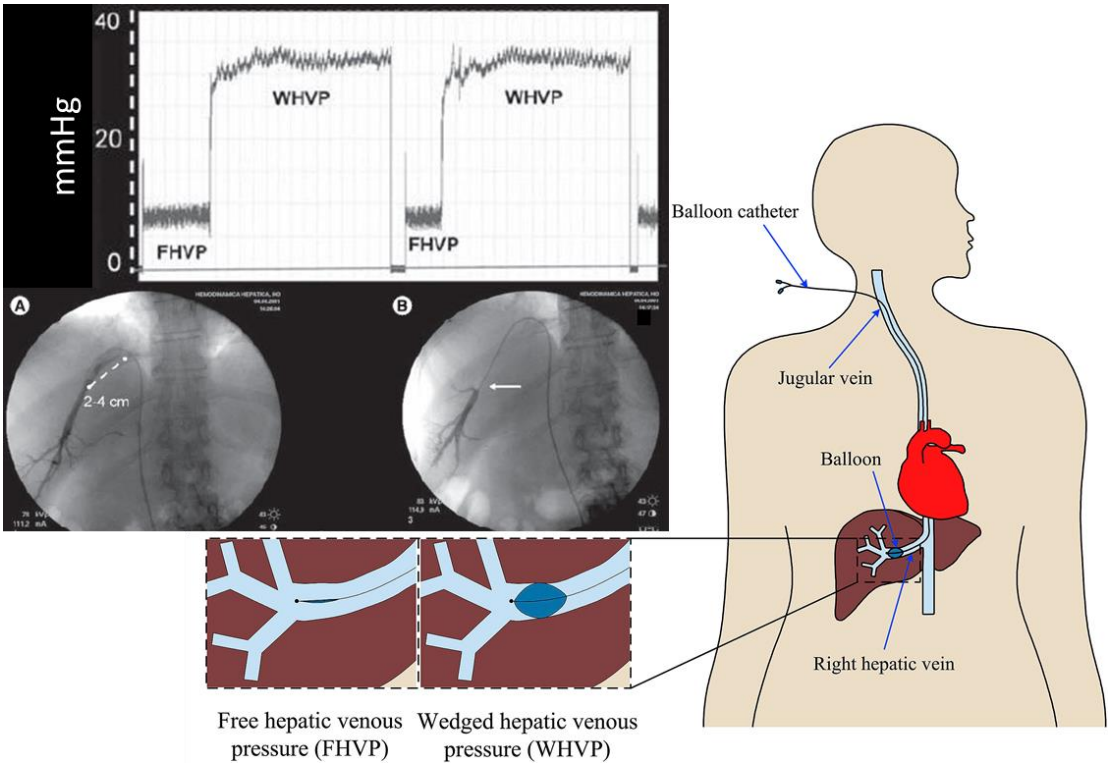

Figure 2.2: Summary of portal pressure measurement with a balloon catheter [7]. (A) FHVP measured by placing the catheter tip 'free' in the hepatic vein 2–4 cm from the inferior vena cava. (B) WHVP measured by occluding the hepatic vein with an inflated balloon (arrow) at the catheter tip. Typical tracing of pressure measures in the hepatic vein shown [8]. HVPG is the difference between WHVP and FHVP.

2.5.2 Technique: wedged vs balloon occlusion

There are two techniques for measuring WHVP, either wedging an end-hole catheter into an end branch of the hepatic vein or inserting an occlusion-balloon catheter in a hepatic vein main branch. The balloon catheter offers theoretical advantages allowing serial measurements from the same location without the need to reposition the catheter. It is likely to avoid the decompressive effects of venous-to-venous shunts proximal to the balloon and gives an average pressure from a number of smaller hepatic veins [143]. WHVP and HVPG measurement with the balloon catheter correlate better with directly measured portal pressure compared to the end-hole catheter [144, 145]. In contrast, the straight end-hole catheter measures the WHVP in small hepatic venules which are very heterogeneous [146]. For these reasons balloon catheters are preferred in most departments to evaluate portal pressure, including Nottingham and Derby.

2.5.3 Reproducibility of HVPG

For a long time there has been concern that there is remarkably little published data to affirm reports that HVPG measurements are very reproducible [147]. The authors described a coefficient of variation of 7.8% in the last 20 patients they had measured. Only two published studies have prospectively evaluated HVPG against invasive portal pressure measurement and reported the reproducibility [144, 145]. One showed a coefficient of variation of 7% with balloon catheter measure of HVPG in 47 patients with cirrhosis, with an intra-class correlation coefficient of 0.72 in another 13 patients with invasive portal pressure measurement [144]. The second study of 174 patients with cirrhosis showed a standard error of measurement of 2.99 mmHg compared to direct measurement and within patient coefficient of variation of 11.7% (*Figure 2.3*) [145].

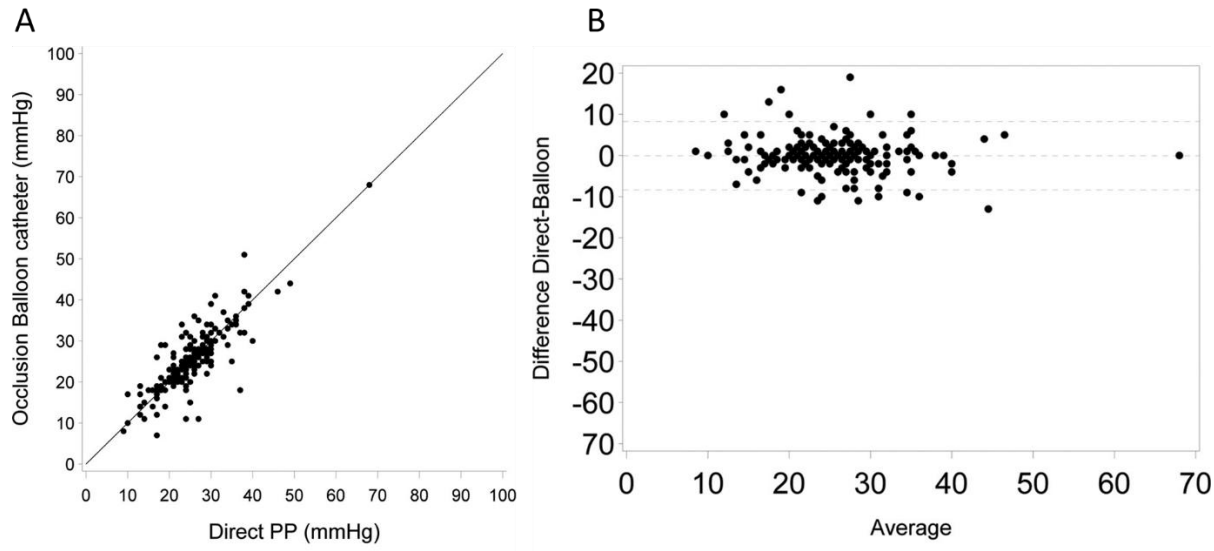

Figure 2.3: (A) Scatterplot of direct portal pressure (PP) measurement and occlusion-balloon WHVP measurement. The diagonal line indicates perfect agreement. (B) Bland-Altman plot of direct portal pressure measurement and occlusion-balloon WHVP measurement. The difference between measurements is plotted against the mean of both. The horizontal lines denote the mean difference and 95% limits of agreement **[145]**.

2.6 MRI

The aim of this thesis is to apply and evaluate non-invasive quantitative MRI measures in patients with advanced chronic liver disease. A detailed understanding of the physics underpinning MRI image acquisition and analysis is beyond the scope of this thesis. The following section provides a summary of the principles of the MRI methodology used in this thesis. I learnt about the underlying principles by attending the University of Nottingham's School of Physics Masters Programme lectures on MRI. I attended the MR safety and assistant courses to enable me to help supervise and undertake research MRI scans for all the participants in these studies at the Sir Peter Mansfield Imaging Centre (SPMIC).

I designed, recruited and ran all three clinical studies within this thesis. I collated all study data before performing the statistical analysis. I physically assisted the subjects and scanner operator during the MRI scans but the MRI analysis of the liver patients was performed by Christopher

Bradley, Eleanor Cox and Susan Francis blinded to HVPG and other clinical information. I performed all the MRI analysis in the healthy volunteer study (under the supervision of Caroline Hoad) blinded to the permeability data with the exception of the small bowel wall T_2 analysis that was developed and performed by Hannah Williams, Caroline Hoad and Penny Gowland.

The work presented builds upon previous development work performed by collaborators at the SPMIC and the Nottingham NIHR Nottingham Biomedical Research Centre (NIHR BRC).

2.6.1 Principles of MRI

Magnetic resonance imaging (MRI) uses the magnetic properties of the hydrogen nuclei (protons) in the body to produce detailed images from any part of the body. Spinning protons produce a small magnetic field as they have electric charge, spin and mass. Each of the magnetic fields is called a magnetic dipole moment, denoted by μ. In the absence of an external magnetic field the dipole moments point in random directions and the net magnetic field will be zero. Other nuclei can also produce MRI signals but this thesis is focused on the hydrogen nucleus because of its abundance in water and fat.

As discussed, the protons have their own magnetic field and are spinning on their axes. When the protons are placed in an external magnetic field (B_0), such as an MRI scanner, they tend to line themselves up with the large external magnetic field (like a magnetic bar). However, since the nucleus is spinning in an external magnetic field, the resultant movement is not simply an alignment and rotation but a precession (like a gyroscope).

Approximately half the spins precess parallel to the external field (low energy state) and half align opposite to the external field (high energy state), but a small number of extra spins precess parallel to the external field compared to anti-parallel resulting in a net longitudinal magnetization (M_0) point in the direction of B_0 (termed z direction). This uniform alignment creates a magnetic vector, M_0, oriented along the axis of the MRI scanner. In the large magnetic field, the protons also precess about the axis of the external magnetic field, B_0 (*Figure 2.4*).

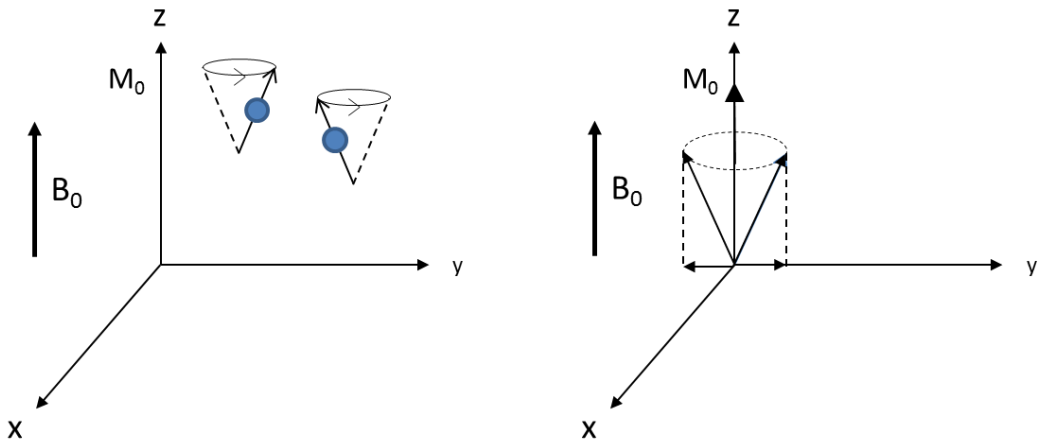

Figure 2.4: Two protons rotating out of phase will lead to a net longitudinal magnetisation M_0 but no component in the x-y plane. The net magnetisation vector M_0 has the same direction as the external magnetic field.

The rate at which the protons precess about the external magnetic field (B_0) is given by the Larmor equation, $\omega=\gamma B_0$, where ω is the angular precessional frequency of the proton and γ is the gyromagnetic ratio. The protons precess about the z-axis but if they are out of phase with each other they do not create a net transverse (M_{xy}) component.

When additional energy (in the form of a radio wave) at a frequency equal to the Larmor frequency is added to the magnetic field, the magnetic vector is deflected. The radio wave frequency (RF) that causes the nuclei to resonate is dependent on the element of interest (usually hydrogen) and the strength of the magnetic field. When the frequency of the RF pulse matches the Larmor frequency ω, resonance occurs. Applying a 90° RF pulse at the Larmor frequency causes protons to be flipped from the low energy state to the higher energy state, eventually equalising the number of protons in both states and removing any measurable longitudinal magnetisation vector. In addition, the RF pulse causes the spins to precess in phase with each other; the vector sum of the in-phase protons results in net transverse plane (transverse magnetisation). This effect can be pushed above with a higher RF pulse.

Once the RF pulse is turned off, the protons realign with the axis B_o magnetic field, returning to equilibrium (the lowest energy state), i.e. returning the longitudinal magnetisation to M_0 whilst the transverse magnetisation decays to zero. Receiver coils around the area of interest detect the emitted signal. The intensity of the received signal is then plotted on a grey scale and spatial localisation gradients are built up. It is this signal which is used to create the MR images. Each of these processes have a different time constant defined by the longitudinal (T_1) and transverse (T_2/T_2*) relaxation time respectively.

2.6.2 Longitudinal (T_1) relaxation time

The longitudinal (T_1) relaxation time refers to the time constant describing the time taken for the spins to realign along the longitudinal (z) axis. It is also called the spin-lattice relaxation time as it signifies the time taken by the spins to give the energy gained from RF pulse back to the surrounding lattice in order to return to the equilibrium state. Following a 90° RF pulse, the magnetisation along the longitudinal axis (M_z) is given by the equation:

$$M_z = M_0(1 - e^{-t/T1})$$

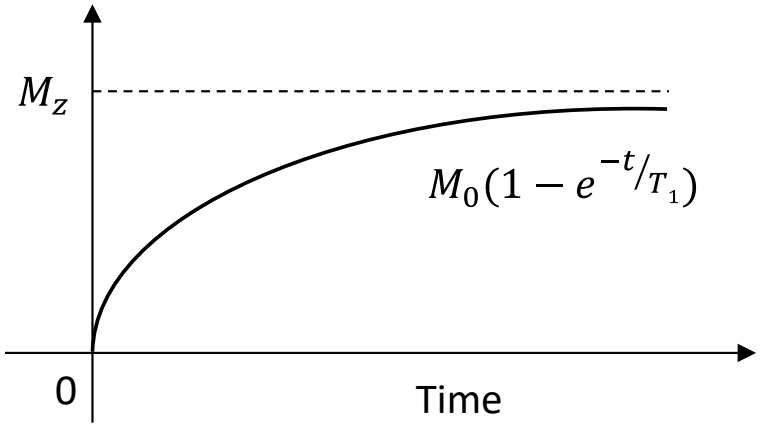

Figure 2.5: After a 90° RF pulse, longitudinal recovery described by the T_1 (spin-lattice) relaxation time.

The T_1 of any tissue depends on how protons are able to transmit their energy to the surrounding lattice. Multiple transmitted radiofrequency pulses can be used in sequence to emphasise particular tissues or abnormalities. A different emphasis occurs because different tissues relax at different rates

when the transmitted radiofrequency pulse is switched off. The time taken for the magnetic vector to return to its resting state in the longitudinal plane (spin lattice) is called T_1.

The T_1 of any soft tissue within the body (brain, heart, kidneys, liver, bowel or spleen) is a measure of the way protons are able to transmit their energy to the surrounding lattice. By focusing on Hydrogen ions in the body, the T_1 relaxation time has been used to study specific tissues of interest within the body to provide a non-invasive measure of its properties in health and disease.

2.6.3 Transverse (T_2 and T_2*) relaxation time

The time needed for the axial components of the spins to lose phase coherences and return to equilibrium is given by T_2. The transverse magnetisation component (M_{xy}) rapidly decays after the RF pulse is turned off at a rate characterised by the T_2 relaxation time constant which is also called the transverse relaxation time.

$$M_{xy} = M_0 e^{-t/T2}$$

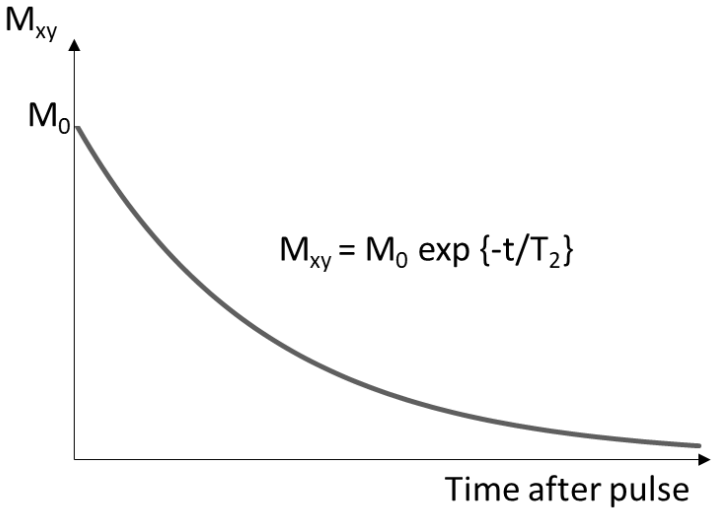

Figure 2.6: After a 90° RF pulse, transverse decay described by T_2 (spin-spin) relaxation time

The decay of M_{xy} results from the spins being dephased, and this is affected by both intrinsic spin-spin interactions and the external magnetic field inhomogeneity. T_2 of a tissue depends only on the spin-spin interactions whilst T_2* decay takes into account the additional dephasing due to the inhomogeneity of the external magnetic field (so $T_2 \geq T_2$*). T_2 relaxation reflects tissue-particular characteristics, primarily those that affect the rate of movement of protons (hydrogen nuclei – mostly found in water molecules). It is therefore a good measure of oedema, inflammation and iron within a tissue of interest.

2.6.4 Longitudinal relaxation time (T_1) of liver and spleen

Due to the limitations of liver biopsy [148], there has been huge interest in developing quantitative MRI markers to evaluate the liver [149]. MRI techniques evaluating the structure of the liver initially focused on liver T_1 measurements (summarised in Table *2.1*). Only recently have these techniques been compared to liver biopsy [136, 137, 150]. Any MR parameter in isolation depends on multiple histological factors [151]. Liver T_1 measurements are influenced by many confounding factors, dependent on the MRI technique employed. These include inflammation [136], iron [151-153], fat [154] and oedema [155, 156] (*Table 2.2*).

Study	MRI measures studied	No. of Slices	No. of Inversion times	N	Compared to liver biopsy?	Uncorrected contributing factors to Liver T_1 measure
Heye et al. 2012 [157]	SRTFL T2 T2*	1	6	61	No	Iron Fibrosis Steatosis Inflammation
Banerjee et al. 2014 [137]	shMOLLI ^{1}H MRS T2*	1	5	79	Yes	Steatosis Inflammation Pulse
Hoad et al. 2015 [136]	IR SE-EPI T2*	9	10	110	Yes	Inflammation

Table 2.1: MRI studies evaluating published liver measures, including liver T_1. SRTFL segmented saturation-recovery turboFLASH pulse sequence, shMOLLI shortened Modified Look Locker Inversion recovery sequence, IR SE-EPI inversion-recovery spin-echo echo planar imaging

Contributing factor to uncorrected MR measures	Liver T_1	Liver T_2
Fibrosis [136, 137, 155, 157]	↑	↑
Fat [154, 158]	↑	↔
Inflammation [45, 136, 156]	↑	↑
Iron [136, 151-153]	↓	↓
Oedema [45, 136]	↑	↑

Table 2.2: Published effects of contributing factors on MRI measures within the liver.

To date, there is no easy way to separate inflammation and fibrosis. Iron accumulation in liver tissue is known to dramatically reduce T_2 and T_2* relaxation times [152, 153], and an increase in iron will also reduce T_1 in the liver [151]. Iron concentrations can accurately be evaluated with T_2*[148]. MRI techniques therefore incorporate iron measures of T_2* to better fit T_1. Researchers have shown MOLLI T_1 is vulnerable to fat interference leading to substantial changes both on phantom models and patients [158].

Fat can be suppressed or attempts can be made to quantify fat to incorporate it into fitting liver T_1. One approach is to incorporate fat saturation pulses for all sequences to suppress the fat signal meaning liver T_1 is independent of steatosis [136]. Alternatively, other protocols attempt to quantify hepatic lipid content by using localised cardiac-triggered proton spectroscopy in an $8cm^3$ voxel trying to avoid vascular and biliary structures [137]. This approach relies on the assumption that liver fat is homogeneously distributed across the liver and that it is easy to locate an area of liver devoid of vascular and biliary structures. Fat-water separation relies on a shift in MR frequency between hydrogen nuclei in fat and water, such as with mDIXON sequences that can more reliably be used to quantify liver fat [159] to correct T_1.

Nottingham researchers have shown longitudinal relaxation time (T_1) varies with degree of fibrosis (*Figure 2.7*) [136]. The technique for acquiring T_1 data in this study differ from other studies as it is

respiratory triggered and multi-slice. This allows a large volume of the liver to be sampled (mean ± SD of 4030 ± 1342) voxels covering 290 ± 97 cm^3 in a reasonable imaging time without the need for breath hold, making this imaging scheme ideal for patient studies. For T_1 measures, the acquisition and analysis is highly repeatable in healthy subjects, with a coefficient of variation between visits of 1.8% and low inter- and intra-observer variability with intra-class correlation coefficients of >0.99 [136].

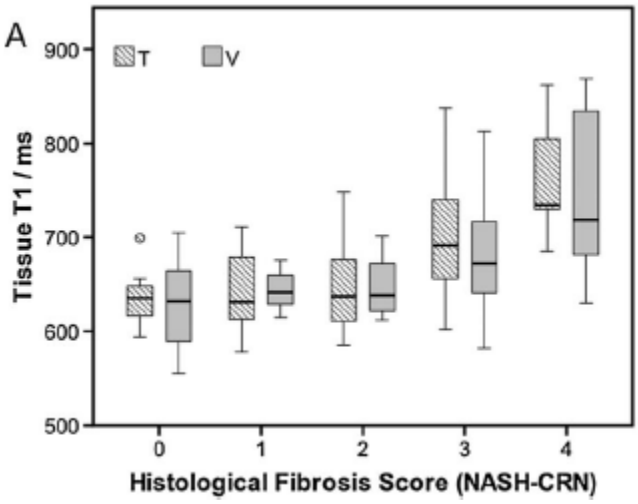

Figure 2.7: Box plot of the distribution of liver tissue T_1 with NASH-CRN histological scoring for fibrosis, split by training (T) and validation (V) cohorts [136]

Moving beyond categorical histological stages of fibrosis, our group has recently demonstrated that this method of measuring liver T_1 also significantly correlates with the percentage of fibrotic tissue relative to the total biopsy area estimated by visual morphometry [45, 150]. Additionally, there is a significant increase in liver tissue T_1 associated with progressive liver disease with differences between both healthy volunteers and patients with cirrhosis, as well as compensated and decompensated cirrhosis. Furthermore, increased liver T_1 has been associated with liver-related outcomes such as decompensation, transplant or death [44, 45].

2.6.5 Splanchnic and portal blood flow

Phase contrast (PC)-MRI is a non-invasive technique to measure flow in a blood vessel without the use of any intravenous contrast agent. Spins that are moving in the same direction as a magnetic field

gradient develop a phase shift that is proportional to the velocity of the spins. This is the basis of phase-contrast angiography. In the simplest phase-contrast pulse sequence, bipolar gradients (two gradients with equal magnitude but opposite direction) are used to encode the velocity of the spins. Stationary spins undergo no net change in phase after the two gradients are applied. Moving spins will experience a different magnitude of the second gradient compared to the first, because of their change in different spatial position. This results in a net phase shift. This information can be used directly to determine the velocity of the spins.

PC-MRI provides velocity measurement for every voxel in the region of interest (ROI) and the average velocity over the measured vessel area can be obtained. The flow rate is the product of the measured velocity and the pixel area of the vessel. A critical parameter in the PC acquisition is the encoding sensitivity velocity, V_{enc}. V_{enc} is a parameter selected by the MR operator depending on the vessel of interest and it represents the maximum velocity present in the imaging volume. Any velocity greater than the V_{enc} will be aliased. This is related to the fact that the velocity in the image volume produces a proportional phase shift of ± 180^{o}. Absolute velocities greater than V_{enc} will produce phase shifts greater than 180, which will be interpreted in the ± 180^{o} range and hence aliased.

Phase contrast (PC)-MRI can be used to quantify the velocity and cross-sectional area of the portal vein and hepatic artery (for hepatic inflow), and the right, middle, left hepatic veins (for hepatic outflow), as well as the splenic artery (SA) and superior mesenteric artery (SMA) (for flow in splanchnic circulation) and azygous vein (for collateral flow). 15 phases through the cardiac cycle are collected for vein measurements and 20 phases for the arteries, with different velocity encoding (V_{enc}) used for each vessel (portal/hepatic/azygous veins V_{enc}=50cm/s, hepatic/splenic arteries V_{ENC}=100cm/s, and superior mesenteric artery V_{enc}=140cm/s) [45, 134]. If aliasing occurs, the V_{ENC} is increased and the measure repeated. Previous work has shown that these measures are highly reproducible (coefficients of variation 1.5-8.3%) [134]. Each measurement is acquired during a 15-20 second breath hold, dependent on the subject's heart rate.

PC-MR data are analysed using Q-flow software (Philips Medical System). For each vessel, a region of interest is drawn manually around the vessel lumen on each phase contrast image, with contour detection used. The mean signal intensity within each region of interest reflects flow velocity in the vessel of interest (cm/s) for each cardiac phase, and the mean velocity across the cardiac cycle is computed. The cross-sectional area of each vessel lumen is multiplied by the mean velocity, to compute mean blood flux (ml/s) in each vessel (examples of which is shown in *Figure 2.8*).

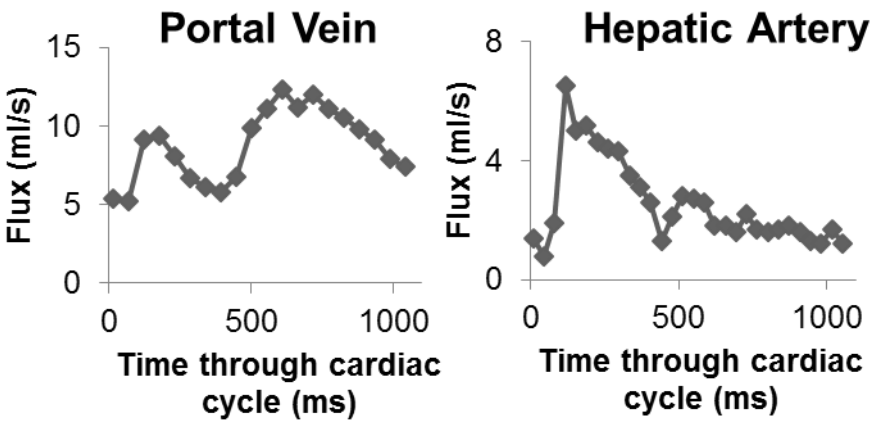

Figure 2.8: Example of Q-flow software (Philips Medical Systems) using a region of interest drawn over a vessel (portal vein or hepatic artery) to calculate the mean cross-sectional area (mm^2), velocity (cm/s) and flux (ml/s) [velocity X area] of blood flow.

2.6.6 Arterial spin labelling (ASL)

ASL is a non-invasive technique to quantify perfusion in a tissue of interest. ASL utilises the magnetic spins of the free diffusible water in the blood as an endogenous contrast agent. The blood water spins are typically inverted (for instance using a FAIR labelling scheme for abdominal ASL) and this labels the magnetisation of the blood water before it enters the tissue of interest (*Figure 2.9)*. The labelled water subsequently exchanges with the water in the tissue, and the tagged magnetisation decays at a rate dependant on the T_1 longitudinal relaxation time of the water in the tissue.

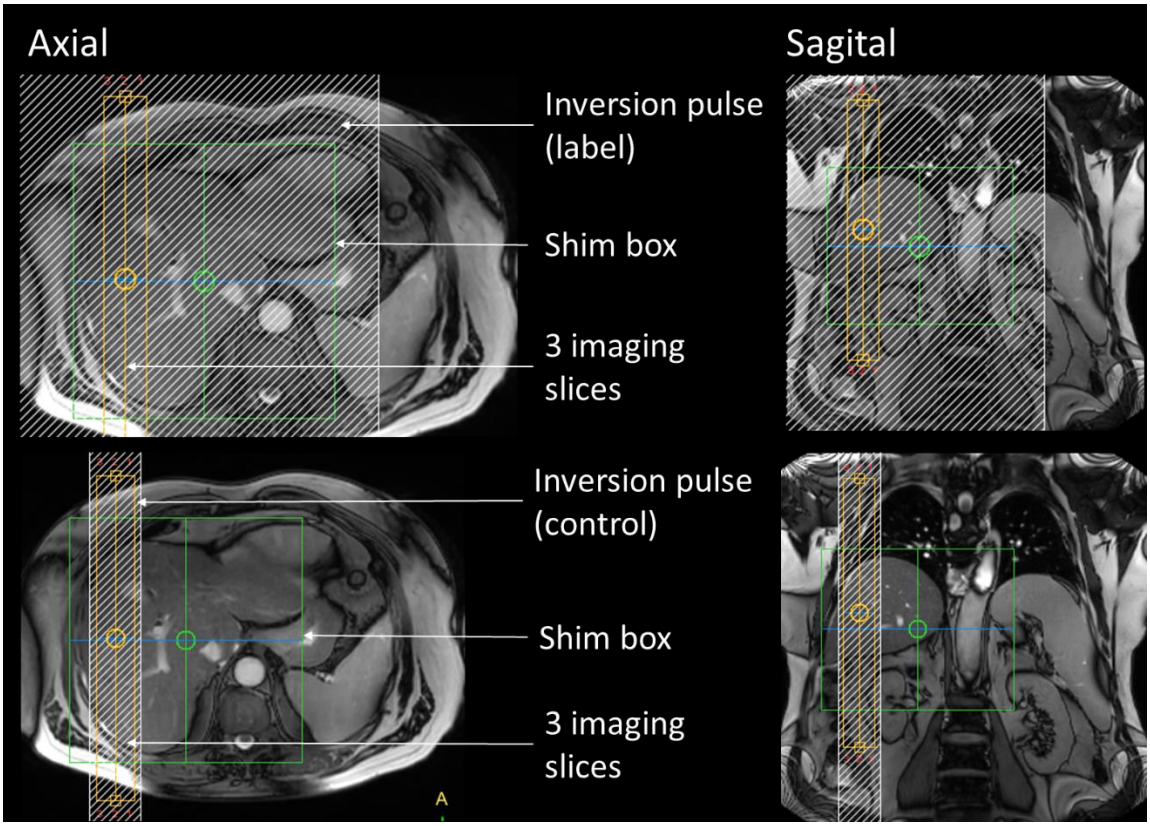

Figure 2.9: Principles of ASL by flow-sensitive alternating inversion recovery **[160]**. *Orange lines indicate the image slices acquired with inflow blood labelled by magnetic inversion (top) and control (bottom).*

A perfusion weighted image is obtained by subtracting the difference of magnetically labelled image from a control image with unlabelled water (*Figure 2.10*). The perfusion-weighted signal change is small and hence the signal-to-noise ratio (SNR) is low. Therefore multiple label and control image pairs are acquired and the difference between them is to calculate perfusion (in millilitres per 100 grams of tissue per minute (ml/100g/min)).

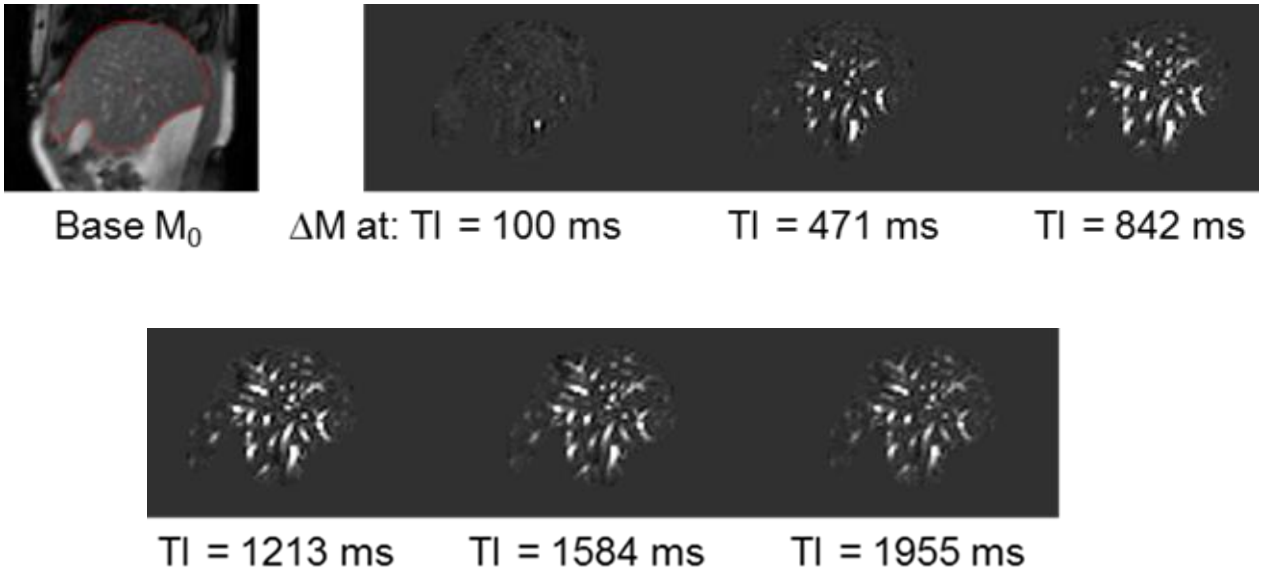

Figure 2.10: Perfusion weighted difference (ΔM) maps calculated (control – label). Individual perfusion weighted difference images (control–label) are calculated for each of readout phase. These are inspected for motion (excluding control/label pairs with movement of >1 voxel) and averaged to create a single perfusion-weighted (ΔM) map for each phase. Mean values of ΔM, the base equilibrium magnetisation M_0 and T_1 are used in an iterative model [160] to calculate tissue perfusion (ml/100g/min) and tissue arrival time of the label (ms).

Liver perfusion significantly reduces with progressive liver disease severity both between healthy volunteers and patients with cirrhosis as well as between compensated and decompensated cirrhosis [45].

2.6.7 Portal pressure

Our group have shown two quantitative MRI markers (liver T_1 and splenic artery velocity) correlate with HVPG in 40 patients in a cross-sectional study at a field strength of 1.5 Tesla [134]. In the same cohort, ELF score and TE correlated well with HVPG (Pearson R=0.758 p<0.001, and Spearman R=0.791, p<0.001 respectively) but neither correlated with portal pressures >10mmHg. Hence, such tools can reasonably dichotomise patients with and without portal hypertension but they are insensitive to stratifying clinical risk or detecting small changes with interventions.

However, quantitative MR parameters related to both hepatic architecture and splanchnic haemodynamics correlated significantly with HVPG along the continuous spectrum. Univariate measures associated with HVPG included liver T_1 (Pearson R=0.835, p<0.001), splenic artery velocity (Pearson R=0.584, p=0.003), superior mesenteric artery velocity (Pearson R=0.534, p=0.002), and azygous vein flow (Spearman R=0.656, p<0.001). A multivariate model combining both measures accurately correlated with HVPG measurement (R=0.90, p<0.001), including those with clinically significant portal hypertension (*Figure 2.11*).

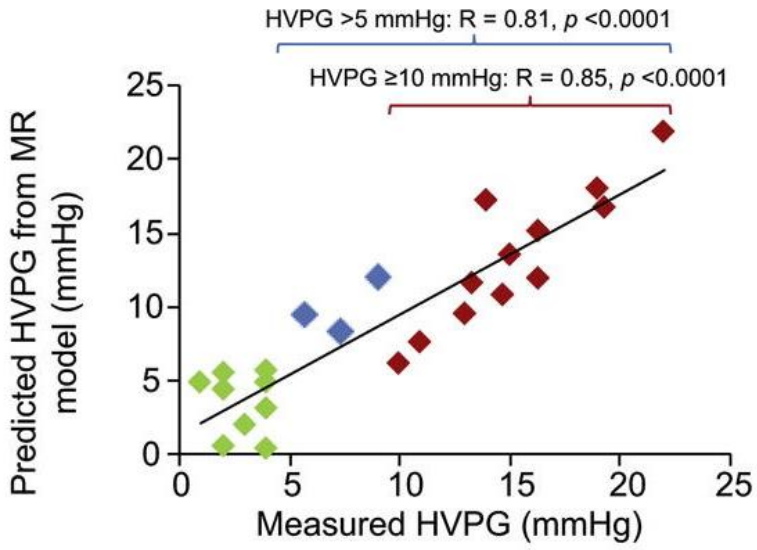

Figure 2.11: Correlation between HVPG and MR model (field strength of 1.5 Tesla) of liver T_1 relaxation time and splenic artery velocity [134]. Green diamonds depict patients with normal HVPG (ie ≤5 mmHg), blue diamonds have portal hypertension (ie ≥5 mmHg), red diamonds are patients with CSPH (ie HVPG ≥10 mmHg).

3. Non-invasive assessment of portal hypertension using quantitative magnetic resonance imaging at 3T

3.1. Abstract

Hepatic venous pressure gradient (HVPG) measurement is currently the only validated technique to assess portal pressure and evaluate changes after interventions. Non-contrast quantitative magnetic resonance imaging (MRI) measures of hepatic architecture and splanchnic haemodynamics correlate significantly with HVPG at 1.5 Tesla. These findings are replicated at 3 Tesla in a separate validation cohort. HVPG significantly correlated with: iron corrected liver longitudinal relaxation time (T_1: R=0.60, p<0.001), Spleen T_1 (R=0.599, p<0.001), SMA velocity (R=0.45, p=0.008) and Splenic artery flow (R=0.456, p=0.017). There was a significant correlation of cardiac index and Splenic artery flow as well as an apparent correlation of differing azygous vein flow in the presence or absence of varices. Combining this data with the derivation data showed a field strength dependent ceiling effect of structural measures and a reduction in SMA and splenic artery velocity >15 mmHg. This may signify a transition in the development of a hyperdynamic circulation. More data is required to build a complex model to accurately predict HVPG >15 mmHg with these MR measures and measure the efficacy of interventions.

3.2. Introduction

Most morbidity and mortality in patients with cirrhosis results from the development and progression of portal hypertension. Portal hypertension is characterised by both increased intrahepatic resistance and progressive splanchnic vasodilation [15]. Distortion of the hepatic architecture resulting from fibrogenesis and nodule formation leads to increased "static" hepatic vascular resistance, whilst a "dynamic" component results from the active contraction of myofibroblasts and increased intrahepatic vascular tone [161]. The rise of portal pressure is perpetuated by the excessive release of endogenous vasodilators, shown to result in splanchnic vasodilation and increased portal blood flow [15]. The modified "peripheral arterial vasodilation hypothesis" combines arterial underfilling with an increase in hepatosplanchnic capillary pressure and filtration with increased lymph formation [14]. The hyperdynamic circulation results in a hyperdynamic multi-organ syndrome [15].

Transjugular hepatic venous pressure gradient (HVPG) is the current reference standard for the assessment of portal pressure and changes following therapeutic interventions [162]. Hepatic venous pressure gradient is the only validated technique to accurately evaluate changes in portal pressure [143] (see 2.5.3 Reproducibility of HVPG). A baseline HVPG of ≥10 mmHg defines clinically significant portal hypertension (CSPH) and predicts the risk of formation of varices [60]. A HVPG of >12 mmHg is associated with variceal bleeding [53]. A HVPG of >16 mmHg has been shown to correlate with increased mortality [55] and decompensation [64], whilst an HVPG of ≥20 mmHg is an independent prognostic marker indicating lower likelihood of response to management of acute variceal bleeding [56]. In patients with varices, interventions that reduce HVPG by 20% from baseline or to <12 mmHg ("haemodynamic responders") have been shown to reduce the risk of variceal bleeding and improve survival [163]. However, HVPG measurements are expensive, invasive and only available in specialist centres which precludes the use of HVPG in routine clinical practice. The development of non-invasive markers of portal pressure is highly desirable to risk stratify, guide treatment [68] and improve outcomes [117].

Liver stiffness measurement (LSM) as assessed with transient elastography (TE) has been suggested as a non-invasive alternative measurement to HVPG. LSM is thought to reflect hepatic fibrosis and the resulting intrahepatic resistance. In a meta-analysis of 18 studies, LSM has been shown to significantly correlate with HVPG [164], but perform poorly in those patients with a HVPG ≥ 12 mmHg [165]. LSM is recommended to risk stratify for clinically significant portal hypertension when HVPG is not available [166]. However, LSM has high failure rates in patients with elevated BMI and ascites, limiting its clinical utility in the setting of patients with suspected portal hypertension [167]. Spleen stiffness measured with TE has been shown to not significantly correlate with HVPG [74, 168], with significant technical challenges related to spleen size and a ceiling effect for tissue stiffness that limit the applicability of this technique. Current non-invasive alternative measures of portal pressure have remained inaccurate and therefore not translated to clinical use [166]. Magnetic Resonance Elastography (MRE) provides a method of non-invasively measuring viscoelastic properties of the liver and spleen, and has been shown to correlate with HVPG (r=0.44, p=0.017, and r=0.57, p=0.002, respectively) [169].

Quantitative MRI is a promising potential non-invasive measure of portal hypertension [134, 135, 170]. Univariate structural and extrahepatic haemodynamic MRI measures have been shown to significantly correlate with HVPG in a cross-sectional study [134]. At a magnetic field strength of 1.5 Tesla, univariate measures associated with portal pressure were hepatic longitudinal (T_1) relaxation time (r=0.797, p<0.001), splenic artery (r=0.584, p=0.003) and superior mesenteric artery velocity (r=0.534, p=0.002). In a multivariate model, liver T_1 and splenic artery velocity significantly associated with HVPG (R^2=0.714, p<0.001). Uniquely, this correlation was maintained in patients with HVPG >10 mmHg (R^2=0.595, p=0.007). Critically, LSM and the Enhanced Liver Fibrosis (ELF) score correlated significantly with HVPG when including the whole population, but not in a sub-analysis of only those patients with HVPG >10 mmHg.

Importantly, since MRI does not involve ionising radiation, repeated assessments are feasible and acceptable. In addition, MRI offers the unique opportunity for contemporaneous assessment of

structural and haemodynamic changes in multiple organs in a single session without the requirement for contrast agent [45]. This can allow the global assessment of the hyperdynamic state to help better define the proposed therapeutic window for the use of beta-blockers in this population [114](1.8.5 Harms and the window hypothesis). Overall, studies using MRI techniques in the assessment of liver fibrosis and portal hypertension performed to date do not meet the rigorous standards set by the STARD (Standards for Reporting of Diagnostic Accuracy Studies) initiative, in particular due to lack of methods tested with 'derivation' and 'validation' cohorts [171]. Here I set out to evaluate which quantitative MRI measures correlate to HVPG at a 3 Tesla (3T) MRI field strength, in a second validation cohort to those collected by the Nottingham group at 1.5 T [134]. NHS hospitals have access to a mixture of 1.5 T and 3 T MRI machines. 3 T field strength offers higher spatial resolution and signal-to-noise ratios increasing the sensitivity of measures across a dynamic range but the effects of field strength on liver measures (T_1, T_2, T_2*) are unknown. In addition, the 3T scanner used has a wider bore enabling subjects with a higher BMI to be scanned.

3.3. Materials and methods

3.3.1. Ethics

This is a prospective cross-sectional study. Ethical approval was granted by the UK National Research Ethics Service; Staffordshire Research Ethics Committee (REC:12/WM/0288) and East Midlands - Nottingham 1 Research Ethics Committee (REC: 16/EM/0323). The study was performed according to the Good Clinical Practice (GCP) principles and sponsored by the University of Nottingham. All patients gave written informed consent in accordance with the principles of the Declaration of Helsinki (revision of Edinburgh 2000).

3.3.2. Study population

Consecutive patients undergoing HVPG measurement for clinical indications both at Nottingham University Hospitals NHS Trust and University Hospitals of Derby and Burton NHS Foundation Trust between July 2016 and August 2018 were prospectively screened and recruited. All patients who

underwent HVPG measurement as part of a transjugular liver biopsy in routine clinical care were screened for eligibility by their usual clinical team. Potential participant details were passed to the research team who provided a patient information sheet and contacted the patient at least 24 hours later. Patients were excluded if they had hepatocellular carcinoma, portal or hepatic vein thrombosis, absolute contraindications for MRI, age <18 years or pregnancy. 43 patients consented to the study. 4 patients were excluded from the final analysis; one patient's images were degraded by retained bullet fragments, one patient had acute alcohol withdrawal, one patient had liver histology showing submassive necrosis due to fulminant autoimmune hepatitis with no fibrosis, and in one there was a technical fault with the MR scanner. MRI and LSM with TE were performed on the same day within 12 weeks of the HVPG measurement. Patients received no therapeutic interventions between the HVPG measurement and MRI scan.

3.3.3. HVPG measurement

HVPG measurements were taken by competent clinical interventional radiologists in the respective hospitals in accordance with established standards after an overnight fast [143]. Under ultrasongrapghic guidance, the right internal jugular vein was cannulated and a 9-French vascular sheath placed by modified Seldinger technique. A 6-French compliant balloon-tipped catheter (Berenstein occlusion catheter, Boston Scientific, UK) was guided into the right hepatic vein for measurement of wedged and free hepatic pressures as recommended [51]. All measures were obtained in triplicate and recorded via a pre-calibrated Philips IntelliVueMP50 patient monitor (Philips Healthcare, UK). HVPG was calculated as the mean difference between wedged and free hepatic pressure, and the mean of triplicate measurements computed.

3.3.4. Liver stiffness measurement (LSM)

LSM was performed prior to the MRI scan, following an overnight fast, using FibroScan® (Echosens, Paris, France) by experienced operators [172]. Due to technical reasons, a LSM was not available on five patients.

3.3.5. MR data acquisition

All patients were scanned following an overnight fast on a 3 T Philips Ingenia DDAS scanner (Philips Medical Systems, Best, The Netherlands) using the anterior body coil and posterior bed coil. All MR measures were acquired in a one hour scan session.

3.3.5.1. Longitudinal relaxation time (T_1) of the liver and spleen

To estimate the tissue longitudinal relaxation time (T_1) in the liver and the spleen, a modified respiratory-triggered inversion-recovery sequence with spin-echo echo planar imaging (SE-EPI) readout (9 contiguous axial slices, 3 x 3 x 8 mm^3 voxel size, 4 mm slice gap (33%), 96 × 96 image matrix, SENSE factor 2, echo time 27 ms) and fat suppression [136] was acquired at 10 inversion times (100 - 1500 ms) with minimal temporal slice spacing (58 ms) for both ascending/descending slice order to increase the inversion times dynamic range at 3 T. This data was collected in approximately 3 minutes, dependent on the patients' respiratory rate.

3.3.5.2. Transverse relaxation time (T_2) of the liver*

Transverse relaxation time (T_2*) mapping of the liver was performed using a multi-echo fast field echo (mFFE) sequence comprising 12 echoes (ET_1=2.5 ms, ΔET =2.5 ms) acquired in a ~ 17 s breath hold. Each T_2* data set was geometrically matched to the T_1 SE-EPI dataset.

3.3.5.3. Splanchnic flow measurements

Phase contrast (PC)-MRI was used to quantify the velocity and cross-sectional area of the flow in the splanchnic circulation in the splenic artery (SA) and superior mesenteric artery (SMA), and collateral flow in the azygous vein (Figure 3.9). Blood flow in each vessel was measured using a vectorcardiogram (VCG) gated 2D PC-MRI on a single slice perpendicular to each target vessel of interest (echo/repetition time = 4.2/7.5 ms, FA = 25°, field of view = 280 x 146 mm^2, 1.5 x 1.5 x 6 mm^3 reconstructed, SENSE 3, 2 averages). 15 phases of a turbo field echo sequence were collected across the cardiac cycle for vein measurements and 20 phases for artery measures, with defined velocity encoding (V_{enc})

applied for each of the vessels (portal/hepatic/azygous veins V_{enc} = 50 cm/s, hepatic/splenic arteries V_{enc} = 100 cm/s, and superior mesenteric artery V_{enc} = 140 cm/s). If aliasing occurred, the V_{enc} was increased and the measure repeated. The portal vein was measured before its split into right and left portal veins; the hepatic artery was measured after splitting from the celiac artery; and the azygos vein was measured between the azygos arch and the accessory hemiazygos vein. Each measurement was acquired during a 15-20 s breath hold, dependent on the subjects' heart rate.

3.3.5.4. Aortic Flow measurement

Aorta flow was collected using PC-MRI with a FOV 280 x 264 mm^2, spatial resolution 0.97 x 0.97 mm^2, slice thickness 10 mm, no SENSE, TE/TR = 2.3/3.7ms, FA = 15°, TFE factor = 5, TFE shots 25, VENC = 300 cm/s, NSA = 3. Scan time was approximately 1 minute, dependent on the subjects' heart rate. [173].

3.3.6. MR data analysis

The physicists (Chris Bradley, Eleanor Cox, Susan Francis) analysing the MR data were blind to the HVPG measurements.

3.3.6.1. Longitudinal relaxation time (T_1) of the liver and spleen

T_1 data was motion corrected across each inversion time. The inversion recovery data were then fit on a voxel-wise basis to an inversion recovery $S(t) = M_0 * abs(1 - 2\exp(-t/T_1))$ to generate T_1 and M_0 maps for the SE-EPI data. Binary masks of both the liver and spleen were formed from manual segmentation of the M_0 image. Histogram analysis was then used to assess the distribution of the T_1 relaxation time values across the all voxels within both the liver and spleen. For the liver and spleen data in each subject, the histogram of voxel values was fit to a Gaussian function and the Gaussian peak (mode of the distribution) was used to represent the T_1 tissue relaxation time. This method provides an automated method to assess the tissue and eliminate those voxels containing blood in vessels [136]. In addition, the full width half maximum (FWHM) of each Gaussian function was calculated to reflect the degree of heterogeneity of T_1 relaxation time values.

3.3.6.2. Transverse relaxation time (T_2) of the liver*

Elevated iron concentrations can be determined from the T_2* relaxation time or R_2* rate ($1/T_2$*) [153]. T_2* is fit on a voxel-wise basis to $S(t) = M_0 * \exp(-t/T_2*)$ to generate T_2* and M_0 maps. As above, the histogram of voxel values was fit to a Gaussian function and the Gaussian peak (mode of the distribution) was used to represent the T_2* tissue relaxation time.

3.3.6.3. Iron-corrected Liver longitudinal relaxation time (T_1)

Iron accumulation in liver tissue reduces the transverse (T_2 and T_2*) relaxation time [152, 153], further an increase in iron can also reduce liver T_1 [136, 151]. Thus it is necessary to remove the bias in liver T_1 values introduced by elevated iron [136, 153]. To do this, the liver T_1 was modelled using a Bloch simulation for iron concentrations, and a correction algorithm applied to result in an iron-corrected liver T_1 as outlined in [174]. To do this, the hepatic iron concentration (HIC) must be estimated from the T_2*/R_2* map [175] and this value is used to compute a corrected liver T_1 [176].

First, the R_2* relaxivity of liver at 3T is converted to that obtained at 1.5T using the following equation [177]:

$$R_2*(3T) = 2xR_2*(1.5T)-35.$$

At 1.5T, the R_2* of liver tissue has been computed as a function of HIC (measured in mg Fe/g dry weight) by St Pierre et al. [175] and Wood et al. [153] as:

$$R_2*(1.5T) = (HIC-0.202)/0.0254$$

Thus it is possible to compute the HIC of liver tissue.

The dependence of longitudinal relaxivity ($R_1 = 1/T_1$) of liver tissue on HIC at 1.5T is given by [178]:

$$R_1 = R_{1,0} + 0.029x4.1xHIC,$$

where $R_{1,0}$ is a function of the extracellular fluid (ECF) fraction. From this, a predicted measured T_1 value for each combination of iron and ECF concentration can be computed. To correct the T_1, the ECF

is computed for each measured liver T_1 value, and then the corrected liver T_1 computed from a look-up table assuming the patient had a normal HIC of 1.2 mg/g.

3.3.6.4. Splanchnic flow measurements

PC-MRI data were analysed using Q flow software (Philips Medical System). For each vessel, a region of interest was drawn manually around the lumen of the vessel on each phase contrast image, with contour detection used. The mean signal intensity within each region of interest reflected the flow velocity in the vessel of interest (cm/s) for each cardiac phase, and the mean velocity across the cardiac cycle was computed. The cross-sectional area of each vessel lumen was multiplied by the mean velocity, to compute the mean blood flow (in ml/s) in each vessel.

3.3.6.5. Cardiac Index

PC-MRI of aortic flow was collected to provide an estimate of Cardiac Index. PC-MRI data were analyzed using ViewForum software (Philips Medical Systems, Best, The Netherlands) to provide an estimate of aortic blood velocity (ml/s), cross-sectional area (CSA) of the aorta (ml^2), from which cardiac flux could be obtained [173] which was corrected for body surface area to yield Cardiac Index.

3.4. Statistical analysis

Statistical analysis was performed using SPSS software version 25 (IBM©). Quantitative variables are expressed as mean±standard deviation (SD), and qualitative variables as absolute and relative frequencies. Normality was tested using Shapiro-Wilk analysis.

HVPG was used as a continuous parameter and associations between continuous variables were tested using the Pearson's correlation coefficient for parametric variables and Spearman's rank correlation coefficient for non-parametric variables. In all analyses, p values of < 0.05 were considered statistically significant. Due to the exploratory nature of this study, no adjustments were made for

multiple comparisons and no formal power calculation was carried out. Instead I aimed to replicate the correlations found at 1.5 Tesla of 30 patients, validated in a further 10 patients [134].

3.5. Results

3.5.1. Patient characteristics

43 patients consented and were enrolled to the study. Two patients were unable to complete the MRI scan and excluded from the final analysis; one due to retained bullet fragments around the liver causing significant image artefact and one due to acute alcohol withdrawal. In one patient the scanner developed a technical fault so no reliable MRI data was collected. One patient (2%) had no histological evidence of any fibrosis with acute massive necrosis due to autoimmune hepatitis (HVPG = 12 mmHg) so was excluded from the final analysis. Figure 3.1 provides a CONSORT diagram of study participants.

The clinical and biochemical parameters of the included participants are presented in Table 1.1. All patients underwent a subsequent transjugular liver biopsy after HVPG measurement as part of their routine clinical care. Seven patients (18%) had histological evidence of bridging fibrosis and 27 (69%) had cirrhosis.

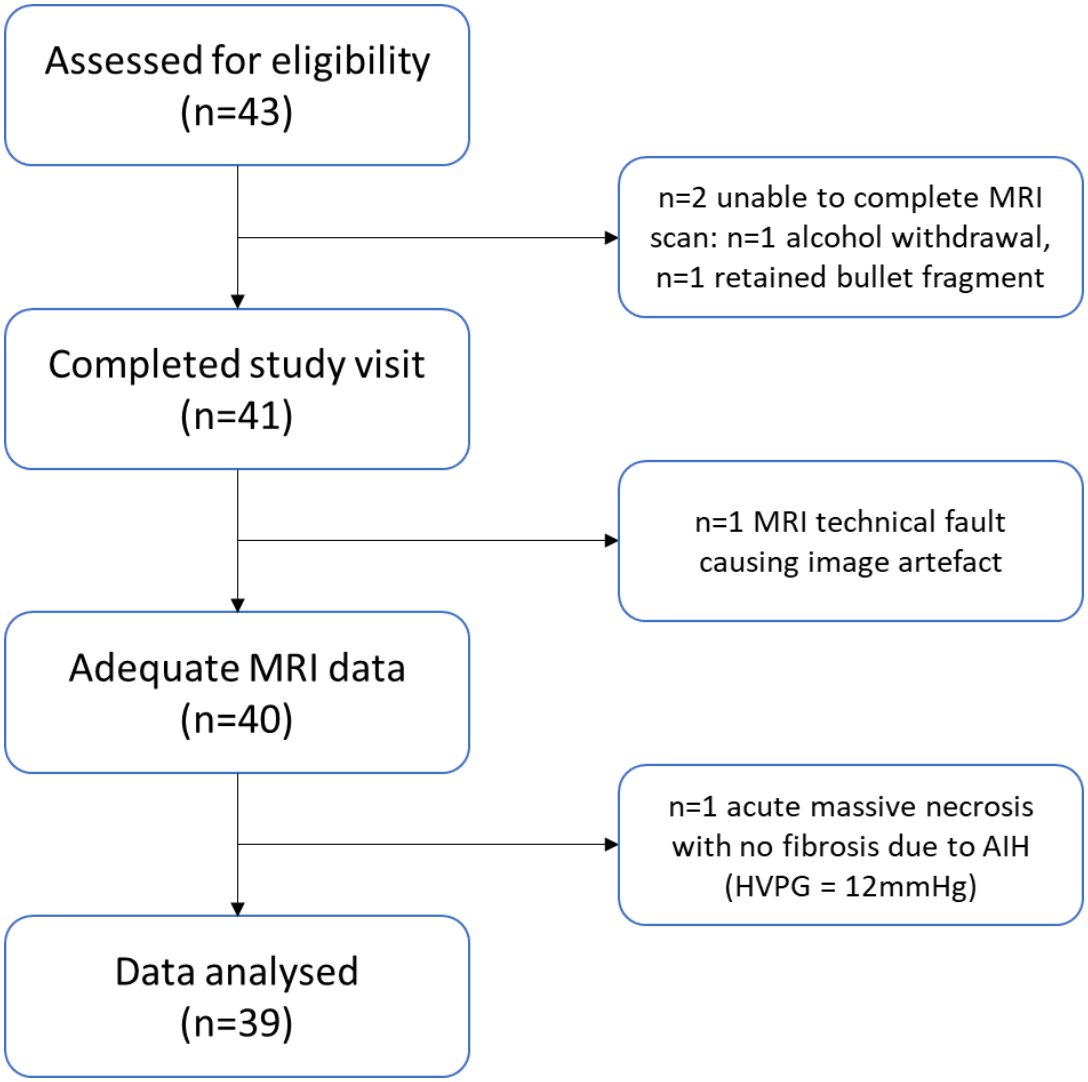

Figure 3.1: CONSORT diagram of study participants

Variable	All patients (n=39)
Age, years	60 ± 11
Gender M/F	23/16
BMI	31.9 ± 7.6
Aetiology (%)	
Alcohol	13 (33%)
NAFLD	20 (51%)
Autoimmune liver disease	2 (5%)
Histological Fibrosis staging (%)	
No Fibrosis	0
Pericellular fibrosis	5 (13%)
Bridging Fibrosis	7 (18%)
Cirrhosis	27 (69%)
Aspartate transaminase (AST), U/L	77.3 ± 99.0
Alanine transaminase (ALT), U/L	66.2 ± 90.4
Bilirubin, µmol/L	26.7 ± 42.2
Alkaline phosphatase (ALP), U/L	123.1 ± 60.9
Albumin, g/L	40.2 ± 6.7
Prothrombin time, seconds	12.1 ± 0.9
Platelet count, x10^9/L	203.8 ± 92.6
Serum sodium, mmol/L	137.5 ± 3.2
Serum creatinine, µmol/L	71.3 ± 21.9
Time between HVPG and MRI, days	44 ± 19
Liver stiffness, kPa	16.4 ± 10.9
HVPG, mmHg	9 ± 5

HVPG >5 mmHg, n (%)	28 (72%)
CSPH, HVPG ≥10 mmHg, n (%)	15 (38%)

Table 3.1: Clinical and laboratory features of the study population (Mean ± SD)

3.5.2. Liver Stiffness Measurement

Valid liver stiffness measurements assessed by FibroScan® were available in 35 (90%) of patients. Liver stiffness measurement as measured by transient elastography did not significantly correlate with HVPG (Spearman R = 0.29, p = 0.10) (Figure 3.2). This remained true for those without portal hypertension HVPG <6 mmHg (Spearman R = -0.197, p = 0.585) and without CSPH HVPG ≤ 10 mmHg (Spearman R = 0.006, p = 0.978).

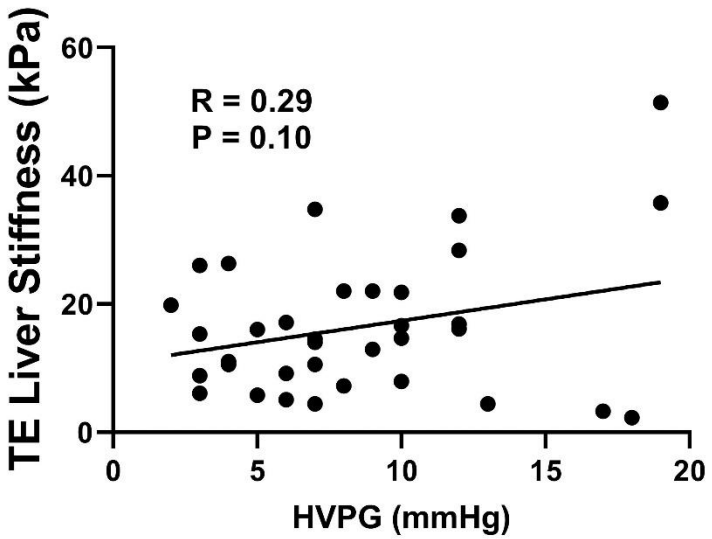

Figure 3.2: Correlation of hepatic venous pressure gradient (HVPG, mmHg) with liver stiffness measurement as assessed by transient elastography (kPa).

3.5.3. Longitudinal relaxation time (T_1) as a predictor of HVPG

3.5.3.1. Liver Longitudinal relaxation time (T_1)

Considering the whole patient group, there was a statistically significant positive correlation between HVPG and SE-EPI liver T_1 relaxation time (Pearson R = 0.63, p<0.0001) (Figure 3.3). This relationship was maintained in patients with portal hypertension with HVPG >5 mmHg (Pearson R = 0.54,

p=0.0046) and in those with an HVPG ≤ 15 mmHg (Pearson R = 0.472, p=0.006), but did not reach significance in those with CSPH with HVPG ≥10 mmHg (Pearson R = 0.428, p=0.112). The mean (± SD) number of voxels in the mask for the liver T_1 measurements was 13458 (±19818). The FWHM of the liver SE-EPI Gaussian distribution showed a significant positive correlation with HVPG (R = 0.330, p = 0.043), reflecting the increased heterogeneity in liver T_1 with increased severity of portal hypertension. Example fat-suppressed inversion recovery (IR) SE-EPI data and T_1 maps are shown in Figure 3.4.

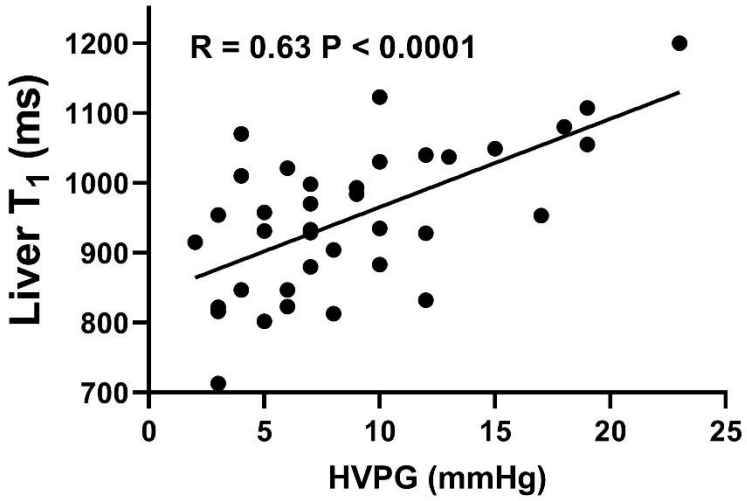

Figure 3.3: Correlation of liver SE-EPI T_1 relaxation time (ms) and HVPG (mmHg).

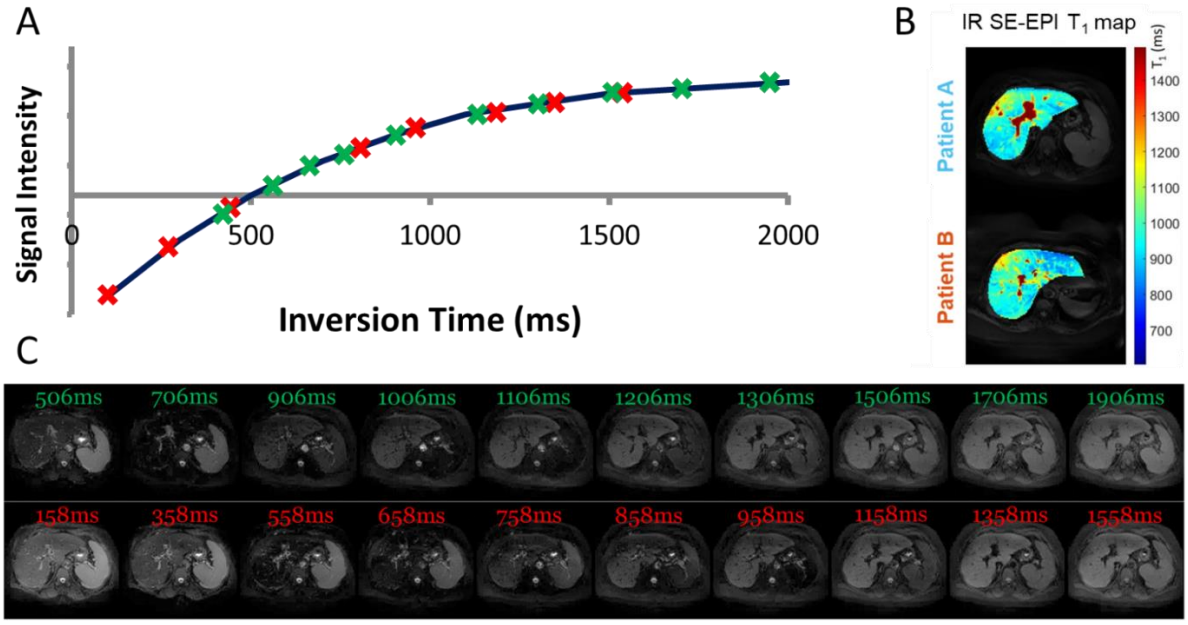

Figure 3.4: Example of fat-suppressed inversion recovery (IR) SE-EPI T_1 mapping. A) shows the IR curve with 20 data points derived from C. C) shows 10 IR SE-EPI T_1 mapping data in ASCEND slice ordering in green and DESCEND slice ordering in red. B show example resultant T_1 relaxation maps for two patients both of whom had a HVPG of 8 mmHg.

*3.5.3.2. Liver T_2**

In the whole patient group, liver T_2* correlated significantly with HVPG (R = 0.401, p = 0.014)(*Figure* 3.5). This relationship was maintained in patients with portal hypertension with HVPG >5 mmHg (R = 0.402, p = 0.038) but not in those with CSPH with HVPG ≥10 mmHg (R = 0.350, p = 0.219). Note, there are a significant number of subjects with high iron content across the participants, highlighting the need to T_2* correct the liver T_1 measures.

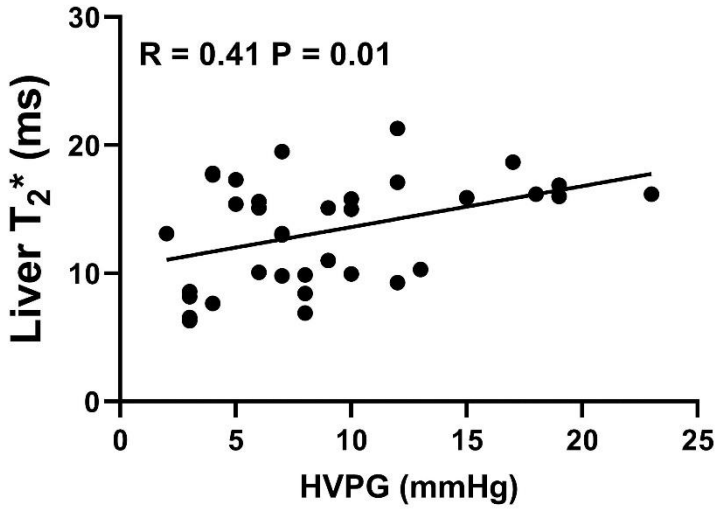

Figure 3.5: Correlation of Liver T_2 (ms) with HVPG (mmHg).*

3.5.3.3. Iron-corrected Liver T_1

In the whole patient group, iron-corrected Liver T_1 correlated with HVPG (R = 0.60, p < 0.001)(Figure 3.6). This relationship was maintained in patients with portal hypertension with HVPG >5 mmHg (R = 0.64, p = 0.0006), in HVPG ≤ 15 mmHg (Pearson R = 0.42, p=0.02) and in those with CSPH with HVPG ≥10 mmHg (R = 0.68, p = 0.01).

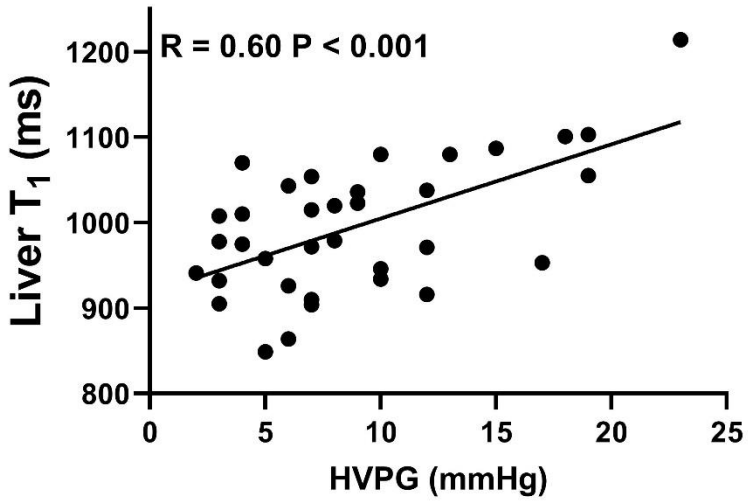

Figure 3.6: Correlation of iron-corrected SE-EPI liver T_1 (ms) and HVPG (mmHg).

3.5.3.4. Spleen longitudinal relaxation time (T_1)

Spleen T_1 did not correlate with HVPG in the whole patient group (Pearson R = 0.294, p = 0.073). However, splenic T_1 did significantly correlate with HVPG < 10 mmHg (R = 0.552, p = 0.006) and HVPG ≤ 15 mmHg (Pearson R = 0.60, p<0.001) but not in those with CSPH ≥ 10 mmHg (R = -0.273, p = 0.324) (*Figure* 3.7).

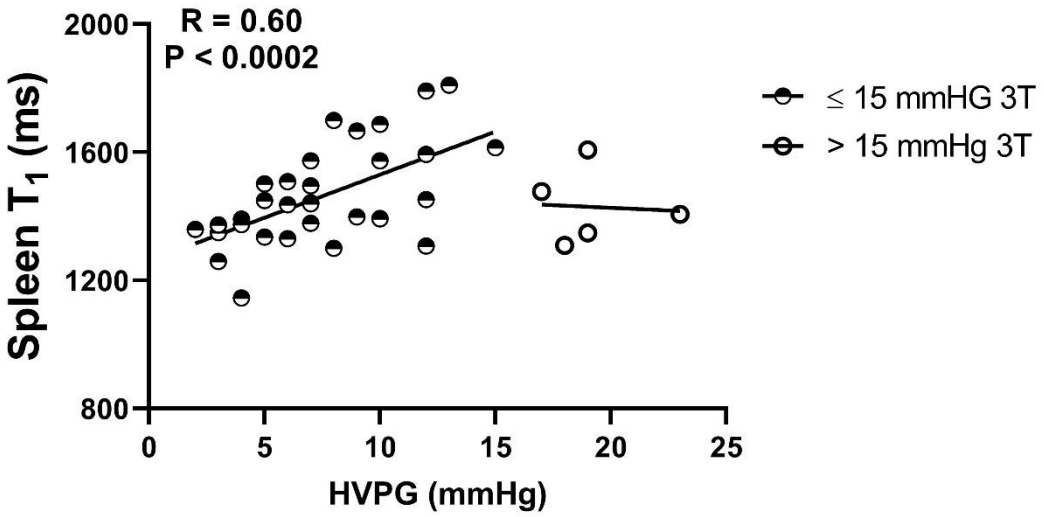

Figure 3.7: Correlation of SE-EPI Spleen T_1 (ms) with HVPG (mmHg).

3.5.4. Splanchnic flow measures and their correlation with HVPG

Table 1.2 shows the correlation of splanchnic flow measures over the whole group with HVPG. Three splanchnic measures can be seen to correlate with HVPG ≤ 15 mmHg; SMA mean velocity (Pearson R = 0.450, p =0.008), SMA mean flow (Pearson R = 0.465, p=0.006) and splenic artery flow (Pearson R = 0.456, p=0.017). Azygous vein flow however did not correlate with HVPG across the whole group (Pearson R = -0.148, p=0.390) or HVPG ≤ 15mmHg (Pearson R =-0.148, p=0.390).

Vessel		All patient group		HVPG ≤15 mmHg	
		Correlation coefficient, R	*p value*	*Correlation coefficient, R*	*p value*
Superior Mesenteric Artery n = 39	*Area*	0.092	0.578	0.181	0.306
	Velocity	0.288	0.075	0.450	0.008
	Flow	0.305	0.059	0.465	0.006
Splenic artery n = 31	*Area*	0.053	0.777	0.290	0.134
	Velocity	0.278	0.130	0.03	0.881
	Flow	0.259	0.167	0.456	0.017
Azygous vein n = 36	*Area*	-0.117	0.495	-0.117	0.495
	Velocity	-0.129	0.453	-0.129	0.453
	Flow	-0.148	0.390	-0.148	0.390

Table 3.2: Correlation coefficient and p value of splanchnic circulation flow parameters as measured by phase contrast MR with HVPG.

Although there was no statistically significant correlation between Azygous flow and HVPG, in the subgroup where patients can be separated into the presence or absence of oesophageal varices there is an apparent relationship between high azygous flow and the presence of oesophageal varices that does not reach significance (Pearson R = -0.687, p= 0.060). The one outlier is a patient in whom the reported HVPG was 3 mmHg (with wedged pressure of 16 mmHg and free pressures of 13 mmHg) but on gastroscopy was found to have three Grade II oesophageal varices.

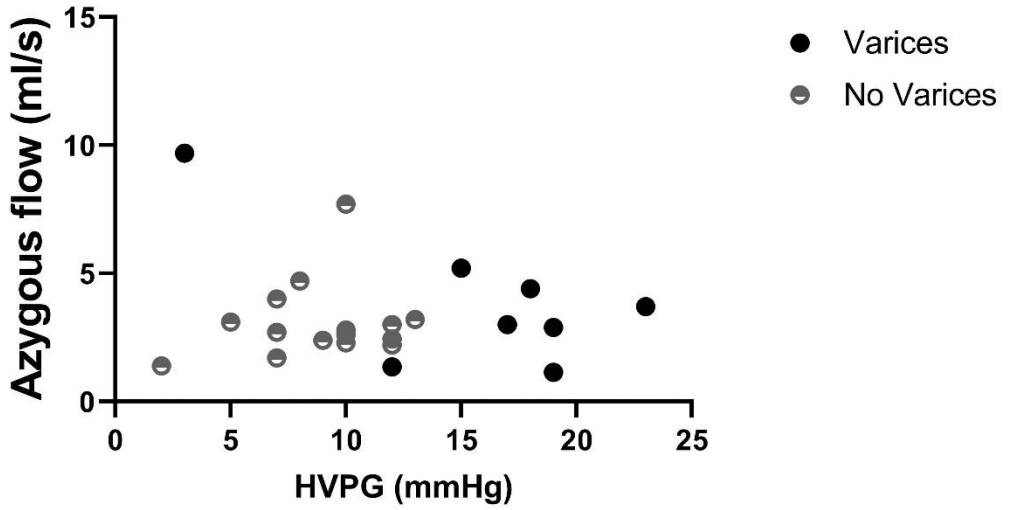

Figure 3.8: Azygous flow (ml/s) against HVPG (mmHg) with patients split into those with and without oesophageal varices at screening gastroscopy after HVPG measurement.

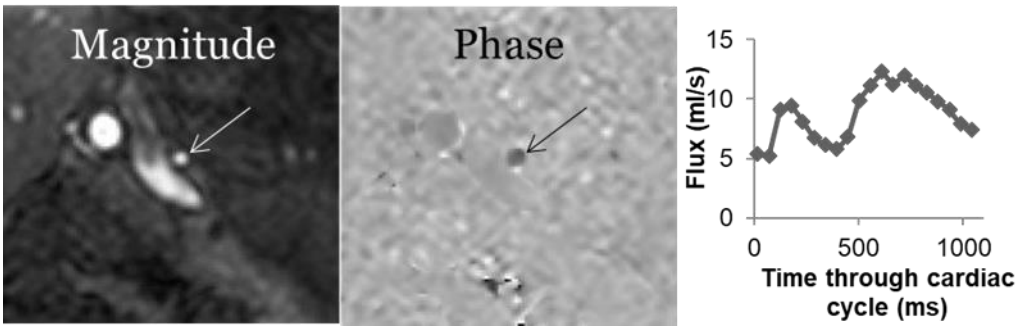

Figure 3.9: Example of phase contrast MRI, the method used to measure flux, surface area and velocity of blood in the Superior Mesenteric, Splenic and Aortic Artery and azygous vein through the cardiac cycle.

3.5.5. Comparing MRI measures at 1.5 and 3 T as markers of HVPG

Here these findings at 3 T are compared with those from the original derivation study conducted at Nottingham at 1.5 T [134]. Results from 1.5 T and 3 T are plotted together to better understand the data, particularly in the context that the participants scanned at 3T are more likely to have higher HVPG values and oesophageal varices compared to those participants scanned at 1.5 Tesla.

3.5.5.1. Liver longitudinal relaxation time (T_1)

Longitudinal realxation time is MR field strength dependent, with the relaxation time for most tissues being about 20%–40% longer at 3.0 T than at 1.5 T [154]. Figure 3.10 compares liver T_1 as a function of HVPG for 1.5 T and 3 T. At both field strengths there is a significant correlation of SE-EPI liver T_1 with HVPG. The correlation at 1.5 Tesla is stronger (Pearson R=0.84, p<0.001) than that of an iron corrected T_1 measure at 3 Tesla (Pearson R = 0.60, p<0.001) principally due to an observed ceiling effect at approximately 1300ms at 3.0 T.

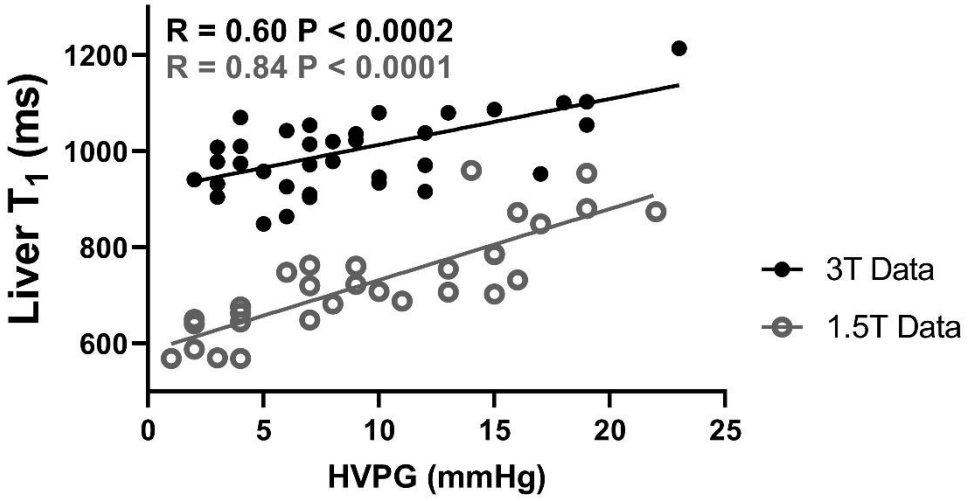

Figure 3.10: Iron corrected liver T_1 (ms) versus HVPG (mmHg) at field strengths of 1.5 and 3 T.

There is also a significant correlation of splenic T_1 with HVPG ≤15mmHg at both field strengths (*Figure* 3.11), with a Pearson R = 0.599, p<0.001 at 3 T and Pearson R = 0.65, p<0.001 at 1.5 T. Plotting the data together, it can be seen that at a HVPG >15 mmHg there is an observed field dependent plateau. At a field strength of 3 Tesla, this ceiling effect occurs at approximately 1800ms, and at approximately 1300 ms at 1.5 T, approaching the T_1 of blood [179].

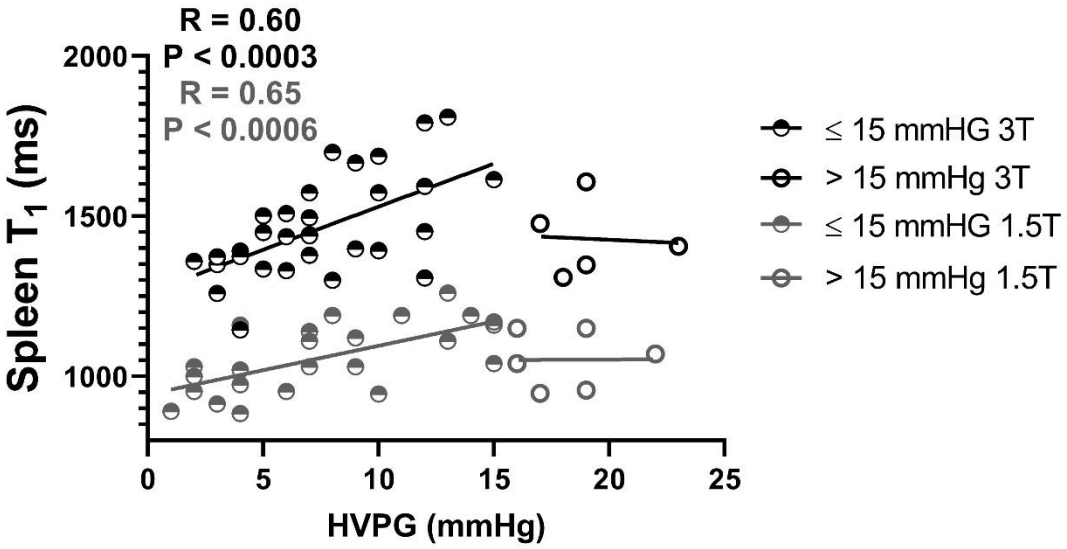

Figure 3.11: Splenic T_1 (ms) versus HVPG (mmHg) for data collected at 1.5 and 3 T.

3.5.5.2. Splanchnic flow

Figure 3.12 shows that there is no theoretical or observed difference in the measured SMA velocity between 1.5 and 3 T data. When the data is pooled, it becomes apparent that there is a significant positive correlation of SMA velocity with HVPG ≤15 mmHg (R=0.55, p<0.001) after which the SMA velocity appears to reduce at HVPG >15 mmHg (*Figure* 3.12). Combining the data across field strengths demonstrates this effect clearly which was difficult to determine when viewing data at each field strength separately.

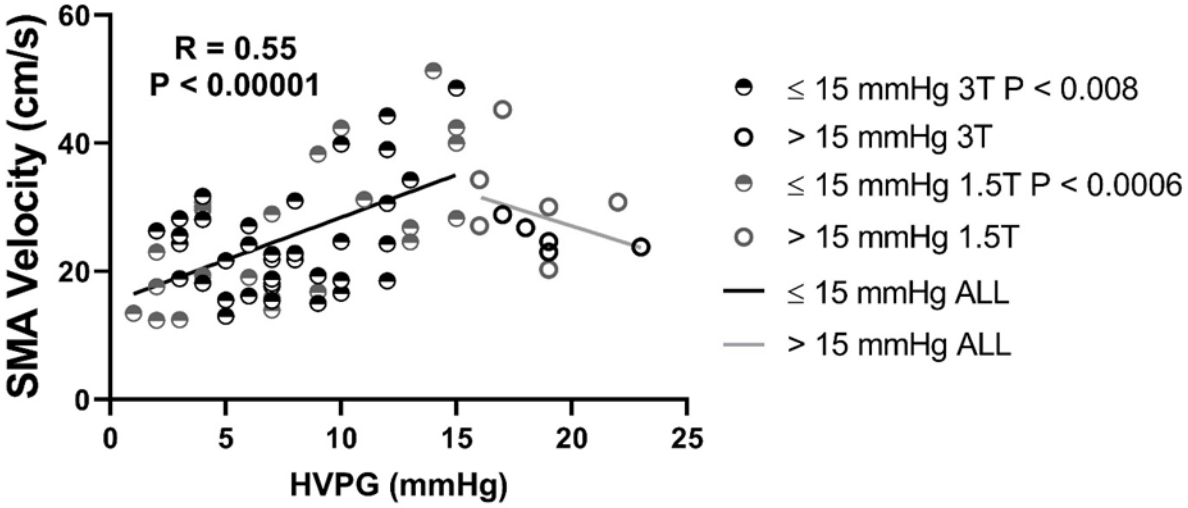

Figure 3.12: SMA velocity (cm/s) versus HVPG (mmHg) shown for data collected at 1.5 and 3 T.

There is similar significant correlation of pooled splenic artery velocity against HVPG ≤ 15 mmHg (Pearson R = 0.46, p<0.001) which becomes less apparent at HVPG >15 mmHg (*Figure* 3.13).

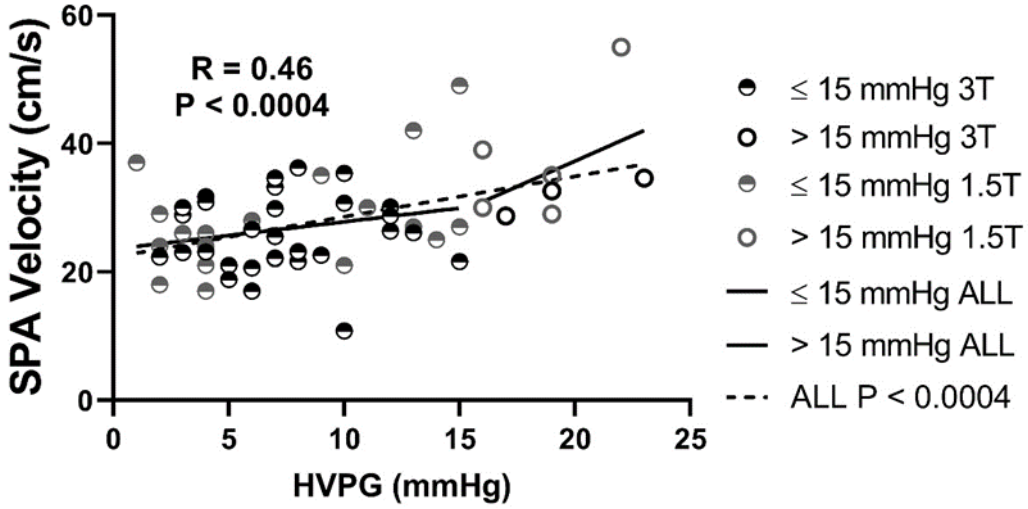

Figure 3.13: Comparison of splenic artery velocity (cm/s) at field strength 1.5 and 3 Tesla against HVPG (mmHg).

Assessing the link between longitudinal relaxation time and haemodynamic measures, there is a significant correlation of splenic T_1 with SMA velocity (Pearson R = 0.47, p<0.002) at a field strength

of 3 Tesla (*Figure* 3.14), but this was not significant at 1.5 Tesla – likely due to the reduced gradient of splenic T_1 versus HVPG at 1.5 T.

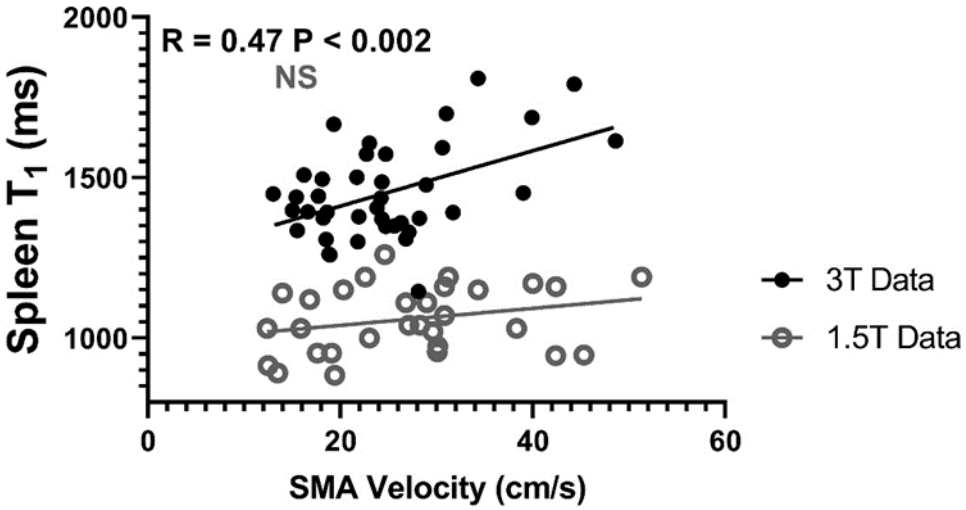

Figure 3.14: Relationship between Splenic T_1 (ms) and SMA velocity (cm/s) at field strength 1.5 and 3 Tesla.

3.5.6. Cardiac Index

Cardiac index (L/min/m^2) did not significantly correlate with HVPG across the whole patient group (Pearson R = 0.39, p=0.053)(*Figure 3.15*), nor in HVPG <10 mmHg (Pearson R = 0.045, p=0.859) or in HVPG ≤15 mmHg (Pearson R = -0.19, p=0.932).

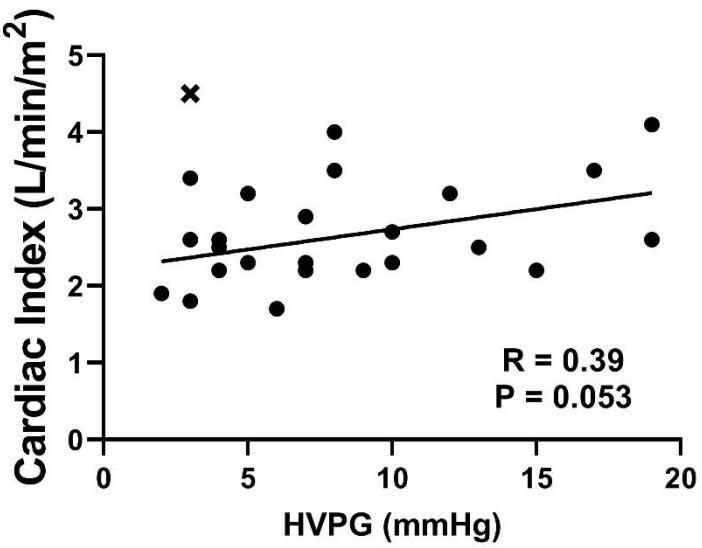

Figure 3.15: Relation of cardiac index (L/min/m^2) at 3 Tesla against HVPG (mmHg). Note the outlier at HVPG of 3 mmHg is the participant with varices.

However, there was a significant correlation (Pearson R = 0.45, p<0.03) between cardiac index (L/min/m^2) and splenic artery velocity (cm/s), although not SMA velocity or splenic T_1 (*Figure 3.16*).

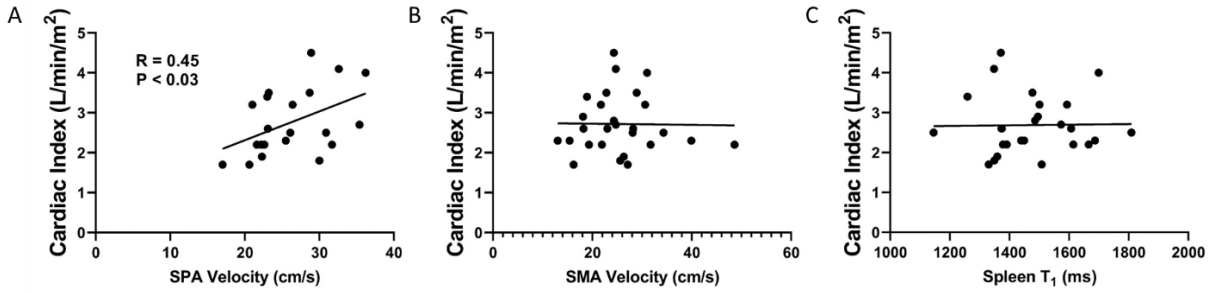

Figure 3.16: Relationship between Cardiac Index (L/min/m^2) and A) Splenic artery velocity (cm/s), B) SMA velocity (cm/s) and C) Spleen T_1 (ms).

3.6. Discussion

3.6.1. Principal findings

In liver cirrhosis, the disruption of sinusoidal architecture with progressive fibrogenesis and intrahepatic vasoconstriction causes increased intrahepatic resistance resulting in elevated portal pressure. This is further accentuated by splanchnic vasodilation and increased portal blood flow which leads to the development of a multi-organ hyperdynamic state. In this study, I have demonstrated that non-invasive quantitative MR measures of iron corrected liver SE-EPI T_1 relaxation time, splenic SE-EPI T_1 and SMA velocity all significantly correlate with portal pressure. When this data is combined with previously published data at a lower field strength of 1.5 Tesla [134], further findings emerge. The correlation with SMA and splenic artery velocity is true up until HVPG ≤15 mmHg at which point it appears to decrease. Splenic artery velocity is significantly correlated with cardiac index and azygous flow appears to change in the presence of oesophageal varices.

3.6.2. Strengths and weaknesses of the study

The Nottingham group have previously shown that liver T_1 relaxation time is associated with the degree of fibrosis and inflammation in the liver [136, 180]. This acquisition and analysis approach is highly repeatable in healthy subjects with a coefficient of variation (CoV) between visits of 1.8% and a low inter and intra-observer variability with intra-class correlation coefficients of more than 0.99. SE-EPI T_1 data is acquired with fat suppression, removing the effect of fat on the calculated liver T_1 value which is apparent in some other liver T_1 measures [158], as such SE-EPI T_1 acquisition provides a measure of the water liver tissue compartment. The SE-EPI T_1 measurement method described here is both respiratory triggered and multi-slice, enabling a large volume of the liver and spleen to be sampled in a reasonable imaging time without the need for breath holds, making this imaging scheme ideal for patient studies.

Liver T_2* significantly correlated with HVPG indicating that at a higher field strength and in this cohort more patients had a short T_2*. This increased the spread of liver T_1 measures and reduced the

correlation with HVPG. On calculating the iron-corrected liver T_1 this reduced the spread of measures across HVPG and yielded a higher correlation. The weaker correlation at 3 T is likely caused by both the increased sensitivity to T_2* correction and a lower relative ceiling measure of liver T_1.

PC-MRI is a non-invasive flow measurement technique without intravenous contrast, whereby the phase shift of flowing blood is proportional to the velocity. PC-MR is a more reliable measure of hepatic blood flow when compared to Doppler ultrasound with lower variability and higher reproducibility [181]. Within session CoV of SMA and SA velocity measurement is less than 10% [134, 182]. Both quantitative MR measures are unaffected by body habitus and presence of ascites in this study, and should yield comparable measures across field strength allowing measures to be pooled.

The scan time required to collect data for the assessment of an individual's hyperndynamic state (Liver T_1, Liver T_2*, Splenic T_1, SMA, Aorta and Azygous vein data) is 10-15 minutes dependent on the breathing rate of the patient, with Liver T_2* and PC-MRI data being planned whilst the respiratory triggered T_1 sequence is acquired. No additional hardware is required to obtain these MR measures, with clinical radiology staff easily able to locate the liver, spleen, SMA, aorta and azygous vein. The well characterised patient population studied are clinically relevant with all patients having HVPG measurements for clinical suspicion of portal hypertension due to a mixture of aetiologies, predominantly alcohol and non-alcoholic fatty liver disease. The results of this study are similar to those of a previous study by our centre in a separate cohort of patients scanned at a field strength of 1.5 Tesla [134], providing a validation cohort in which similar findings are reproduced.

The main limitation of the study is the relatively small number of patients included within a single expert imaging centre and exclusion of non-cirrhotic portal hypertension. Combining patient level data at 1.5 and 3 T field strengths increased the sample size to 79 subjects. A multi-site, multi-vendor study would provide external validation of the findings in patients with chronic liver disease and portal hypertension.

3.6.3. Relation to literature

3.6.3.1. Liver T1

3 T MRI offers higher signal-to-noise ratio compared to 1.5 Tesla [183], with a theoretical doubling of the overall signal-to-noise ratio (SNR) at 3.0 T. Further the T_1 relaxation time of tissues is longer at 3.0 T than at 1.5 T. In this study liver T_1, measured by SE-EPI, correlates independently with HVPG along its continuous range from normal to CSPH. The relationship between the degree of hepatic fibrosis and portal pressure has long been reported. Quantitative liver biopsy analysis with collagen proportionate area measurement correlates significantly with HVPG [184]. Our group previously showed that at 1.5 T liver T_1 relaxation time is associated with the degree of fibrosis and inflammation in the liver [136] and independently correlates with HVPG [134]. A separate research group have similarly shown that the shMOLLI liver T_1 is associated with the degree of hepatic fibrosis [137], although it did not correlate with HVPG [185]. Liver T_1 reflects the water liver tissue compartment and collagen formation. Liver T_1 measurements are influenced by confounding factors, dependent on the MRI technique employed and field strength of the scanner. These include inflammation [136], iron [151-153], fat [154] and oedema [155, 156]. Iron accumulation in liver tissue reduces T_2 and T_2* relaxation times [152, 153], and an increase in iron will also reduce T_1 in the liver [151]. Iron concentrations can be accurately evaluated with T_2*[148, 153]. Correction of liver T_1 relies on assumptions that R_2* can be corrected for field strength based on data from primate livers at lower field strengths extrapolated to higher field strengths [176]. The quantification of hepatic iron then depends upon a non-linear equation at 1.5 Tesla before correcting liver T_1 back to 3 T. In this study liver T_1 measures had to be corrected for significant iron overload, reflected in those patients with short liver T_2* measurement, in contrast to our work at lower field strength where no patients had significant iron [134].

The distribution of liver T_1 values (described by the FWHM of the Gaussian curve) was also shown to increase with worsening portal hypertension reflecting the increasing heterogeneity of T_1 values

within the liver. This may explain the sampling variability associated with liver biopsy [186-188], potentially TE, and highlights the need for whole liver assessment. Higher field strength accentuates differences in liver composition within the water liver tissue compartment but there also appears to be a ceiling effect of liver T_1 at approximately 1300ms at 3 Tesla as it approaches the T_1 of blood [179]. Hence, the overall liver T_1 did not correlate as closely to HVPG, particularly at higher values, at a field strength of 3 Tesla compared to 1.5 Tesla [134].

3.6.3.2. Spleen T_1

Spleen parameters are routinely used to assess for portal hypertension. Clinical splenomegaly is a common but insensitive and subjective sign of portal hypertension [189]. Thrombocytopaenia is an objective measure used in some clinical algorithms to exclude clinically significant portal hypertension [68, 69, 74]. It is hypothesised that portal hypertension leads to splenic congestion and consequent increased splenic stiffness. Spleen stiffness does correlate to HVPG with variable results, predominantly performing well in patients with chronic viral hepatitis and less well in mixed aetiologies [74, 168, 190, 191]. Significant technical issues remain that limit the clinical utility, which include adequate spleen size [130]. Two-dimensional MRE demonstrates a significant correlation of spleen stiffness and oesophageal varices [192] but has not yet been compared to HVPG. Here spleen T_1 correlated significantly with HVPG ≤15 mmHg, but not at higher HVPG as the T_1 then reached a plateau. This replicates the same finding in a previous study at 1.5 Tesla [134]. A recent study demonstrated a similar finding in an external smaller study with wedged catheter HVPG measurements [185]. All three data sets illustrate a ceiling effect, where no significant further increases are found once CSPH is developed. I hypothesise this is due to splenic T_1 signal approaching a limit of fibrosis and/or blood pooling and thus the blood T_1 relaxation time [179], where further changes are due to increasing pressure effects that cannot be measured within the spleen structure and probably explains the same ceiling effect seen with elastography [74, 168, 190, 191].

3.6.3.3. Vessel flow

The only published data on splanchnic PC-MRI has been published by Nottingham and demonstrated significant univariate associations with HVPG at 1.5 Tesla of SMA (R = 0.584, p = 0.003) and splenic artery (R = 0.534, p = 0.002) velocity together with Azygous vein flow (R = 0.656, p < 0.001) [134]. One study using Doppler US showed SMA and splenic artery flow is significantly increased in patients with cirrhosis and portal hypertension compared to healthy subjects [193] , but not was directly compared to HVPG. Another study that directly compared Doppler US to HVPG found no difference in the SMA velocity in patients with and without CSPH [194]. In this study only SMA velocity significantly correlated with HVPG ≤15 mmHg and then appeared to reduce. When combined with patient level data from our previous study at 1.5 Tesla this is a common finding that becomes apparent because this study population contains more people with advanced portal hypertension. To our knowledge this is the first time a reduction in SMA velocity has been reported in HVPG >15 mmHg. It is intriguing that HVPG ≥ 16mmHg has been found by other research groups to be an independent risk factor associated with an increase in mortality and liver decompensation [51, 55, 57, 64].

The SMA (n=39) PC-MRI scan is considerably easier to plan acquire data perpendicular to the vessel as compared to splenic artery (n=31), replicating previous published data where n=30 had SMA measures compared to n=24 in the splenic artery [134]. The splenic artery runs a more tortuous course so requires good planning, or is sometimes impossible to plan due to its small tortuous nature. Further it is also more sensitive to artefacts at 3 Tesla such as susceptibility effects which make imaging of the vessel and assessment of area difficult [183]. In contrast the SMA is a larger vessel with a more robust measurement, making it far more suited to larger multi-site studies.

Invasive catheterisation to measure azygous blood flow has been correlated with HVPG [195, 196]. PC-MRI demonstrated significantly higher azygous flow in portal hypertensive patients compared to healthy subjects [197]. PC-MRI of the azygous vein flow also significantly reduced following the placement of transjugular intrahepatic portosystemic shunt (TIPSS)[198]. In this study, we found no

significant correlation between the azygous vein flow and HVPG but did observe a clear difference between those with and without oesophageal varices. The fact that this study group contained a larger number of participants with clinically significant portal hypertension and oesophageal varices likely explains the difference to the data at 1.5 Tesla [134].

To our knowledge the significant correlation between cardiac index and splenic artery velocity has not been shown before in patients with liver cirrhosis. This finding fits with increased cardiac output being a key component of the hyperdynamic state [15].

3.6.3.4. Liver stiffness

LSM did not correlate to HVPG in this study. This is likely due to the high prevalence of NAFLD, the mean BMI over 31 kg/m^2 and the presence of ascites in our patient group, which are all recognised factors that limit LSM and its clinical utility in this setting [167]. This finding echoes a smaller recently published study in a comparable patient group where LSM did not correlate with HVPG (R = 0.35, p = 0.244) [185].

3.6.4. Meaning of the study

In conclusion, in a well characterised patient population, I have shown that a combination of quantitative MR measures of liver T_1, spleen T_1 and SMA velocity correlate significantly with HVPG along a continuous spectrum at a field strength of 3 Tesla. This replicates previous work at a lower field strength. Combining the data with previous work at 1.5 Tesla, reveals that it is complicated to accurately non-invasively estimate HVPG with a simplistic linear model. Splanchnic flow measures do add value, with SMA velocity consistently significantly correlated to HVPG ≤ 15 mmHg but then appears to start reducing at HVPG >15 mmHg. Azygous flow appears to significantly correlate with the presence or absence of oesophageal varices. Cardiac Index and Spleen T_1 also appear to demonstrate significant changes at various ranges of portal hypertension. Non-invasive, contrast-free, MR measures can accurately evaluate patients with suspected portal hypertension and characterise the haemodynamic changes that contribute to portal pressure and the hyperdynamic state. It will require

a more complex algorithm with hierarchal or machine learning or multiple measures of the mulita-organ hyperdynamic state that results from portal hypertension to make a comprehensive individual assessment and stratification of therapy. It may be that non-invasive multi-organ MR measures can be combined to define the proposed therapeutic window for beta-blockers [114]. A non-invasive model including both architectural (liver T_1 relaxation time) and splanchnic haemodynamic (SMA velocity) measures together with other factors (Splenic T_1, azygous vein flow, cardiac index) could be used as a surrogate of HVPG in clinical trials of portal hypertension as well as monitoring efficacy of treatment in clinical practice. These MRI measures can be performed without the need to purchase additional hardware and so could potentially be accessed outside traditional expert centres.

3 T measures of blood flow are directly comparable to those at a field strength of 1.5 T. The higher signal-to-noise ratio at 3 T leads to a greater dynamic range across patients with advanced chronic liver disease but is associated with field strength dependent issues compared to the same measures at 1.5 T. Firstly, there is a ceiling effect of T_1 within the liver seen at higher field strength. Secondly, there is a field-strength dependent effect of iron on T_1 that in this study required correction. The effects of inflammation, fat and oedema are unknown but likely to cause more confounding at higher field strengths. The advantage of using the wide-bore scanner was that all the patients who consented to the study could be scanned. Future studies will have to balance the known and unknown confounding effects of field strength on liver measures with the increased sensitivity and wider bore available at higher field strength.

3.6.5. Unanswered questions and future research

External validation across vendors and field strengths will have to be tested in larger multi-site studies to strengthen the validity and applicability of this data. Only with larger numbers of patients will it be possible to formulate a more accurate iterative model that can accurately provide a non-invasive measure of HVPG and measure the effect of interventions. In addition, long term follow up studies will be able to provide information as to whether these MR measures can stratify clinical outcomes as

has been shown with HVPG [37, 52, 60, 64]. Two separate research groups have published suggesting these quantitative MR measures may predict clinical outcomes [44, 45], although neither were specifically investigating the effects of portal hypertension.

4 MRI parameters to evaluate the effect of therapeutic intervention in Hepatitis C Virus (HCV) infection

4.1 Papers related to this chapter:

1. Bradley C & Scott RA (joint first authors), Cox E, Palaniyappan N, Thomson BJ, Ryder SD, Irving WL, Aithal GP, Guha IN, Francis ST. *Short-term changes observed in multi-parametric liver MRI following therapy with Direct Acting Antivirals in chronic Hepatitis C Virus Patients.* European Radiology. 2019 Jun;29(6):3100-3107.
2. Scott RA, Aithal GP, Francis ST, Irving WL. *Pre-treatment Lesions on Magnetic Resonance Imaging in Patients With Hepatitis C Virus Infection Diagnosed With Hepatocellular Carcinoma After Initiating Direct-Acting Antiviral Therapy.* Gastroenterology. 2018 May;154(6):1848-1850.

4.2 Abstract

Directly Acting Antiviral (DAA) therapy has revolutionised treatment, achieving >95% sustained virological response in patients with chronic infection with Hepatitis C Virus (HCV), even in those with cirrhosis. However, little is known about the impact of viral clearance on the liver. Multiparametric MRI, in a time window of 3-6 months between pre- and post-treatment scans, demonstrated changes in hepatic composition. Liver longitudinal relaxation time (T_1, 35±4 ms), transverse relaxation time (T_2, 2.5±0.8 ms; T_2*, 3.0±0.7 ms) and liver perfusion (28.1±19.7ml/100g/min) all significantly reduced. These measures are likely linked to reduced pro-inflammatory milieu, including interstitial oedema, within the liver. By chance, seven patients were diagnosed with hepatocellular carcinoma (HCC) after starting DAA treatment in whom pre-treatment MRI lesions could be identified on the research scans.

4.3 Introduction

Globally, chronic Hepatitis C virus (HCV) infection is estimated to affect 71 million people [199]. Direct-acting antivirals (DAAs) have revolutionised HCV treatment, with sustained virological response (SVR) rates approaching 100% in compensated cirrhosis [200-202], and emerging data suggesting excellent SVR in decompensated liver disease [203, 204]. Despite high SVR rates, there is an incomplete understanding of the effect of viral clearance on the liver in the context of DAA therapy. The progression or regression of fibrosis and/or portal hypertension caused by DAA therapy could have implications for each patient wider than chronic HCV management alone. Potential changes include those reflecting liver composition (including volume, inflammation and fibrosis) and hepatosplanchnic haemodynamic changes (including liver perfusion and blood flow).

Improvement in clinical outcomes following HCV eradication with treatment regimens of pegylated interferon and ribavirin are established. Large cohort studies show differences in liver decompensation rates between SVR and non SVR groups; hazard ratio (HR) 0.24 (95% CI 0.14-0.42), p <0.001 [205], HR 0.26 (95% CI 0.17-0.39), p <0.001 [206] and HR 0.15 (95% CI 0.06-0.38), p =0.04 [207]. Assessment by invasive liver biopsy in HCV patients with established cirrhosis has shown regression of cirrhosis in 61%, and reduction of collagen in 89% of patients at 61 months following an SVR [208]. Further studies using liver biopsy have shown cirrhosis regression rates of 46 to 75% after 3 - 10 years [209-212]. Although promising, regression was not ubiquitous nor studied in those with the most advanced liver disease due to the known risks of treatment with interferon and ribavarin. It remains unproven whether the regression seen was due to selection bias of those who achieved SVR, aviraemia or an immunomodulatory effect of the interferon itself [213]. Hepatic venous pressure gradient (HVPG), an invasive measure of portal hypertension, also improves with SVR [214-216]. Together, this published data builds a strong case for the concept of fibrosis and portal hypertension regression.

However, individual and invasive techniques for measuring fibrosis and portal hypertension respectively do not assess the complex pathophysiological changes associated with progression and

regression of chronic liver injury. Furthermore, ethical and practical constraints limit serial liver biopsy sampling with DAA therapy. A multicentre prospective study, with paired invasive HVPG and non-invasive transient elastography (TE), demonstrated DAA therapy significantly reduced HVPG but patients continued to have clinically significant portal hypertension and remained at risk of decompensation [217]. In a detailed study of 41 patients with compensated advanced chronic liver disease (cACLD) [68] due to HCV, the TE of both the liver and spleen rapidly improved during the first 4 weeks of DAA treatment with no significant changes thereafter up to the end of treatment and 48 weeks later [218]. Currently available clinical non-invasive markers, including TE, over-estimate regression compared to biopsy after SVR [217-219]. In a bicentre study of 572 patients with cACLD due to HCV who achieved SVR with DAAs, patients continued to be at risk of HCC despite an improvement in TE [220]. In an era of novel anti-fibrotic therapy on the horizon, robust non-invasive biomarkers for use in advanced liver disease patients who receive DAA therapy to understand the structural and functional changes in the liver, and stratify ongoing risk post SVR and focus interventions are required.

This study collected quantitative MRI data in patients with liver cirrhosis who underwent DAA therapy from the NHS England expanded access programme [203]. This study describes the early changes in structural and haemodynamic MRI measures in the liver between baseline (pre-treatment) and immediately post-treatment at a 3-6 month time window following the start of DAA therapy, in patients with advanced end-stage liver disease.

4.4 Aims

The aims of this study were to characterise any changes in the structural or haemodynamic multiparametric MRI measures in patients with advanced liver disease caused by chronic HCV infection who receive DAA therapy.

During the study a debate developed around increased reports of hepatocellular carcinoma in those who received DAA therapy. As a result, an additional aim became to evaluate whether non-contrast

MRI research scans can detect any pre-treatment lesions in those patients who are subsequently diagnosed with hepatocellular carcinoma after initiating DAA therapy.

4.5 Methods

In this prospective, observational, study patients were recruited through the NHS England expanded access programme, established to prioritise treatment for patients with greatest clinical priority, including compensated and decompensated liver disease. Treatment was with sofosbuvir plus, by clinician choice, ledipasvir or daclatasvir, with or without ribavirin [203, 221]. The study received ethical approval from the NRES Committee East Midlands - Derby 1 (Research Ethics Committee reference 11/EM/0314). Once enrolled in the study, if a subject did not attend a study visit after treatment, they were sent a letter and telephoned twice by the research team.

Patients underwent a detailed MRI study before DAA therapy and after treatment completion (within 12 weeks of last DAA tablet swallowed). Patients followed standard management protocols for DAA therapy and monitoring. Routine clinical information including medical history, clinical examination and laboratory values were recorded for each participant. Laboratory values were used to calculate validated scores of ALT, Fib4 [25], APRI [26], MELD [35] and UKELD [222] using freely available online calculators.

4.5.1 Sustained Virological Response (SVR)

The target endpoint of therapy is to achieve an SVR, defined by undetectable HCV RNA in serum or plasma 12 weeks (SVR12) or 24 weeks (SVR24) after the end of therapy, as assessed by a sensitive molecular method with a lower limit of detection ≤15 IU/ml [223]. Both SVR12 and SVR24 have been accepted as surrogate endpoints of therapy by regulators in Europe and the United States, given that their concordance is >99% [224]. Long-term follow-up studies have shown that an SVR corresponds to host control of HCV infection in the vast majority of cases [225]. For the purposes of this study SVR corresponds to SVR12 – i.e. undetectable HCV RNA 12 weeks after the end of therapy.

4.5.2 Fib4

FIB-4 is a simple index composed of readily available routine laboratory tests (platelet count, ALT and AST) as a non-invasive marker of liver fibrosis in patients with chronic HCV infection [226]. It is calculated using freely available online calculators by the following equation:

[Age (years) x AST (U/L)] / [Platelet count (10^9/L) x (ALT [U/L])$^{1/2}$]

4.5.3 APRI

The AST to platelet ratio index (APRI) is a non-invasive marker of liver fibrosis in patients with chronic HCV infection [227]. It is calculated using freely available online calculators by the following equation:

APRI = [AST (/ULN) / Platelet counts (10^9/L)] x 100

4.5.4 UKELD

United Kingdom Model for end-stage liver disease is derived from routine laboratory tests of serum bilirubin, INR, creatinine and sodium on freely available online calculators to predict short-term mortality in patients with chronic liver disease [222].

UKELD Score = 5.395 × In(INR) + 1.485 × In(creatinine, µmol/L) + 3.13 × In(bilirubin, µmol/L) - 81.565 × In(sodium, mmol/L) + 435

4.6 MRI measures

MRI data were acquired on a 1.5T Philips Achieva scanner (Philips Healthcare Systems, Best) in a single 40 minute scan session using methods described in [136]. Subjects were scanned feet first supine after an overnight fast, using a body transmit and 16-element SENSE XL torso coil. The MRI protocol comprised of a series of non-invasive measures to assess liver composition and haemodynamics. Multi-slice balanced-Fast-Field-Echo (bFFE) images were initially acquired in 3 orthogonal planes (35 slices of 1.75 × 1.75 × 7 mm^3 resolution, single breath holds per orientation) to locate the liver and vessels of interest, and to estimate liver volume.

4.6.1 Liver Composition

Liver T_1, T_2 and T_2* were mapped in 9 axial slices through the liver (field of view (FOV) 288x288mm^2, voxel size 3x3x8mm^3, 4 mm slice spacing). A modified respiratory-gated inversion recovery sequence with a fat suppressed spin echo, echo-planar imaging (SE-EPI) readout scheme was used to measure liver T_1 [22, 27, 28] (inversion times for SE-EPI image slice were 100 - 1000 ms in 100 ms increments). For all inversion times, SE-EPI imaging slices were collected at end expiration such that the first slice was collected at 1500 ms after the respiratory trigger with subsequent slices collected with a 65 ms temporal slice spacing. The T_1 mapping sequence was acquired with slices collected in ascend and descend slice ordering to increase the dynamic range of inversion times. In total, 20 inversion times were acquired in < 3 minutes. A respiratory-gated SE-EPI sequence was used to map liver T_2 comprising six echo times (ET=27, 35, 42, 50, 60, 70 ms) in approximately 2 minutes. T_2* mapping was collected using a multi-echo fast field echo (mFFE) sequence comprising 12 echo times (ET_1=5 ms, ΔET =2.5 ms) acquired in a ~ 17 s breath hold. T_2 and T_2* data sets were geometrically matched to the T_1 dataset.

In-house software was used to create T_1, T_2 and T_2* maps (MATLAB, The Mathworks Inc., Natick, MA). Prior to data fitting, images affected by motion (due to missing the respiratory trigger) were discarded. To create T_1 and M_0 maps, data at the 20 inversion times were fit using a voxel-by-voxel 2 parameter fit. For T_2 and T_2* mapping, a voxel-by-voxel log-linear least-squares method was used to fit the echo intensities and to create T_2 and T_2* maps. To assess the quantitative T_1, T_2 and T_2* maps, a region of interest covering the liver was selected and a histogram of values within computed. A Gaussian curve was fitted to the histogram to determine the mode of the T_1, T_2, and T_2* distribution within the liver, this procedure excludes regions where vessels are visible within the liver.

4.6.2 Blood Flow

Phase Contrast (PC)-MRI assessed blood flow through vessels in the hepatic circulation (portal vein, hepatic artery) as well as vessels critically related to portal hypertension (splenic artery, right renal artery, superior mesenteric artery (SMA)) with reconstructed voxel size of 1.17x1.17x6 mm^3 [22]. PC-

MRI was performed using a single slice turbo field echo (TFE), slice placed perpendicular to each vessel. 15 phases were collected across the cardiac cycle for the portal vein, 20 phases for all other vessels, with velocity encoding in the portal vein of 50cm/s, in the hepatic, splenic, renal arteries of 100 cm/s, and 140 cm/s in the SMA. Each measurement was acquired in a single <20 s breath hold. Using Q-flow software (Philips Medical Systems, Best, NL), mean artery cross sectional area (mm^2), mean velocity (cm/s), and hence mean bulk flow (ml/s) over the cardiac cycle, was calculated for each vessel.

4.6.3 Liver Perfusion

Respiratory-triggered flow-sensitive alternating inversion recovery arterial spin labelling (FAIR-ASL) data (288x288 mm^2 field of view, 3x3x8 mm^3 voxel, 3 sagittal slices, slice gap 5mm) were collected with a balanced fast field echo (bFFE) readout in approximately 5 minutes. A base (M_0) equilibrium scan and T_1 map was also acquired for quantification of hepatic tissue perfusion using a kinetic model. In-house software was used to motion correct the images and perform automatic outlier rejection of images affected by movement prior to quantification of tissue perfusion [29].

4.7 Statistical Analysis

Statistical analysis was performed with *Graphpad Prism7* software. Continuous variables are expressed as mean ± standard deviation for normal data otherwise median (interquartile range), while categorical variables are reported as number of patients with (proportion of patients with) the certain characteristic.

A paired Student's t-test is used for comparisons between pre- and post- treatment for normally distributed data and Wilcoxon matched pairs signed rank test when not normally distributed. All statistical analysis is Bonferroni corrected for multiple comparisons.

4.7.1 Repeatability of Multiparametric MRI Measures

To determine between session repeatability of MRI measures, the intra-subject Coefficient of Variation (CoV) (defined as the standard deviation/mean) of multiparametric MRI measures were

assessed. A subset of 10 healthy participants (age 23-37 years, body mass index 20-26 kg/m^2) had three scans, at least one week apart and within four weeks, at the same time of day and after an overnight fast to limit diurnal and dietary variability. This healthy participant study was approved by the University of Nottingham Ethics committee.

4.8 Results

Of the 41 patients enrolled, 39 completed treatment (one died during treatment and one declined treatment after two doses). Pre-treatment MRI scans were performed 1 (0 – 29) day(s) before the start of DAA treatment. 17 HCV patients with advanced liver disease underwent DAA therapy within 1 week of their pre-treatment MRI scan and returned for their post-treatment MRI scan at a median of 22 days (3 – 79 days) after the last DAA taken (Figure 4.1). Study demographics are provided in Table 4.1. 16 of 17 patients (94%) achieved SVR, defined as undetectable serum viral RNA 12 weeks after treatment completion. Validated serum clinical liver markers of ALT, Fib4 and APRI were collected at pre- and post- MRI time points. The majority of patients had significantly improved liver function test scores post-treatment compared to pre-treatment (Figure 4.1), with a significant group reduction in ALT, Fib4 and APRI.

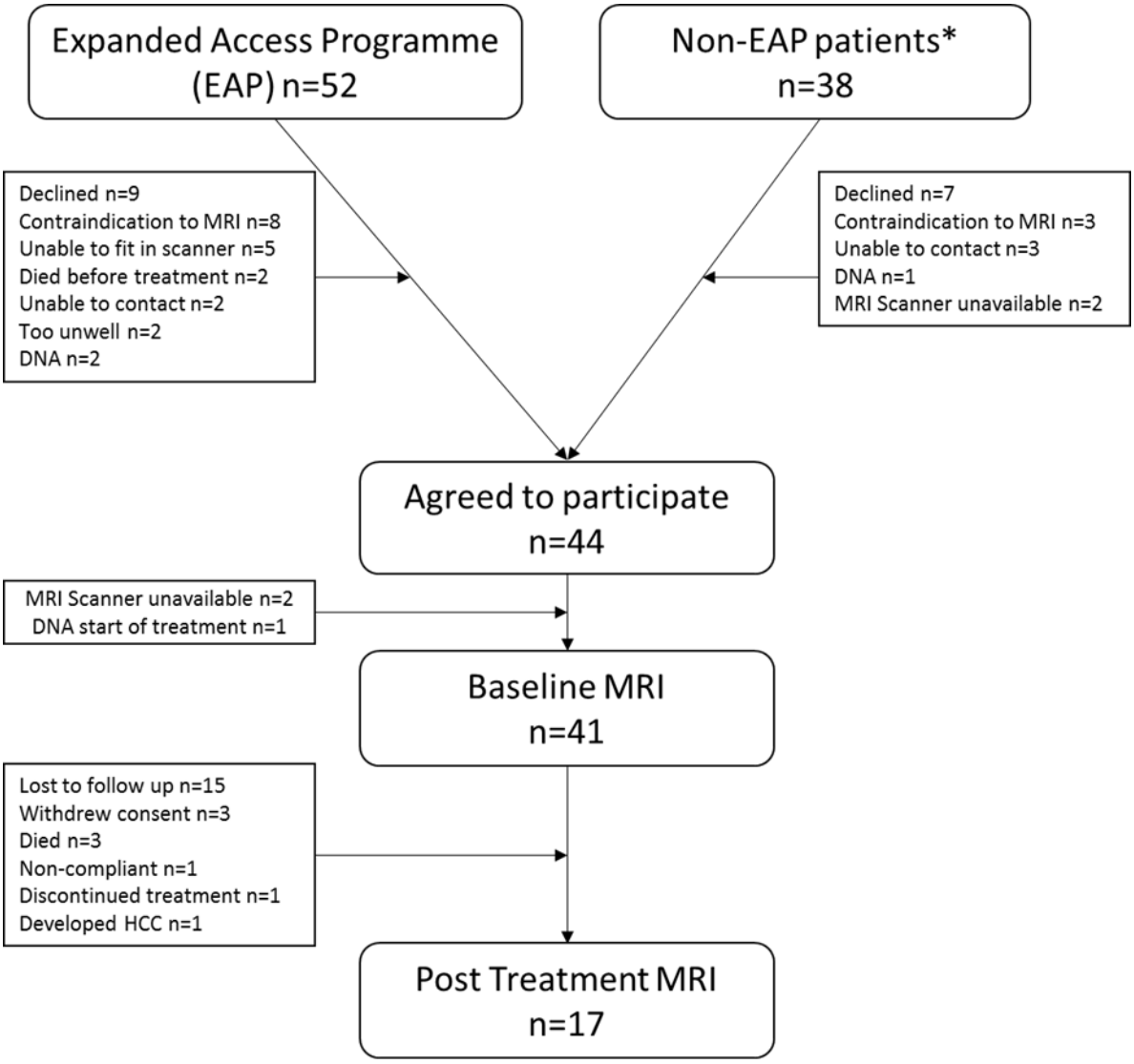

*Figure 4.1: Flow diagram illustrating recruitment and retention to the study. All eligible patients were recommended for DAA treatment at the East Midlands viral Hepatitis multi-disciplinary team. *From July 2015, treatment with DAAs was extended to include compensated cirrhosis.*

Demographic Table	
Variable	All patients
Age - Mean (S.D.)	53 (8)
Male (%)	14 (82 %)
Transplant (%)	3 (18 %)
Cirrhosis (%)	15 (88 %)
MELD (IQR)	8 (7 – 8.25)
Compensated (%)	7 (41 %)
Decompensated (%)	8 (47 %)
Previous variceal haemorrhage	4 (23 %)
Ascites	2 (12 %)
Jaundice	2 (12 %)
Diabetes (%)	2 (12 %)
Body Mass Index median (IQR)	25.6 kg/m^2 (24.0 – 27.9)
HCV Genotype	
1 (%)	9 (53 %)
2 (%)	1 (6 %)
3 (%)	7 (41 %)

Table 4.1: Pre-treatment characteristics of the 17 Hepatitis C Virus patients consented to the study who returned for a post-treatment MRI scan.

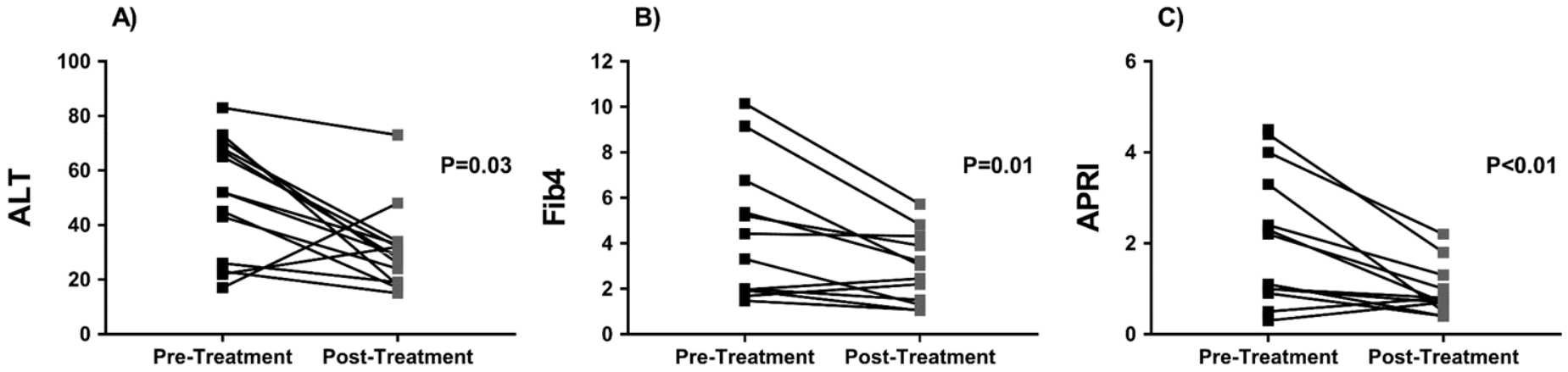

Figure 4.2: Liver enzymes (ALT) and non-invasive markers of liver fibrosis (FIB4 and APRI) pre- and post- treatment showing A.) Significant reduction in ALT of 54±25 (p=0.03); B.) Significant reduction in Fib4 1.6±0.5 (P=0.01). C.) Significant reduction in APRI score of 31.0±0.3 (p<0.01).

Table 4.2 shows that all MR volume and relaxometry measures had a CoV<5 %, and all haemodynamic measures <15 %, apart from hepatic artery blood flow. There were significant changes in the liver microstructure as assessed by MR relaxation times with DAA therapy, with a significant reduction in liver T_1, T_2 and T_2* after treatment. No change was observed in splenic T_1 (*Figure* 4.3). Figure 4.4 shows example liver T_1, T_2 and T_2* maps pre- and post- DAA therapy. No significant differences were observed in liver or spleen volume. No significant changes were observed in any blood flow measure (hepatic artery, splenic artery, superior mesenteric artery or portal vein); however, there was an increase in liver perfusion following DAA therapy *(Figure* 4.5). Paired perfusion data presented is presented for n=9 participants, all of whom achieved SVR. The remaining subjects had inadequate paired data due to insufficient anatomical matching between visits.

MRI Measure	CoV (%)
Liver volume	4.6
Liver T_1	1.5
Liver T_2	4.3
Liver T_2*	3.7
Portal vein flow	13.6
Hepatic artery flow	22.7
Liver Perfusion	12
Spleen volume	5.2
Spleen T_1	1.8
Splenic artery flow	11
SMA flow	7.6

Table 4.2: Coefficient of variance (CoV) of MRI measures.

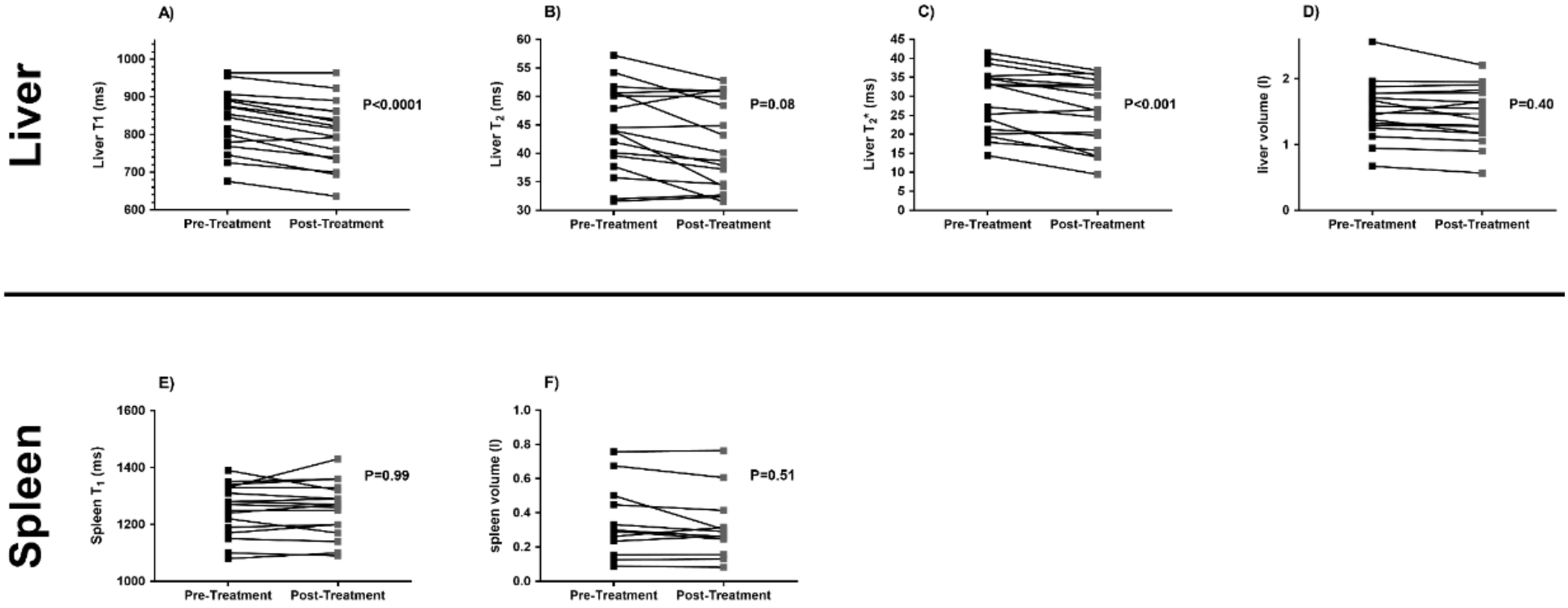

Figure 4.3: Effects of DAA therapy on liver composition A.) Significant reduction in liver T_1 of 35±4ms ($p<0.0001$). B.) Significant reduction in liver T_2 of 2.5±0.8 ms ($p=0.08$). C.) Significant reduction in liver T_2 of 3.0 ±0.7ms ($p<0.001$). D/E/F.) No significant difference was observed in spleen T_1, liver volume or spleen volume between pre and post DAA treatment.*

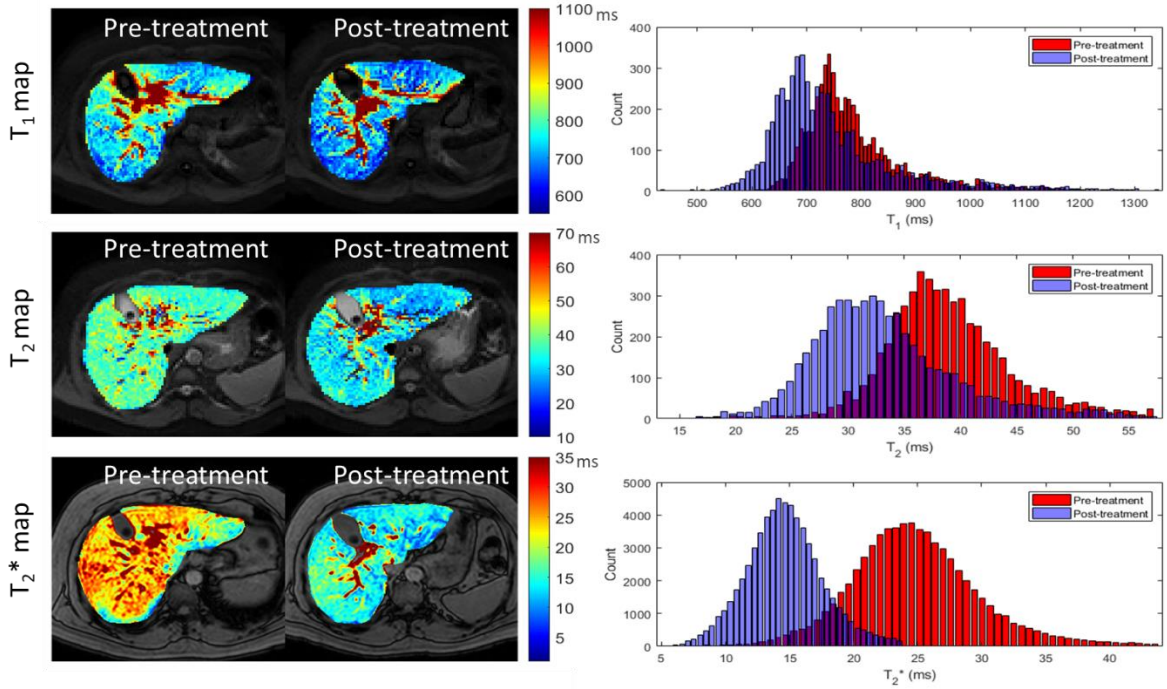

Figure 4.4: Example axial T_1 map, T_2 map and T_2 map of the liver pre and post DAA treatment and associated histograms of measures highlighting the reduction in the mode of the distribution post DAA treatment.*

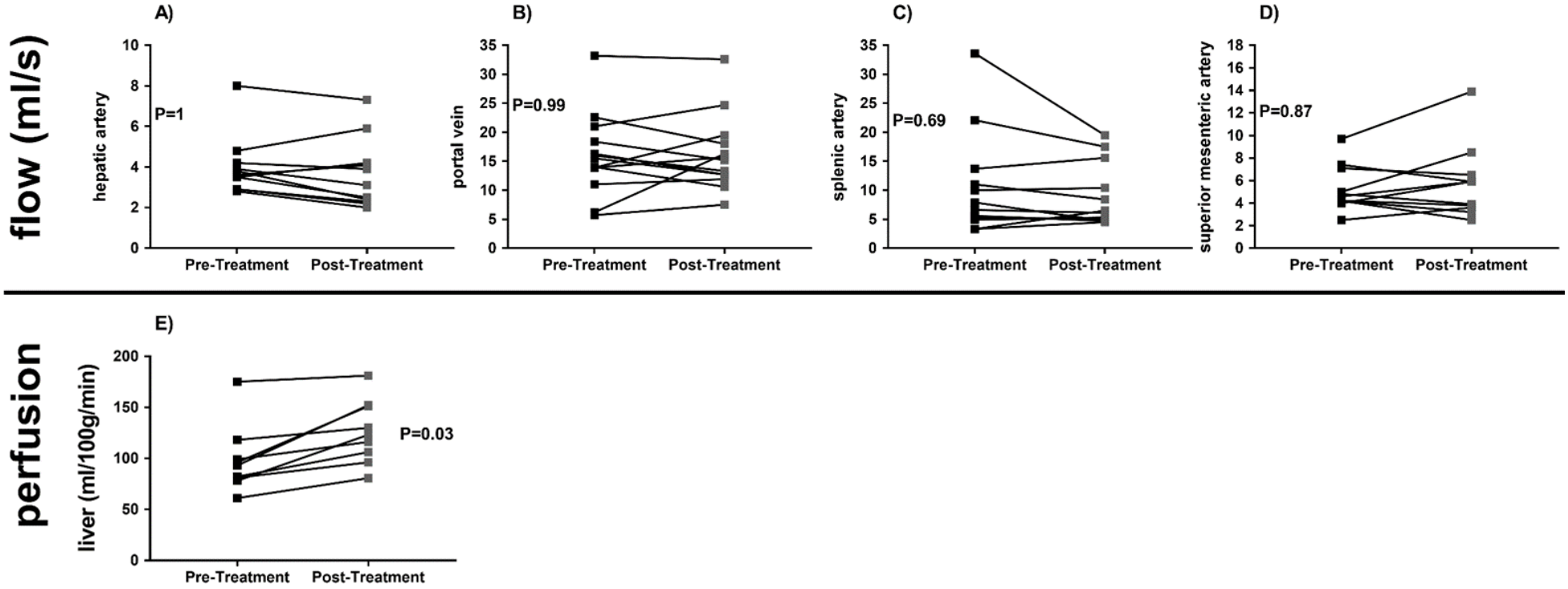

Figure 4.5: Bulk flow to the liver in the portal vein and hepatic artery, as well as superior mesenteric and splenic artery flow show no significant changes between pre and post DAA therapy. An increase in liver perfusion of mean change of 28±20 ml/100g/min is observed following DAA therapy (p=0.03).

The patients who subsequently attended the post-treatment MRI scan (n=17) had a lower pre-treatment MELD (7.8 ± 2.2 vs 10.5 ± 4.2, p = 0.027) than those who did not (n=24) attend the post-treatment MRI scan, but were otherwise similar (Table 4.3).

Variable	Did not attend post treatment MRI (n=24)	Attended post treatment MRI (n=17)	Statistical significance
Characteristics:			
Age (years)	52.7 ± 10.5	52.7 ± 8.5	p = 0.990
BMI (kg/m^2)	29.2 ± 6.7	26.0 ± 2.6	p = 0.099
Diabetes	3 (14.3%)	2 (10%)	p = 0.524
Serum markers:			
MELD	10.5 ± 4.2	7.8 ± 2.2	p = 0.027
UKELD	50.0 (48.0 – 53.0)	48.5 (47.0 – 50.0)	p = 0.151
Fib4	6.3 ± 4.5	5.5 ± 4.8	p = 0.568
APRI score	2.3 (1.1 - 3.9)	2.2 (0.9 – 3.8)	p = 0.633
MRI measures:			
Liver SE-EPI T_1 (ms)	827.6 ± 94.5	839.3 ± 87.7	p = 0.698
Liver T_2 (ms)	43.4 ± 4.5	45.2 ± 7.6	p = 0.396
Liver T_2* (ms)	27.1 ± 6.9	30.7 ± 8.3	p = 0.196

Table 4.3: Comparisons of pre-treatment characteristics of patients. Data shown separately for those patients who did not attend MRI post DAA treatment MRI and those who did post DAA treatment MRI.

4.9 Discussion

Using multiparametric MRI in patients with HCV related cirrhosis pre- and post-DAA therapy, there were demonstrable significant changes in the liver composition (T_1, T_2 and T_2*) and haemodynamics over a short time period following clearance of HCV infection. No changes in bulk hepatic or splanchnic blood flow were observed in the short time frame between MRI scans.

This is the first study to document changes in MR parameters following DAA therapy. Few previous studies have assessed the effect of HCV treatment on MRI measures. One previous study assessed the effect of HCV treatment (pegylated interferon, ribavirin, telaprevir) on liver diffusion, demonstrating reduced apparent liver diffusion coefficient reflecting ultrastructural changes such as cell necrosis/apoptosis and inflammatory cell infiltration [228]. A recent study showed a small increase in liver volume following anti-viral treatment, which was larger in patients with SVR [31], interpreted to indicate liver regeneration and/or recovery and reduced fibrotic load of the liver.

The strengths of this current study are the prospective recruitment and phenotyping of the patients. The quantitative MRI parameters have been previously validated against “gold standard” measures including liver biopsy [19, 20] and HVPG [22]. More recently specific MR liver biomarkers, including liver T_1, liver perfusion, and haemodynamic measures, were associated with clinical outcomes in independent cohorts of patients [44, 45]. Liver T_1 acquisition and analysis has been shown to be highly repeatable [19], with an intra-subject CoV < 1.8%, and a low inter- and intra-observer variability with intra-class correlation coefficient > 0.99 [22]. Here the intra-subject variability in MR relaxation time is low, with a CoV of 1.5, 4.3, 3.7 % for liver T_1, T_2 and T_2* respectively, considerably lower than inter-subject variability. Capturing data pre- and post-treatment enables direct intra-individual comparisons, strengthens the validity of the data, since each subject is their own control. In response to DAA therapy the reduction in T_1 is more significant compared to that of T_2 and T_2*. This could be attributed to the smaller CoV. However, there is also variability within the literature in terms of a T_2 change, with preclinical models of liver fibrosis shown to result in an increase as well as decrease in T_2 [229]. It is

hypothesized that increased T_2 is related to hepatic inflammation associated with the development of fibrosis or the proliferation of small biliary ducts in models of bile duct ligation [230].

The limitations of this study are the small sample size from a single UK centre, with some variation in patient disease severity. Due to practical constraints it was not possible to perform parallel invasive assessments such as liver biopsy or HVPG. The timing of the MRI scans in close proximity to drug therapy, enabled characterisation of changes at an early time point in subjects who achieve SVR at a later time point. Although all patients had a baseline TE measurement, very few had a repeat TE measurement at the return visit due to a lack of available expertise.

The observation that only a few specific MR parameters changed in the study time period is relevant. Notwithstanding the possibility of Type 1 and Type 2 errors, the lack of significant changes in liver haemodynamic blood flow potentially indicate the natural history of "regression". Reversal of fibrotic and vascular networks, which of course may be incomplete [10], is thought to occur over months to years. To date, there is limited data showing histological changes associated with DAA treatment in HIV co-infection [231] and post-transplant populations [232], both demonstrating a significant reduction in necroinflammation with SVR. It is widely recognized that both TE and serum markers of fibrosis are influenced by necroinflammation [219, 233-235]. Moreover, short-term studies have shown that TE dynamically changes during treatment, particularly within the first four weeks [218], with DAA therapy and long-term studies having shown that both TE and serum fibrosis markers may over-estimate regression [10, 217, 220].

Pegylated interferon and ribavirin ameliorates portal hypertension in patients with HCV infection [214-216] and HIV/HCV-coinfection [236]. Multiple studies similarly show that DAA treatment results in statistically significant reductions in HVPG [217, 231, 237, 238] but interestingly may not alter clinically significant portal hypertension [217].

The key findings of reduced liver T_1, T_2, T_2* and increased liver perfusion are likely linked by a reduction in the pro-inflammatory milieu within the liver, including interstitial oedema, aligned with a reduction

in serum ALT. DAA treatment changes necroinflammation which may improve liver function over a longer period of time [221], portal hypertension (provided treatment in the early stage of portal hypertension [217]), and may also underlie the reported change in TE [218-220]. A reduction in necroinflammation on liver biopsy in the short term, even when associated with a short duration of viral suppression using Interferon based treatment, has a positive impact on future clinical outcomes at 6 years and fibrosis regression [239]. Chronic inflammation might be expected to increase perfusion but is unknown in the context of advanced liver disease. A recent MRI study showed reduced perfusion is associated with progressive liver disease and linked to adverse outcomes [45], and CT has shown worsening perfusion with progressive fibrosis in HCV [240]. This is consistent with the finding presented of a significant increase in liver perfusion with the likely acute resolution of chronic necroinflammation after DAA treatment in HCV related advanced liver disease.

A multi-modal technique including MRI that captures how the different aspects of liver composition, perfusion and blood flow change over time could provide additional confidence for clinical decision making. In addition, robust non-invasive tests that are specific to the liver would be valuable to drug development for anti-fibrotic compounds as they can be repeated at multiple time points to evaluate drug efficacy. MRI has the potential to be a key non-invasive tool to evaluate the efficacy of interventions in chronic liver disease and stratify patients according to the potential clinical outcomes.

In summary, for the first time, this MRI study has shown that treatment of HCV with DAAs in patients with cirrhosis leads to an acute reduction in liver T_1, T_2, T_2* and increase in liver perfusion measured. The ability of MRI to characterise changes in the angio-architecture of patients with cirrhosis after intervention at such short intervals will enhance our understanding of the progression/regression of chronic liver disease and potentially assist clinical decision making. The sensitivity of these MR measures should be exploited to accelerate early phase of clinical development of novel anti-fibrotic agents.

In future work, the intention is to use quantitative MRI measures to observe the long-term effects of DAA therapy on liver composition, perfusion and surrounding haemodynamics to characterise the extent of fibrosis regression, vascular remodelling and reduction in portal hypertension that may occur after DAA therapy. Secondly, to assess whether MRI changes correspond to, or are predictive of, histological regression of fibrosis, as described in long term studies with interferon and ribavirin [208, 241, 242].

4.10 Hepatocellular carcinoma (HCC)

Although attainment of sustained virological response (SVR) reduces the incidence of hepatocellular carcinoma (HCC) in patients with chronic hepatitis C virus (HCV) infection, increased risk of HCC is not completely abolished [220, 243]. In the largest series to date, risk factors associated with persistent HCC risk after SVR achievement included increasing age, presence of cirrhosis and diabetes [244]. It is striking, however, that 35% of HCC cases in that cohort arose within the first year following SVR attainment and the overall median time between SVR and HCC detection was 1.66 years [244]. This observation raises the possibility that HCC was present prior to SVR attainment.

During the study detailed above, seven (of 41) patients were diagnosed with HCC subsequent to onset of DAA therapy (6 de novo and 1 recurrence). In each case there was, serendipitously obtained, radiological evidence of the presence of HCC before onset of DAA therapy. Here I describe these cases of HCC, 6 of which would have fulfilled criteria for development after SVR according to classification criteria [245, 246].

Six (of seven) patients were male, median age 55 (range 50 – 69), BMI 25.9 (23.4 - 32), MELD 9 (7-15). Six (of seven) had decompensated cirrhosis, 5 had HCV genotype 3, 2 genotype 1a. All patients had a normal pre-treatment α-fetoprotein, median 9 ng/mL (7 – 15). 4/7 achieved SVR, one died during treatment and two underwent transplant. Post-hoc processing of pre-treatment research MRI scans showed 6/7 lesions were detectable 36 - 511 days before clinical diagnosis of HCC (Figure 4.6). No pre-treatment lesion was identified in Patient 7, but a lesion was detectable on the post-treatment research scan 106 days before clinical diagnosis.

Only one patient (Patient 3) had recurrent HCC, with radio-frequency ablation 3 years prior to this study. The other six were de novo HCCs. 4 HCCs were detected by routine abdominal ultrasound surveillance at 14 days following initiation of DAA treatment (Patient 6), or 199 - 389 days post completion of DAA treatment (patients 2, 5 and 7). Of the remaining three patients- Patient 1 presented with a raised screening alpha-fetoprotein (49 days post DAA treatment completion), Patient 3 presented with acute decompensation (ascites) 50 days after starting DAAs, and the HCC in Patient 4 was detected on routine imaging at transplant work-up (34 days post DAA treatment completion). Radiological reports and multi-disciplinary team notes were retrieved. 5/7 patients had 'clinical' MRI scans to confirm the diagnosis of HCC. These clinical scans were anonymised, randomised and the DICOM files exported. Clinical MR images then underwent identical post-hoc processing to the research scans and were reconstructed into 3D images by researchers blinded to the patients' identity. An independent researcher was tasked with matching the clinical and research scans – and succeeded in doing so for all 5 patients (Figure 4.6). All lesions identified on the DIXON scans were in the same segment as the HCCs that were subsequently diagnosed. The matching of HCC lesions between the clinical "diagnostic" scans and preceding research DIXON MRI scans, both in terms of anatomical location and similarity in size, is highly suggestive that the HCCs were present pre-treatment, but were not clinically evident.

Three patients had a screening ultrasound that was reported as normal (9-367 days) after the research MRI scan, analysed post hoc, had a demonstrated a lesion. 5/7 cases of HCC had a normal surveillance ultrasound in the 6 month period prior to DAA therapy (median interval 36 days). This is consistent with the known relative insensitivity of ultrasound in the detection of tumours [247, 248].

This data unequivocally demonstrate that lesions which ultimately co-localise with subsequently formally diagnosed HCCs exist *before* DAA therapy is started, and support the argument that the increased prevalence of HCC following DAA treatment is because DAA-treated patients have more advanced liver disease [243, 244] rather than the risk attributable to DAA therapy [249].

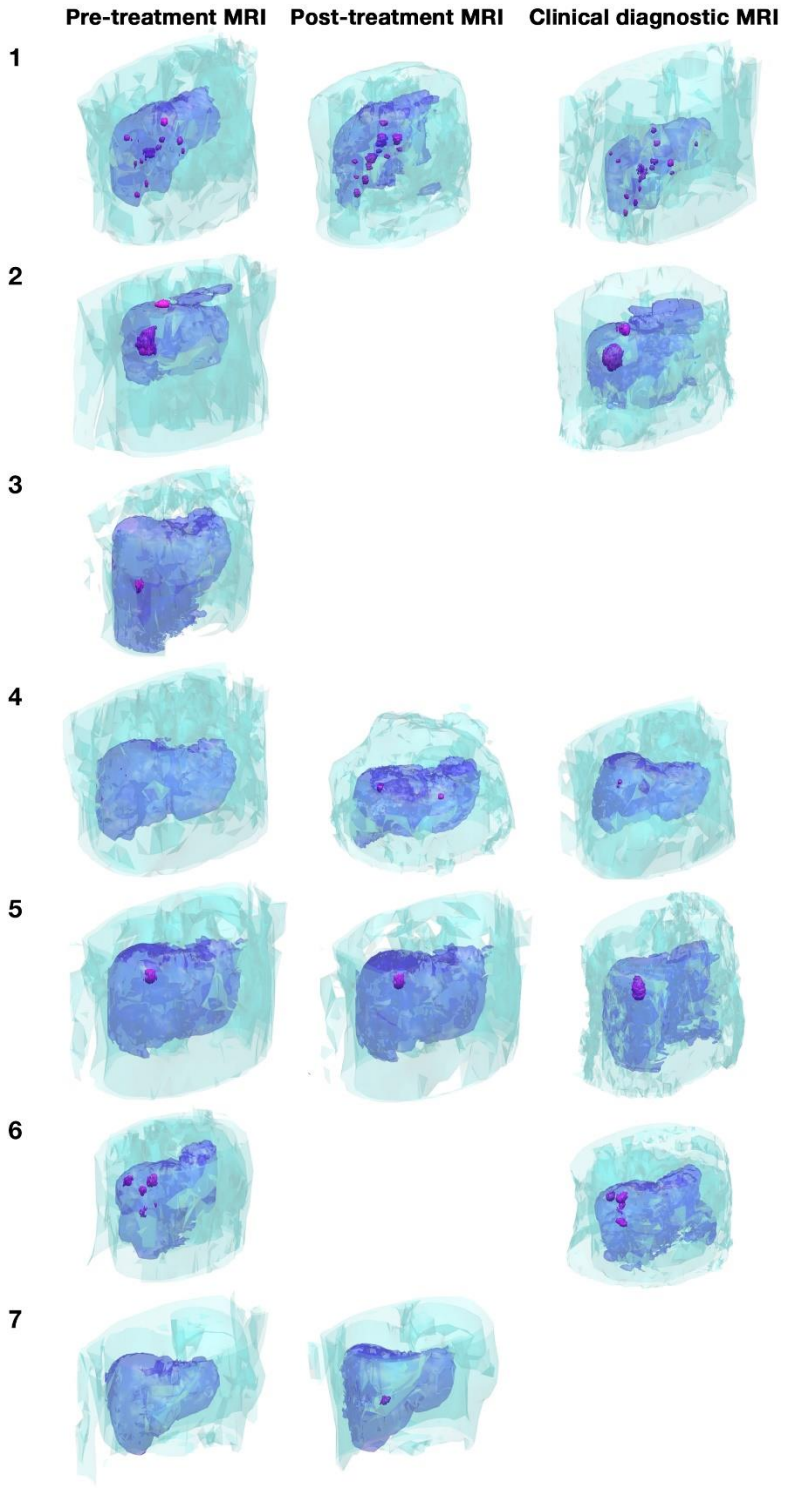

Figure 4.6: Post hoc image analysis could retrospectively identify lesions (pink) within the liver (blue) on the water-only DIXON MRI scans of all 7 patients who developed hepatocellular carcinoma before the clinical diagnosis was made. Using in-house software (MATLAB, The MathWorks Inc, Natick, MA), the DIXON water-only images of the pre- and post-magnetic resonance imaging scan sessions were thresholded at

80% of the mean liver intensity to automatically segment the lesions from the liver tissue. These images were then 3-dimensionally rendered.

5. Measures of small bowel permeability

5.1. Abstract

Increased gut permeability and subsequent bacterial translocation are believed to be important steps in the pathogenesis of several acute and chronic diseases, including cirrhosis of the liver. There are numerous published methods for measuring gut permeability none of which have been linked to hard clinical outcomes. In the absence of a true gold standard, this chapter compares the best available tools to evaluate gut permeability with a newly developed MRI assessment of the small bowel. Provocation with enteral Indomethacin administration, an accepted positive control for experimental medicine studies, is used to compare the MRI measures to bowel permeability assessed by the Lactulose/Mannitol urinary excretion ratio (LMR). Only small bowel T_2 significantly increased and correlated with increased LMR following indomethacin administration. Performance characteristics of the newly developed MR measure to predict clinical outcomes related to increased bowel permeability can now be evaluated in a longitudinal cohort of patients with cirrhosis.

5.2. Gut permeability

The gut wall is a complex, dynamic, porous barrier existing between the host organism and the environment [250]. There is no standardised definition as to what constitutes increased gut permeability, other than reporting a difference in measures between groups of interest. Increased gut permeability is implicated in the pathophysiology of a number of disorders, such as coeliac disease, inflammatory bowel disease, alcoholic hepatitis, non-alcoholic fatty liver disease, liver cirrhosis with portal hypertension, irritable bowel syndrome, obesity, diabetes and HIV [251]. All these diseases are characterised by inflammation which may be associated with increased permeability or alternatively, inflammation may be triggered by bacterial translocation through areas of increased permeability.

Bacterial translocation is defined as a passage of bacteriae and/or bacterial products through or across the intestinal barrier to the mesenteric lymph nodes [252]. It is a normal physiological process in healthy conditions and crucial for host immunity.

5.2.1. Small bowel focus

There are several pieces of evidence that suggest the small bowel is the principle focus of pathological bacterial translocation and increased permeability. The amount of bacteria increases from 10^3 units per gram of content in the small intestine up to 10^{12} in the colon [253]. It has been suggested that this larger number of bacteria has led to the colon being efficient at elimination of translocating bacteria. The colon has higher transepithelial resistance than the small bowel [254]. Experimental studies inoculating equal concentrations of E. coli into small or large bowel show that bacteria translocate predominantly from the small bowel [255]. In addition, proximal bowel colonisation has been associated with increased bacterial translocation and septic morbidity in surgical intensive care patients [256, 257], indicating that small intestinal bacterial overgrowth has the greatest potential for promoting bacterial translocation. There are numerous poorly validated proposed serum markers of bacteria-related markers, biomarkers of epithelial cell integrity, intestinal inflammation and immune activation. Three major mechanisms promote **bacterial translocation;** intestinal **bacterial** overgrowth, deficiencies in host immune defences and increased permeability or damage to the intestinal mucosal barrier.

5.2.2. Bacterial translocation in liver cirrhosis

Recently, a modified version of the arterial vasodilatation hypothesis has been proposed to explain the transition to decompensated cirrhosis in the “systemic inflammation hypothesis” [17]. This hypothesis suggests bacterial translocation is associated with increased systemic inflammation exacerbating the hyperdynamic circulation leading to decompensation, hepato-renal syndrome and acute on chronic liver failure (ACLF). Evidence to substantiate the claim that bacterial translocation

directly leads to clinical outcomes is lacking, arguably due to a lack of a gold standard test [258]. Several bits of circumstantial evidence point towards it being an important prognostic event.

First, bacterial infections appear to be a crucial prognostic event in patients with cirrhosis. A systematic review proposed a 'fifth' stage in the natural history of cirrhosis in addition to previously described Baveno classification [29]; bacterial infections were associated with a 4-fold increase in mortality (pooled OR 3.75; 95% CI 2.12 – 4.23) [259]. This data was confirmed by a large US epidemiology study of hospital admissions showing that sepsis was the highest independent risk factor for death in patients with cirrhosis (RR 4.70; 95% CI 4.61 – 4.79) and increasing over time [260]. Two large studies have recently demonstrated bacterial infections are important precipitants of ACLF [261] and mortality in alcoholic hepatitis [262]. In the latter study levels of circulating bacterial DNA before corticosteroid treatment could identify patients at high risk of infection within 7 days (OR 4.68; 95% CI 1.80 – 12.17) [262].

Second, a cross-sectional study of 101 patients with cirrhosis and 35 patients with no cirrhosis undergoing surgery showed enteric organisms were grown from mesenteric lymph nodes in proportion to the severity of liver disease, up to 30.8% in Child C cirrhosis [263]. Lastly, in a cross-sectional study of 52 patients with cirrhosis compared to controls, ^{51}Cr-EDTA (a surrogate measure of gut permeability) was observed in the ascites of patients with SBP suggesting increased permeability is linked to bacterial translocation and clinical outcomes [264].

5.2.3. Structural changes of the bowel in cirrhosis

Structural changes of the intestinal mucosa in cirrhosis are associated with portal hypertension. They include widening of intercellular spaces, vascular congestion, oedema, fibromuscular proliferation, decreased villous to crypt ratio, and thickening of the muscularis mucosae [265-267]. Only one retrospective study in a transplant centre using Computed Tomography with intravenous contrast has ever evaluated the radiological appearances of the bowel in 57 patients with cirrhosis [268]. 37% had

significantly increased (>200%) bowel wall thickness, 76% had associated small bowel wall thickening and the changes mostly resolved post liver transplant (44% pre- vs 6% post- liver transplant).

1.2.4.Small bowel motility in cirrhosis

Small intestinal bacterial overgrowth in cirrhotic patients ranges from 48-73% [269-273]. Its presence correlates with the severity of liver disease [274-276] and is linked to decompensating events in cirrhosis [277, 278]. This is thought to occur due to bacterial translocation, SBP and endotoxaemia [271, 273, 279]. Small intestinal bacterial overgrowth in cirrhosis has traditionally been attributed, at least partly, to a decrease in small-bowel motility and intestinal transit time [270, 280-284]. NSBBs have been shown to result in faster intestinal transit and lower rates of bacterial overgrowth and translocation in rats [104]. Although bowel transit and motility have never been directly measured in patients with cirrhosis, a large proportion of patients experience a protective effect from NSBBs regardless of haemodynamic response suggesting there is another unknown mechanism of benefit [101], possibly related to bowel permeability [102]. Reducing portal pressure with NSBBs has a significant protective effective against infection, such as SBP [103].

5.3. Methods for the assessment of In-vivo small bowel permeability

Methods for measuring bowel permeability have employed a variety of measures performed with non-standardised protocols and heterogeneous outcomes [285] that fall short of the recommendations of STARD initiative [171]. In addition, it remains unclear as to whether increased permeability is an epiphenomenon, an early manifestation of disease or a critical step in disease pathogenesis.

In vivo measurement of bowel permeability involves differential excretion of sugars or sugar alcohols that are absorbed in the bowel and poorly metabolised (eg lactulose, mannitol, rhamnose, sucralose etc). Thus measuring the urinary concentrations provides a measure of passive absorption and hence intestinal permeability [286].

5.3.1. Lactulose/Mannitol ratio

The lactulose:mannitol excretion ratio (LMR) is the widest used and most evaluated marker [287, 288]. It measures the urinary excretion of two probes of different sizes, calculating the excretion ratio of a monosaccharide (mannitol) and a disaccharide (lactulose), but with similar transit and uptake processes. LMR has been included as a treatment efficacy endpoint in clinical trials [289, 290].

5.3.2. ^{51}Cr EDTA

An alternative measure is the use of a single isotope 51chromium labelled ethylene-diamine-tetra-acetate (^{51}Cr-EDTA). It shares many of the same physical properties as oligosaccaherides. ^{51}Cr-EDTA is dissolved into water and consumed after an overnight fast. Volumes of urine are recorded and measured for the presence of radioioactivity. Results are expressed as the percent urinary excretion of the orally administered dose of ^{51}Cr-EDTA as a surrogate marker of intestinal permeability. Artificial ^{51}Cr-EDTA does not degrade as it does not undergo fermentation by colonic bacteria.

However, the use of a single probe molecule is thought to not account for inter-individual differences unrelated to permeability (e.g. bowel transit, renal function and tissue distribution) [291]. This can be partially overcome with the use of a standard liquid meal (200 mL/300 kcal of a nutritional supplement Fortisip), which makes inter-individual variability of probe permeation and permeability index very low [292]. Only one comparison study has been performed between LMR and ^{51}Cr-EDTA which showed they were equally suitable, although LMR may be more specific for the small bowel [293].

5.3.3. Confocal Endomicroscopy

Direct visualisation of the bowel wall *in vivo* with confocal endomicroscopy can demonstrate local barrier dysfunction or increased permeability as evidenced by the leakage of fluorescein, peripherally injected contrast agent [294]. Differences can be observed in conditions where the mucosal surface is inflamed, such as in patients with inflammatory bowel disease [295]. The invasive nature of the techniques, its costs and necessary deep sedation required limit this technology to highly selected patients in specialist centres. However, the technology has established the principle of real-time *in*

vivo observation with imaging of disruptions in the bowel wall associated with increased bowel permeability.

5.3.4. CT

Computed Tomography (CT) uses ionising radiation to take a series of cross-sectional images to visualise the bowel *in vivo*. It has been used to visualise the bowel in inflammatory bowel disease [296], and as a quantitative tool of small bowel inflammation [297, 298]. The use of ionising radiation together with injected contrast medium precludes it as a technique for serial measurement for risk stratification.

5.3.5. MRI

MRI has not previously been used to measure bowel permeability directly, but various aspects of bowel structure and function related to bowel permeability can be monitored with MRI. MRI can be used to monitor changes in the bowel wall thickness and inflammation, for instance in relation to Crohn's disease activity [299]. Increased bowel permeability has been associated with active Crohn's disease [300], is reversible with anti-TNF alpha therapy [301] and may occur prior to the onset of disease in susceptible individuals [302]. Contrast-based Magnetic resonance enterography has a diagnostic accuracy of up to 90% to detect ulcer healing in Crohn's disease [303]. The use of gadolinium contrast agents in healthy volunteers however has been limited due to an FDA safety alert regarding the use in humans [304].

There are many publications identifying subjective T_2-weighted measures being important in the MR assessment of the bowel wall, particularly in relation to Crohn's disease. In a meta-analysis of Magnetic Resonance enterography variables, wall T_2 hyperintensity was one of three most consistently specific signs for bowel wall inflammation [305]. In the same meta-analysis, MR parameters with the consistently highest sensitivity were bowel wall thickness, wall T_2 hyperintensity and motility [305].

There is a compelling case for a standardised, widely available, technique of evaluating small bowel permeability to enable experimental studies investigating pathogenic mechanisms underlying diseases as well as to stratify patients for clinical management and evaluate the efficacy of interventions aimed at reducing the consequences of increased gut permeability.

5.4. Hypothesis and Aims:

I hypothesised that there would be detectable differences in quantitative MRI measures of the small bowel which would reflect increased small bowel permeability among healthy volunteers when exposed to indomethacin compared to placebo.

Two relatively small doses of oral indomethacin have been well validated and can safely provoke increase in small bowel permeability [306]. A two week washout period has been demonstrated to be adequate in preventing cross-contamination [288].

Specifically, the aim of the study was to characterise, using non contrast enhanced MRI, any objective differences between the small bowel wall thickness, T_2 relaxometry and motility under both conditions. In the absence of a true gold standard, these measures were compared to LMR as a recognised measure of gut permeability. Given the lack of data, I also evaluated the most evidence based serum biomarkers of increased small bowel permeability as covariates of interest [285].

5.5. Materials and Methods

5.5.1. Design

This was a single centre double blind 2-way crossover provocation study with two doses of 75mg Indomethacin slow release (or placebo) in healthy volunteers (*Figure 5.1*). The study was approved by the University of Nottingham School of Medicine ethics board (Reference number B10112015). The trial ran from April 2016 until December 2016.

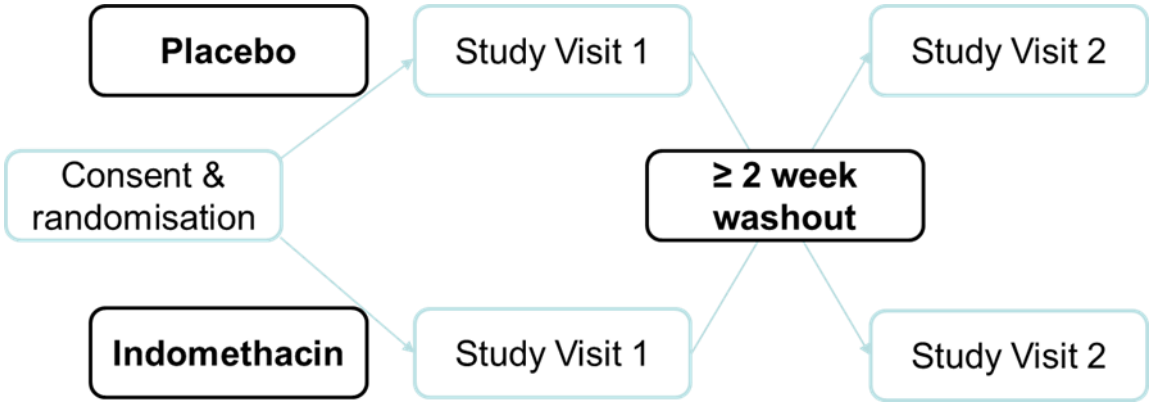

Figure 5.1: Schematic of participant journey through the study

5.5.2. Randomisation and Blinding

Participants were randomised to either treatment first with a 1:1 ratio by a member of the department not directly involved in the study. Participants were randomised into two blocks; the first 8 "training subjects" and the 16 subsequent "validation subjects". The placebo and indomethacin were manufactured to appear identical. Analysis of MRI data, LMR data and serum ELISA data were performed blind. All entries into the study database were made before unblinding occurred.

5.5.3. Participants

Participants were screened for eligibility and consented prior to randomisation. To be eligible participants had to not have any exclusion factors known to increase small bowel permeability.

Exclusion criteria included: pregnancy, chronic gastrointestinal disorders or symptoms, diabetes mellitus (type 1 or 2), smoking, psychiatric disease, coeliac disease, food allergy, history of atopy, allergy or intolerance to non-steroidal anti-inflammatory drugs (NSAIDs), first degree relative with inflammatory bowel disease, coeliac disease or type 1 diabetes mellitus, alcohol dependency, estimated glomerular filtration rate < 45mL/min or any contraindications to MRI. During the last 2 weeks before the study, volunteers were not taking any regular medications other than the contraceptive pill. Participants were informed not to smoke, drink alcohol and refrain from ingestion of all artificial sweeteners for 72 hours prior to either study visit. In addition, all NSAIDs were prohibited throughout the study.

5.5.4. Interventions and Procedures

The order of the procedures is shown in *Figure 5.1* and *Figure 5.2*. To ensure adherence to the study protocol, participants took time-stamped digital images of treatment pill consumption (placebo or indomethacin) 16 hours and 4 hours before the planned midway point of the urinary excretion test (usually 1030). Participants were fasted on the day of the study. A cannula was inserted and blood samples taken prior to a two hour Lactulose/Mannitol urinary excretion test. Subjects emptied their bladders and ingested 5g of lactulose and 2g of mannitol dissolved in 100ml of water. The solution was ingested within 1 minute in the presence of an investigator and within 5 minutes after voiding the bladder. 500ml of water was given 30 minutes after sugar administration to aid in the collection of urine. Water was allowed ad liberatum thereafter. Prior to the MRI scan participants were given oral contrast solution made following a standard operating procedure on the morning of the study (consisting 1L of water, 25g/2.5% Mannitol and 2.0g/0.2% locust bean gum). 500ml was given 45 minutes prior to the start of the MRI scan. A further 500ml was ingested equally over the 15 minutes prior to the start of the MRI sequences to obtain optimal distension of the small bowel and terminal ileum.

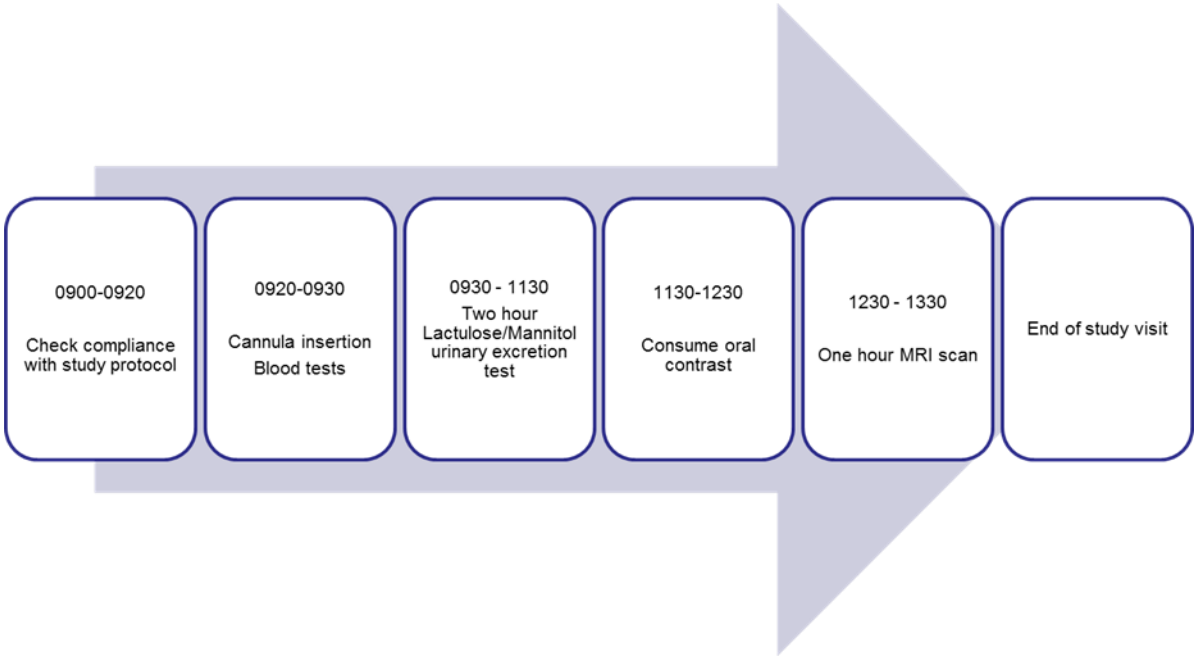

Figure 5.2: Schematic of participant experience during each study visit

5.6. MRI Acquisition

All images were acquired using a whole-body Philips 3T Achieva (N=46) or Phillips 3T Ingenia (N=2) (Philips Healthcare, Netherlands). Participants lay in the prone position with their arms by the head. After acquisition of the anatomical scans to locate the regions of interest, small bowel motility scans are acquired. Subjects are subsequently given two doses of 20mg intravenous Buscopan™ separated by a minimum of 10 minutes. This enables the T_2 and bowel wall thickness acquisition to be acquired without peristalsis degrading image quality.

Images to determine bowel wall thickness are obtained from a balanced Turbo Field Echo (bTFE) sequence covering the whole of the small bowel in two 16 second breath holds. 20 high resolution coronal slices are acquired at resolution 1.2mm × 1.22mm × 3mm with an in plane reconstruction of 0.78mm × 0.78mm. A ET/TR of 1.79/3.59 ms were used. Half fourier acquisition (0.7) and a SENSE factor of 1.5 were used. The field of view (FOV) was 340mm x 352mm.

For the T_2 decay a single slice spin echo prepared bTFE is acquired at echo times of 20, 50, 80, 120, 180, 300ms [307]. The number of echo times is limited by the time that Buscopan™ remains effective (~8 minutes). A ET/TR of 1.68/3.4 ms are used with a flip angle of 50°. The images are acquired at 1.3mm x 1.5mm x 5mm voxel size with half Fourier acquisition (0.625) and in plane reconstruction of 1mm x 1mm. The FOV is 340mm x 350mm. A coronal imaging slice is placed in the plane where the terminal ilium enters the cecum. The positioning limits the amount of SB in the imaging plane however it is chosen to ensure consistency of the image location across the two study days. Each echo time is taken using a separate breath hold with a minimum wait time of 15 seconds between scans to ensure that full recovery of the magnetisation is achieved before the next acquisition.

The method for measuring small bowel wall motility has been published in detail previously [308, 309]. For this study we altered the published protocol. Images are acquired free breathing at a rate of 1 acquisition per second for 60 seconds. A flip angle of 50° is used with a ET/TR of 1.16/2.32. The 7 or 8 image slices are acquired at 1.5mm x 1.5mm x 1mm and in place reconstruction 1mm x 1mm. The

number of slices is set so that the whole small bowel wall is covered. Half Fourier acquisition (0.7) and a SENSE factor of 1.5 were used.

5.7. MRI Analysis

All MRI analysis was performed blinded to the treatment arm allocation.

5.7.1. Small bowel wall thickness

The bTFE image series are reviewed to establish anatomical landmarks (eg terminal ileum, large bowel, small bowel). Developed in house software (IDL® Research Systems Inc, Boulder, CO, USA) is used to calculate the mean small bowel wall thickness. Regions of interest are selected in the right lower quadrant around the terminal ileum at sites of opposing loops of small bowel wall across the whole image series (blue lines in *Figure 5.3*). The programme then automatically calculated the small bowel wall thickness (in mm) along each data point in the region of interest bowel wall segment. A minimum of 200 data points are used in each individual in each quadrant at each study visit and the average of all data points used to calculate the mean small bowel wall thickness (millimetres).

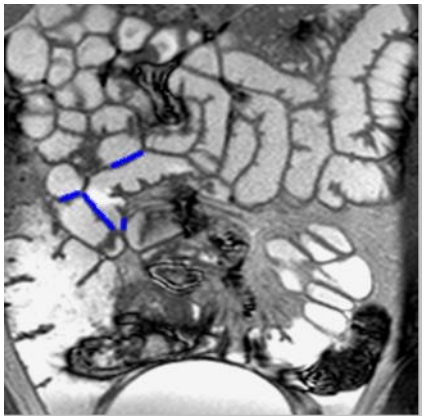

Figure 5.3: Developed in house software (IDL) calculates the mean small bowel wall thickness across >200 profiles on 16 second breath hold balanced Turbo Field Echo (bTFE) sequence high resolution coronal slices (2 breath-holds to cover full anatomy). The blue lines indicate a region where profiles have been acquired between opposing loops of the small bowel in the right lower quadrant.

5.7.2. Small bowel wall T_2

The concept, imaging protocol and analytical tool are subject of intellectual property of the NIHR, Nottingham University Hospitals NHS Trust and the University of Nottingham. This analysis was performed by researchers (Hannah Williams, Caroline Hoad and Penny Gowland) at the Sir Peter Mansfield Imaging Centre.

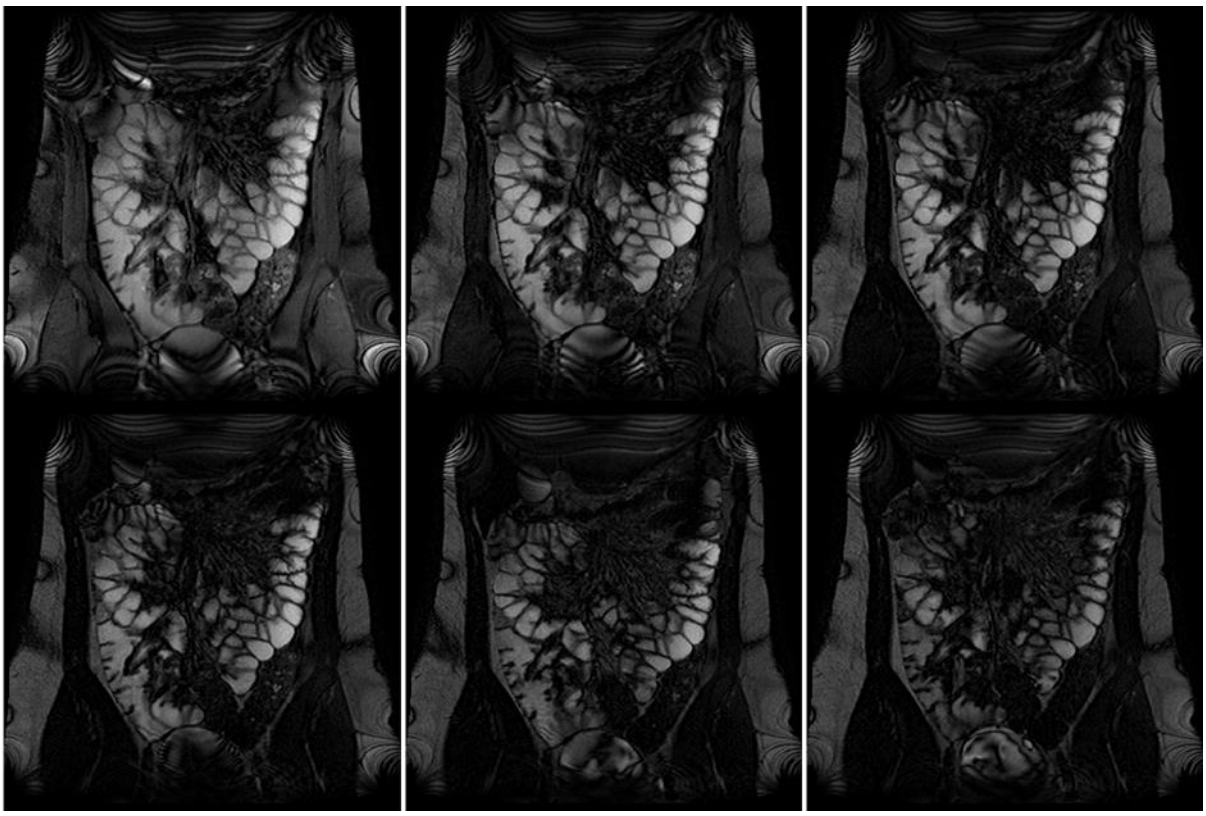

Figure 5.4: T_2 decay with echo times 20, 50, 80, (top left to right) and 120, 180 and 300 ms (bottom left to right) using a T2-prepared bTFE sequence.

Manual drawing of regions of interest along the bowel wall is time consuming and inaccurate. In order for quantitative T_2 to become a viable clinical measure, the analysis is required to be fast and automated. Thus we developed in house software in Matlab to automatically identify the bowel wall from T_2 weighted images. The software creates a map of the wall and then extracts the signal from different segments of the small bowel wall.

Using a series of thresholds and boundary conditions the bowel is isolated by removing subcutaneous fat, muscle and visceral fat (*Figure 5.5*). Following motion correction the location of the small bowel wall is found using edge detection (*Figure 5.6B*). The edges are dilated (*Figure 5.6C*). The contents of the bowel is isolated using thresholding (*Figure 5.6D*). The threshold is determined using histogram analysis to identify a value that enabled separation of the wall and contents. The inverse of the threshold image provided a map of all voxels not containing bowel content (*Figure 5.6E*). The inverted threshold image is multiplied by the dilated edge detection image to provide a map of the bowel wall at every echo time (*Figure 5.6F*). The binary maps of the wall for each echo time are then multiplied together. This created a map of bowel wall voxels that have consistent spatial location across all echo times (*Figure 5.6G*).

The map is visually inspected for false identifications (e.g. vasculature in the mesentery) which are manually removed. Any sections of bowel wall that are broken due to missing voxels in the map are completed by finding edges of lines and connecting any edges that have 1 empty voxel separating them (*Figure 5.6H*) [310]. This results in a completed map of bowel wall spatially consistent throughout all echo times.

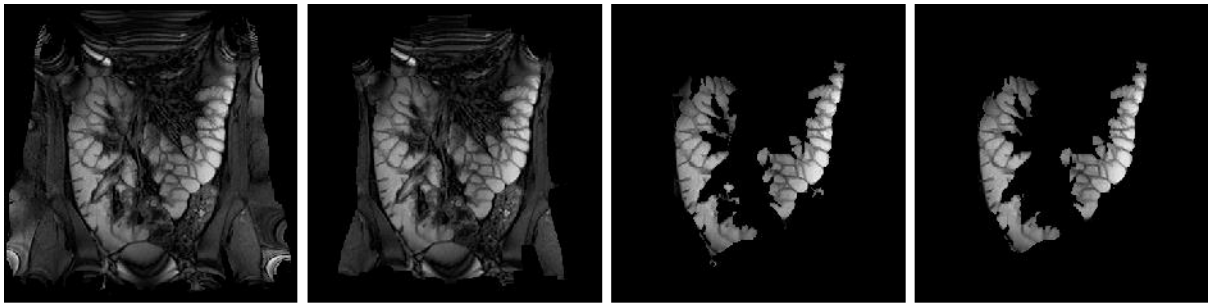

Figure 5.5: Thresholds and boundary conditions to remove (from left to right) noise, subcutaneous fat, muscle and visceral fat to leave the isolated bowel.

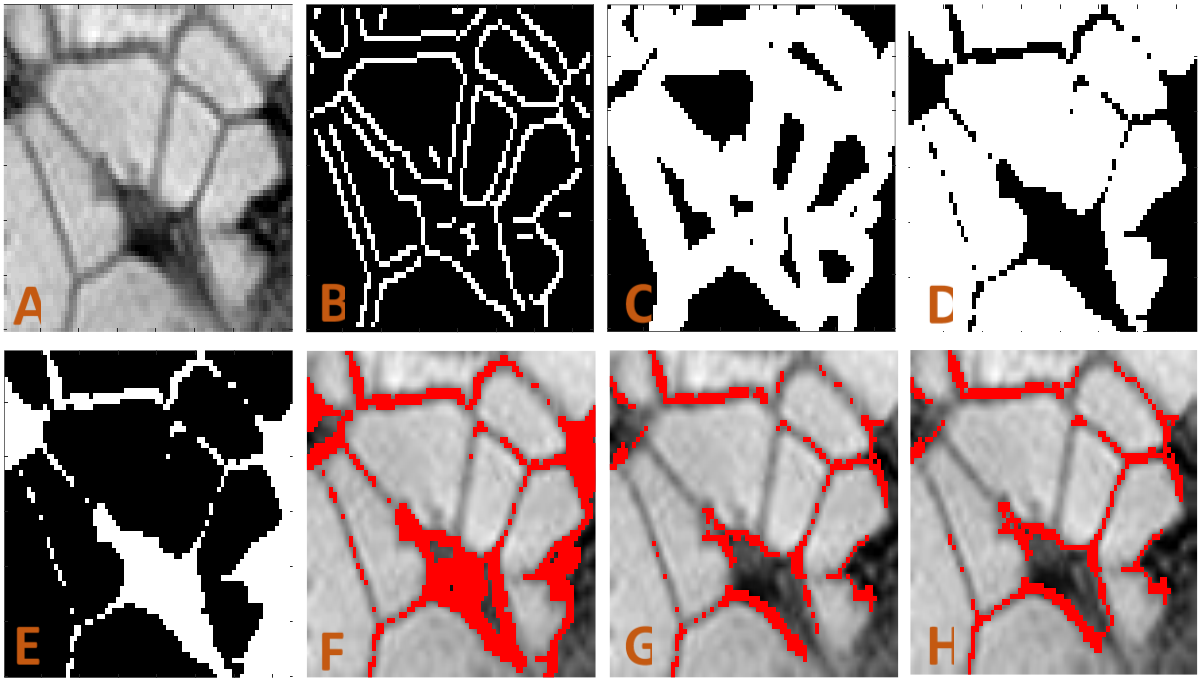

Figure 5.6: A – Close up of bowel wall. B - edge detection. C – Dilated edge detection D – threshold to isolate bowel content E – inverted threshold image F - map of bowel from a single echo time G – map of bowel wall from all echo times H – final map of bowel wall.

To investigate heterogeneity of the small bowel wall the map is automatically segmented into small regions of interest. The signal from each continuous section is analysed separately giving T_2 values for different sections of the bowel wall. Any sections larger than 25 voxels are split into multiple regions to allow for the heterogeneity along the wall to be investigated. Participants in which three or less small sections of bowel wall are identified are removed.

Data points subject to through plane motion are removed by an automated process using the signal of the bowel content to determine whether through plane motion has occurred during acquisition.

To overcome partial volume effects the region of interest data is fitted to a two-compartment model (small bowel and content). The T_2 of the contents is taken as the average T_2 measured from regions of interest of contents. The T_2 fit takes account of the full bTFE readout [307]. T_2 measurements are averaged across all subjects and the standard deviation of the mean calculated. Any region of interest

which has a T_2 more than 5s is deemed an outlier and removed. Any T_2 fit which produces an R squared value of less than 0.9 is also removed.

5.7.3. Small bowel motility

MR measures of small bowel motility and the analysis techniques have been previously published in detail [308, 309]. In brief, Robust Data Decomposition Registration (RRDR) is used as a pre-processing step to remove respiratory motion. The global motility index is determined using GI-Quant® (Motilent, London, UK) on a region of interest which encompasses the whole visible small bowel region across all slices acquired.

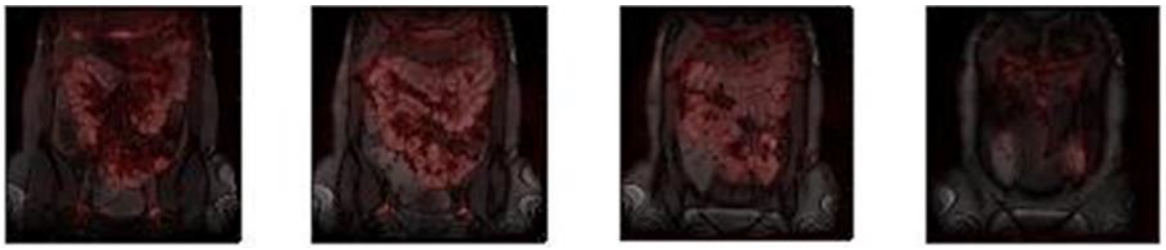

Figure 5.7: Motion corrected mean motility index for global SB measurement overlaid on a single frame from free-breathing CINE acquisition using previously published methods [309].

5.7.4. Small bowel permeability

The in vivo permeability test is a standard differential urinary sugar excretion test using hydrophilic interactions liquid chromatography (HILIC) with electrospray ionization tandem mass spectrometry (ESI-MS/MS) [251, 311]. In brief, after collection the total urine volume is noted and 1.5 mL sample aliquots are filtered with 450 nm filters (Merck Millipore, Billerica, Massachusetts, USA) and stored at −20°C until batch analysis is performed. All the samples are coded without reference to the test condition. The measurements are performed by a lab technician (Catherine Ortori, Centre for Analytical Bioscience, School of Pharmacy, University of Nottingham) blinded to the test condition.

20µl aliquots are diluted to precipitate any excess salt with 980µl 90% acetonitrile to which internal standards xylitol and raffinose are premixed at 0.5µg/ml final concentration. These are vortexed, incubated at -20^{o}C overnight, centrifuged and the supernatant decanted into amber HPLC vials. Calibration standards are made as a dilution series from 2.5 to 500ug/ml of the analytes mannitol and lactulose from stocks made in water. The method is validated by creating 6 independently prepared dilutions of 5, 50 and 500µg/ml. To accurately identify lactulose, sucrose standards are also prepared.

Two LC columns, for convenience, were used in series, a Sequant ZIC®-pHILIC pHILIC 100 x 2.1mm 5µm and a ZIC®-HILIC 150 x 21.mm 5µm kept at 15^{o}C. The mobile phase was A, acetonitrile and B 5mM ammonium acetate adjusted dropwise to pH 6.85 with 0.05% ammonium hydroxide solution. The flow rate is 0.3ml/min. The detector is a Sciex 4000 QTrap operating in –ve ion electrospray mode at with the source at 350^{o}C with curtain, nebuliser and auxiliary gases set to 10, 40 and 20 respectively. The ion-spray voltage is -4200V. As the two analytes are found to have very different ranges of concentrations, samples are quantified against the appropriate region of the line. A minimum of 5 points are used for each analyte.

5.7.5. Serum markers

Serum markers with the strongest evidence base are evaluated; namely Lipopolysaccharide Binding Protein (LBP) an acute phase protein, intestinal fatty acid binding proteins (i-FABP) as a marker of intestinal barrier function and circulating endotoxin core antibodies (EndoCAb) IgG [285]. Serum samples are stored at -80C prior to assaying in duplicate. All enzyme-linked immunosorbent assay (ELISAs) are performed with commercial kits as per the manufacturer's instructions (Hycult® Bioetech, Netherlands). Data values obtained are within assay limits and the coefficient of variance <15%.

5.8. Sample Size and Statistical Analysis

A previous study showed normal mean small bowel thickness is 1.5mm with a standard deviation (SD) of 0.5mm [312]. Assuming a 66% increase in bowel thickness (mean=2.49, SD=1.78) with inflammation as a result of indomethacin [306] would be comparable to active Crohn's disease [305, 313, 314], we

anticipated that 24 patients will give us more than 90% power to reject the null hypothesis with alpha of 0.05 and between group correlation of 0.5.

The data was tested for normality using Shapiro-Wilk's test. Paired testing (either parametric or non-parametric) was then carried out to determine whether paired differences between measures with placebo and indomethacin were significant. Paired differences in small bowel wall thickness (in mm) and motility were compared with Wilcoxon signed rank test and T_2 with a paired t test. Exploratory comparisons between participants were made by the chi-squared test. All statistical analyses were performed using SPSS version 22 (IBM Armonk, NY).

5.9. Results

24 healthy volunteers consented to the study, which consisted of two study visits (Figure 5.1). 15/24 volunteers were female (62.5%). Median age was 23 years (inter-quartile range (IQR) 22 – 25). The median body mass index is 23.7 (21.8 – 27.8) kg/m^2. The median interval between study visits is 21 (18 – 27) days. Two participants are excluded from the per-protocol final analyses as one was non-compliant with the study protocol and one had an incidental finding of an asymptomatic thickened terminal ileum prior to the intervention on review of the MRI data (*Figure 5.8*). This participant was subsequently diagnosed with inflammatory terminal ileal Crohn's disease on colonoscopy, confirmed by histology. No participants suffered any adverse events caused by administration of indomethacin.

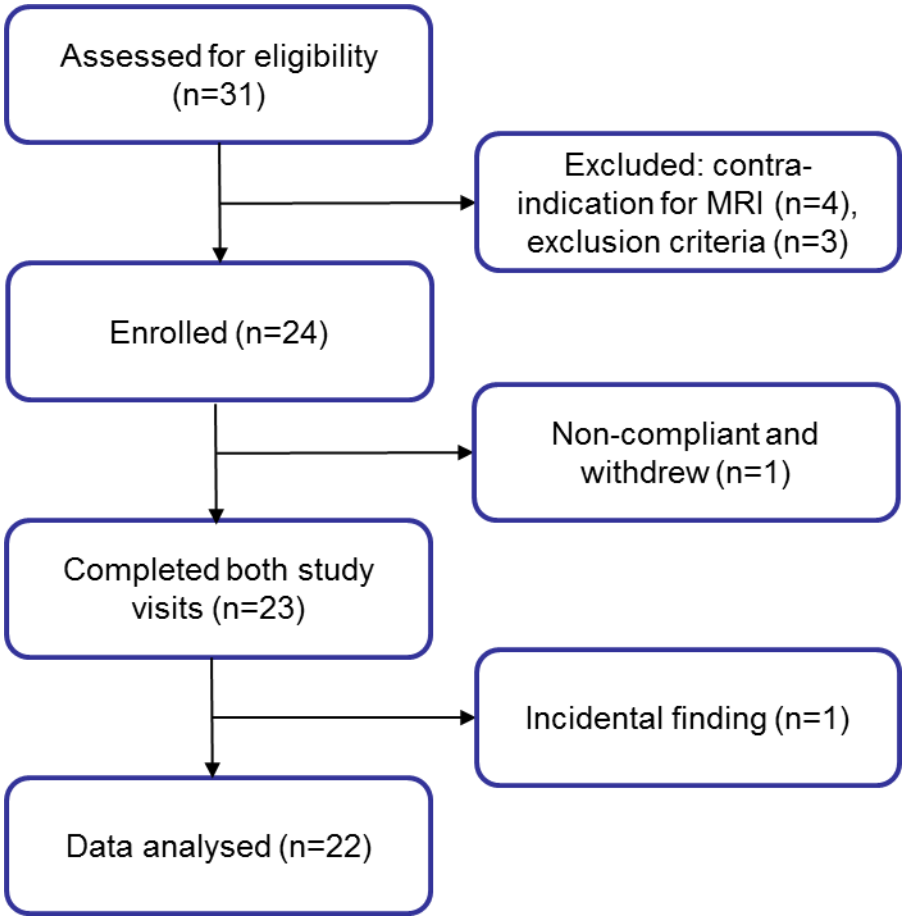

Figure 5.8: CONSORT diagram of study participants.

5.9.1. MRI measures

There is no significant measurable difference between paired small bowel wall thickness in the right lower quadrant of participants between placebo (1.28 mm, IQR 1.21 – 1.36 mm) and provocation with indomethacin (1.29 mm, IQR 1.25 – 1.36 mm), p=0.170. Nor is there a detectable difference between the small bowel wall thickness between placebo (1.27 mm, IQR 1.20 – 1.32 mm) or indomethacin provocation (1.27 mm, IQR 1.18 – 1.42 mm) in the right upper quadrant, p=0.741.

For the T_2 measurements N=6 data sets were note used as they had significant respiratory or bowel motion that could not be corrected. Indomethacin provocation induces a statistically significant increase in small bowel wall T_2 compared to placebo (*Figure 5.9*) (from 70 to 115 ms, p=0.017). The interquartile range of the T_2 measured for each participant increased from 97ms to 147ms with the

administration of indomethacin (p=0.065) (*Figure 5.10*). There is a significant positive correlation between LMR and SB wall T_2 (Pearson correlation coefficient 0.68, p<0.01) (*Figure 5.10*).

Global SB motility showed a decreasing trend with the indomethacin challenge 0.300 (0.251-0.353) to 0.272 (0.253-0.305) with no statistical significance difference, p = 0.149.

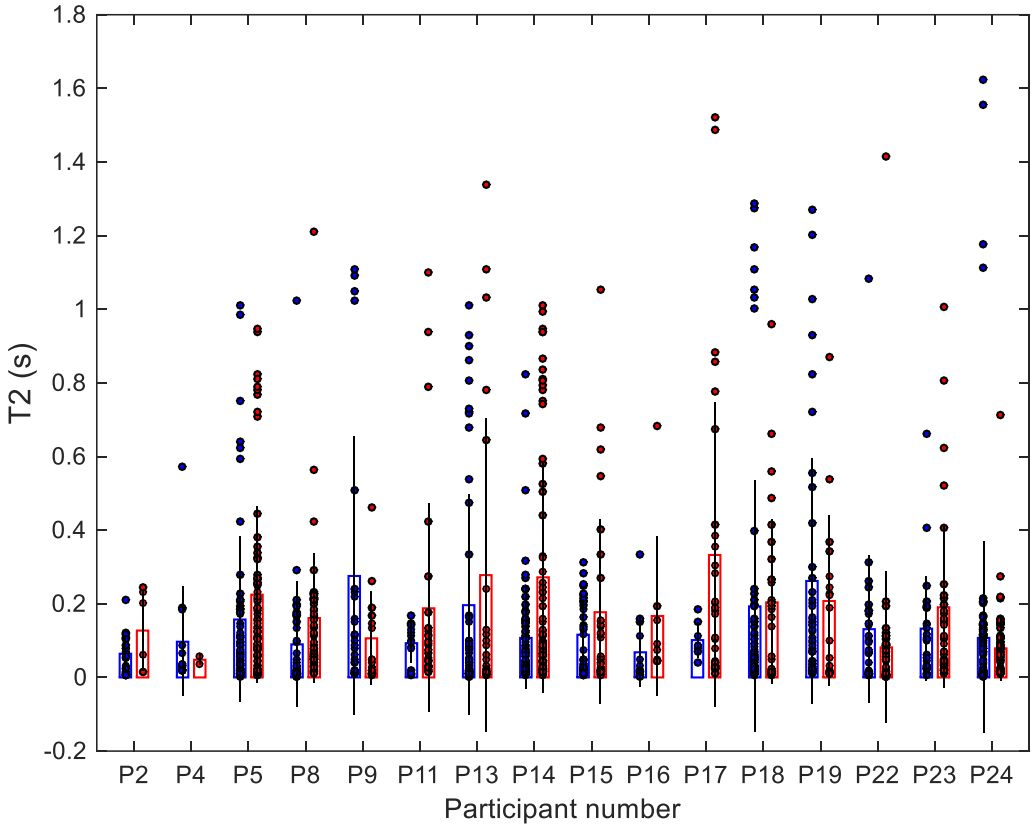

Figure 5.9: Box plots show median placebo (blue) and median indomethacin (red) values of T_2 measurements with the lower and upper quartiles marked by the limits of the box. Circles show individual results for each ROI. Whiskers mark the upper and lower range. Overall placebo median T_2 from all subjects is 70ms and for indomethacin is 115ms. The IQR range of T_2 was 97ms for placebo and 147ms for indomethacin, p=0.065.

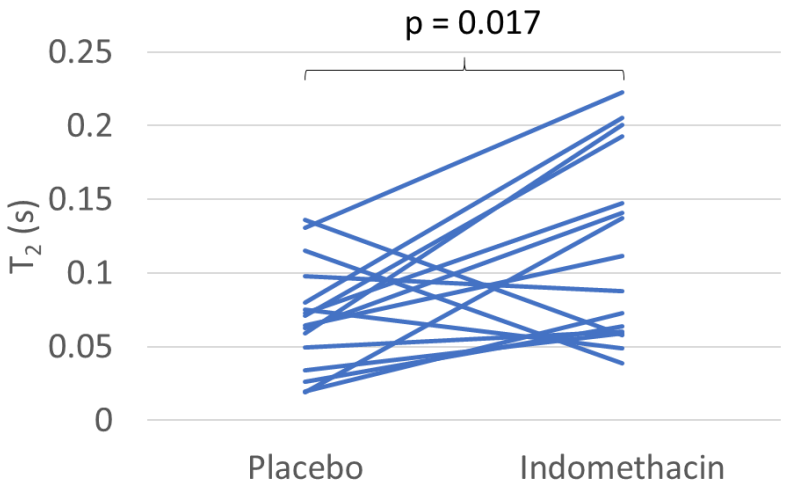
p = 0.017
0.25
0.2
0.15
0.1
0.05
0
T2 (s)
Placebo
Indomethacin

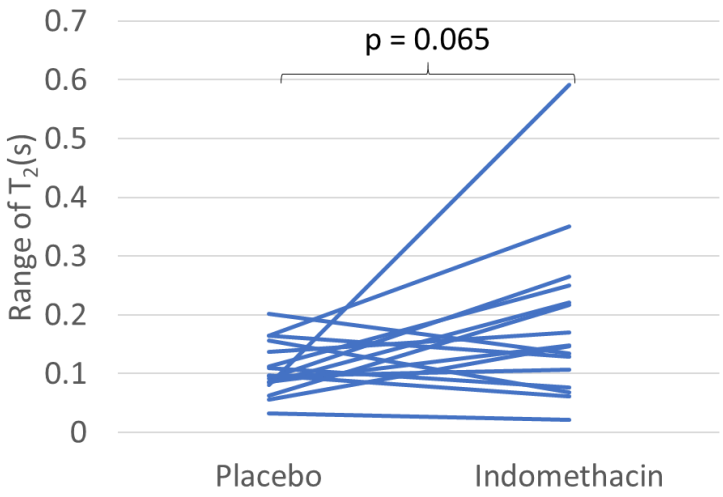
p = 0.065
0.7
0.6
0.5
0.4
0.3
0.2
0.1
0
Range of T2(s)
Placebo
Indomethacin

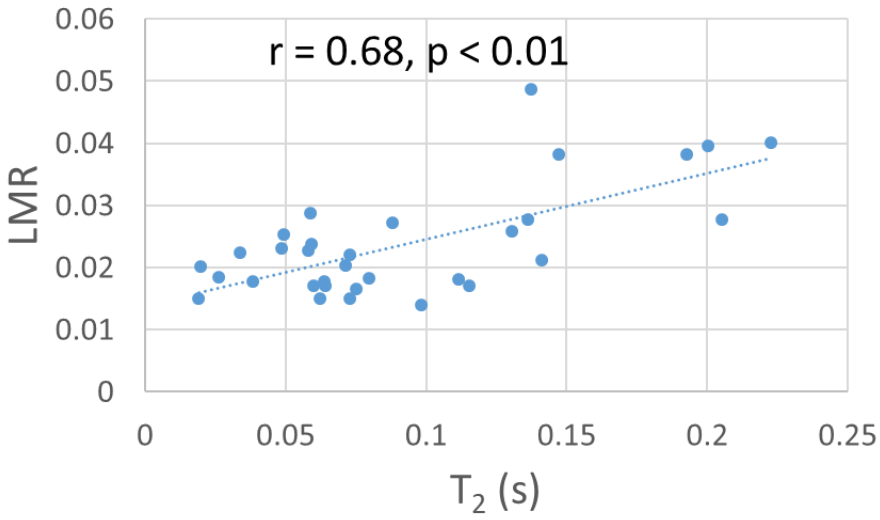
r = 0.68, p < 0.01
0.06
0.05
0.04
0.03
0.02
0.01
0
LMR
0
0.05
0.1
0.15
0.2
0.25
T2 (s)

Figure 5.10: Top-median T_2 for each participant. Middle–range of T_2 across regions of interest for each participant. Bottom-correlation of median T_2 for each participant and LMR

5.9.2. LMR results

The LMR in the urine collection of the first two hours after ingestion of the respective sugars was used to quantify the small bowel permeability [286, 287]. As expected, two oral doses of indomethacin significantly increased the small bowel permeability [288]. Indomethacin induced significant changes from placebo in LMR from 0.019 (IQR 0.016-0.026) to 0.025 (IQR 0.021-0.039) (p=0.002).

5.9.3. Serum biomarkers

Three potential serum indicators of bacterial translocation: LBP, iFABP and endoCab-IgG, were determined in the study samples. There were no significant differences in the levels of these markers in paired indomethacin provocation or placebo samples (*Table 5.1*).

Commercial ELISA	**Placebo**	**Provocation with indomethacin**	**Statistical significance**
LBP (ng/ml)	12.0 (10.7 – 15.1)	12.4 (10.9 – 17.5)	p = 0.550
EndoCab IgG (GMU/ml)	0.447 (0.254 – 0.546)	0.473 (0.357 – 0.545)	p = 0.455
i-FABP (pg/ml)	256.5 (220.1 – 434.9)	290.1 (241.0 – 495.0)	p = 0.109

Table 5.1: Levels of LBP, endoCab IgG and i-FABP in serum after provocation with indomethacin or placebo. The proposed paired serum biomarkers are of bacteria-related markers, epithelial cell integrity, intestinal inflammation and immune activation. None showed any statistically significant difference between study visits. Lipopolysaccharide

Binding Protein (LBP), intestinal fatty acid binding proteins (i-FABP) and circulating endotoxin core antibodies (EndoCAb) IgG.

5.10. Discussion

In a randomised, double blind, placebo controlled, prospective cross-over provocation study with indomethacin in healthy volunteers, I have shown that objective MRI measures of small bowel wall T_2 relaxometry are increased following indomethacin provocation and these correlated with increased permeability as demonstrated by a 2 hour Lactulose/Mannitol urinary excretion ratio (LMR), the current standard method of evaluating small bowel permeability. Other MRI measures of small bowel wall thickness and motility remained unchanged with indomethacin provocation. Indomethacin provocation did not significantly change any of the serum ELISA biomarkers. Thus, I have shown that a novel quantitative measure of small bowel wall T_2 is a sensitive marker of bowel wall inflammation associated with increased gut permeability (as measured by the LMR). Objective small bowel wall measures of wall thickness and motility are reproducible in healthy volunteers but two small doses of Indomethacin was not a sufficient provocation to induce measurable changes in either of these measures nor commercial serum ELSIA biomarkers.

This study has several strengths. A prospective, double blind, cross-over study design minimises confounding and increases the power of the study. The observed differences are therefore most likely caused by provocation with indomethacin. All the participants were well selected healthy volunteers. All analysis was performed blinded to treatment allocation and compared to small bowel permeability as defined by 2 hour LMR, the current gold standard measure of small bowel permeability [251, 285]. Each MRI measure is quantitative, bringing greater weight and credibility to the study findings when compared with commonly used qualitative MRI measures used to describe the small bowel. These MRI techniques do not require administration of intravenous contrast and are therefore safe and appropriate for repeated measurements - especially in the context of recent FDA warnings [304]. The protocols are based on widely available scan sequences and as such could be rapidly adopted into clinical pathways and research programmes.

Whilst two doses of indomethacin is safe and does increase small bowel permeability of small sugars [288, 306] the relatively low dose may be too transient and subtle to cause bacterial translocation or to mimic the structural changes of the small bowel associated with disease. This may explain why none of the commercial serum markers claimed to be surrogates to bacterial translocation in the literature showed any significant change (Table 5.1). Higher or more frequent doses of oral NSAIDs are known to cause variable patchy small bowel erosions [315, 316] which may also explain the heterogeneity and intra subject range of the small bowel wall T_2 measurements (suggested by the IQR differences in T_2 measures between the two conditions). Combined with previous MR data in Crohn's [299, 305, 313, 314, 317], it is reasonable to assume the increased small bowel wall T_2 may reflect oedema of the small bowel wall causing the integrity of the barrier function to become impaired.

Both MRI parameters and 2 hour Lactulose/Mannitol urinary excretion ratio (LMR) changed significantly following indomethacin provocation test, vindicating the choice of the latter method. The moderate correlation between the MRI results and the LMR test is expected since the results of LMR are not a continuous outcome variable and is sensitive to whole bowel permeability not just the small bowel. Although LMR is the most used measure of small bowel permeability, it does have known shortcomings. First, up to 30% of participants have detectable urinary mannitol at baseline (prior to administration of test sugars) or disproportionate excretion relative to the mass of mannitol administered for the test. This is thought to be as a result of inadvertent ingestion of mannitol in diet or medications [318]. Second, measurement at 0-2 hours is mostly, but not exclusively, a measure of small bowel permeability and may partially reflect colonic permeability.

The developed analysis tools for small bowel wall T_2 automatically motion corrects and isolates the bowel wall for objective quantitative analysis, but does require manual quality control to remove misidentified regions of wall. The remaining MR analysis tools require manual selection of regions of interest which is inherently subjective and only partly addressed by averaging several regions of interest in each subject. Lastly, inherent to the *in vivo* study design, it is not possible to elucidate the

microstructural details of the changes in the small bowel wall that are associated with increased permeability.

For the first time, this study suggests non-contrast quantitative MR measures of small bowel wall T_2 could be a sensitive biomarker associated with increased permeability. If validated in patients and linked with clinical outcomes, this newly developed MRI tool to evaluate small bowel permeability in-vivo has far reaching applications. A widely available, non-invasive, in-vivo measure of small bowel structure and integrity would be an important tool for mechanistic studies as well as evaluate efficacy of specific interventions. Arguably the lack of robust, accessible and affordable biomarkers of these potentially pathophysiological changes has hampered research in this area.

The three candidate markers (LBP, EndoCab IgG and i-FABP) tested in this study did not indicate any change in small bowel permeability associated with indomethacin. LBP) is a type 1 acute phase protein marker, with elevated levels associated with ischaemic heart disease [319] and chronic liver disease [320] Circulating endotoxin core antibodies to gram negative bacteria (EndoCab IgG) are an acute phase surrogate marker of intestinal barrier damage, demonstrated to reduce post-operatively [321, 322]. Intestinal fatty acid binding proteins (i-FABP) reflect the physiological turnover of enterocytes [285]. Increased levels indicate epithelial cell damage and are reported in bowel ischaemia [323], systemic inflammatory response syndrome [324, 325], liver transplantation [326] and coeliac disease [327, 328].

In summary, I have developed non-contrast MRI techniques that can sensitively measure in-vivo small bowel wall thickness and T_2 relaxometry in healthy volunteers. MR measures of small bowel wall T_2 are significantly increased in association with increased gut permeability following indomethacin provocation. The method used here for mapping the small bowel wall is not restricted to T_2 weighted images but can be applied to any images in which the small bowel content and wall have a different signal intensity. These newly developed measures can now be applied to characterise the changes of the small bowel in patients with advanced chronic liver disease associated with increased gut

permeability. The findings need to be validated and the hypothesis will be tested in future studies with patients in whom increased permeability and bacterial translocation are thought to be clinically significant. Quantitative *in vivo* measures of the changes in the small bowel can now be measured. This will enable understanding of the mechanisms associated with both portal hypertension and gut permeability believed to underpin bacterial translocation in patients with advanced chronic liver disease. This is believed to be a key prognostic event precipitating decompensation and life threatening complications but remains an area where there is currently no test to help risk stratify. Performance characteristics of the newly developed MR measures to predict clinical outcomes related to increased bowel permeability can now be evaluated in a longitudinal cohort of patients with cirrhosis. A widely available validated measure would permit researchers to investigate mechanisms of bacterial translocation, risk stratify patients and evaluate the efficacy of interventions.

6 Overall Discussion

6.1 Summary of findings in this thesis

- Chapter 3 demonstrated non-invasive quantitative MRI measures significantly correlate with portal pressure in patients with suspected portal hypertension. In a well characterised patient population, a combination of MR measures of iron corrected liver T_1 relaxation time and superior mesenteric artery velocity significantly correlate with the invasive HVPG measurement. This finding validates our previous published work at a lower field strength. In addition, Splenic T_1, Splenic artery flow significantly correlate with HVPG. Cardiac Index and Azygous flow appear to become important at certain ranges of HVPG. Combining this data with the derivation data showed a field strength dependent ceiling effect of structural measures and a reduction in SMA and splenic artery velocity >15 mmHg. This may signify a transition in the development of a hyperdynamic circulation. More data is required to build a complex model to accurately measure HVPG >15 mmHg with these MR measures and measure the efficacy of interventions.
- Chapter 4 evaluated Multiparametric MRI in patients with cirrhosis caused by chronic Hepatitis C and the observed effect of interventions with Direct Acting Antiviral treatments. In a time window of 3-6 months between pre- and post-treatment scans, there were significant changes in hepatic composition. Liver T_1, T_2 and liver perfusion all significantly reduced. These measures are likely linked to reduced pro-inflammatory milieu, including interstitial oedema, within the liver. By chance, seven patients were diagnosed with hepatocellular carcinoma (HCC) after starting DAA treatment in whom pre-treatment MRI lesions could be identified on the research scans.
- Chapter 5 showed the development of novel quantitative MRI measures compared to currently available measures of small bowel permeability. Provocation with enteral Indomethacin administration, an accepted positive control for experimental medicine studies, was used to compare the MRI measures to bowel permeability

assessed by the Lactulose/Mannitol urinary excretion ratio (LMR). Only small bowel wall T_2 significantly increased and correlated with increased LMR following indomethacin administration.

6.2 Interpretation and clinical consequences

Overall this thesis has highlighted the shortcomings of our ability to stratify patients with advanced liver disease. In terms of clinical outcomes the best currently available tool is HVPG, a surrogate measure of portal pressure. However, this measure is invasive, expensive and restricted to specialist centres. Several non-invasive measures can be used to dichotomise patients with and without clinically significant portal hypertension but all have their limitations [166]. The introduction of TE in clinical practice has allowed the early identification of patients with advanced chronic liver disease at risk of developing clinically significant portal hypertension, without the need to undergo a liver biopsy. The Baveno VI guidelines proposed a new alternative term “compensated advanced chronic liver disease (cACLD)” in asymptomatic patients [68]. Once diagnosed, there is a desperate need to stratify these patients with widely available non-invasive tools into those who can be monitored and those who require invasive tests (eg varices surveillance) and interventions to improve outcomes. There are a variety of poorly validated competing non-invasive measures for this role [118](outlined in Chapter 1.9). The most promising measures to date, developed by the Chinese portal hypertension group (CHESS), require ionising radiation with CT [131, 132] unsuitable for the repeated measures necessary for adoption into routine clinical care.

The work presented suggests quantitative, contrast free, MRI measures could offer a widely available non-invasive alternative to stratify patients with cACLD beyond a simple dichotomisation offered by competing non-invasive measures and characterise the haemodynamic changes that contribute to portal pressure and the hyperdynamic state along a continuous scale. A non-invasive model derived from a targeted short (10-15 minute) MRI sequence including both architectural (liver T_1 relaxation time) and splanchnic haemodynamic (SMA velocity) measures together with other factors (Splenic T_1,

azygous vein flow, cardiac index) could be used as a surrogate measure of HVPG in clinical trials of portal hypertension as well as monitoring efficacy of treatment in clinical practice. These MRI measures can be performed without the need to purchase additional hardware and so could potentially be accessed outside traditional expert centres. This validation of a previous study's findings at lower field strength [134] suggests MRI measures can be used across field strengths commonly available in clinical centres to provide an estimate of portal pressure. A more complex algorithm with hierarchal or machine learning or multiple measures of the mulita-organ hyperdynamic state that results from portal hypertension is required to make a comprehensive individual assessment and stratification of therapy. It may be that non-invasive multi-organ MR measures can be combined to define the proposed therapeutic window for beta-blockers [114]. The data requires external validation across MRI platforms in order to become an accepted surrogate measure of portal pressure and established end point of clinical trials.

In an era of emerging anti-fibrotic therapies, MRI is shown to be a sensitive marker of liver scarring and inflammation that can detect immediate differences after treatment of chronic hepatitis C viral infection with direct acting anti-virals. A multi-modal technique including MRI that captures how the different aspects of liver composition, perfusion and blood flow change over time could provide additional confidence for clinical decision making. In addition, robust non-invasive tests that are specific to the liver would be valuable to drug development for anti-fibrotic compounds as they can be repeated at multiple time points to evaluate drug efficacy.

The added ability to visualise lesions later diagnosed as hepatocellular carcinomas also suggests a potential role for MR measures to also incorporate HCC screening. It is likely to be very hard to supplant current contrast-enhanced MRI for characterisation of focal liver lesions identified by screening. If patients were to undergo regular MRI scanning to stratify risk as part of their routine clinical care in the future, however, it may offer a more sensitive screening tool than ultrasound to identify liver lesions for further evaluation.

Lastly, the development of bacterial translocation is believed to be a key prognostic event precipitating decompensation and life threatening complications in patients with advanced chronic liver disease [29]. There is no validated test currently available to identify those patients at risk of either bacterial translocation or the life-threatening clinical sequalae. If validated in patients and linked with clinical outcomes, the newly developed MRI tool to evaluate small bowel permeability in-vivo has far reaching applications. A widely available, non-invasive, in-vivo measure of small bowel structure and integrity would be an important tool for mechanistic studies as well as to evaluate efficacy of specific interventions. Arguably the lack of robust, accessible and affordable biomarkers of these potentially pathophysiological changes has hampered research in this key area of liver cirrhosis.

6.3 Future work

I have identified and planned four initial avenues of investigation following this thesis.

6.3.1 Portal pressure

The key question for any non-invasive measure of portal pressure is whether it can stratify clinical outcomes and evaluate the efficacy of interventions. In order to assess this paired quantitative MRI measures and invasive HVPG will need to be taken in patients with oesophageal varices that require primary prophylaxis before and after treatment with non-selective beta-blockers. Any change in portal pressure will be compared with any changes observed in quantitative MRI measures along a continuous spectrum to evaluate haemodynamic response [99]. In addition, clinical outcomes for 5 years after enrolment to the study should be recorded to evaluate prognostic performance of quantitative MRI measures.

6.3.2 Fibrosis and inflammation

In an era of novel anti-fibrotic therapy on the horizon, robust non-invasive biomarkers for use in patients with advanced liver disease to understand the structural and functional changes in the liver and stratify ongoing risk post intervention to focus future interventions are required. Ethical and practical constraints limit serial liver biopsy sampling but is the only currently accepted measure of changes in liver composition over time. There are two potential longitudinal studies that would enable study of MRI measures to be directly compared with histopathological changes to study the effect of interventions and quantify any fibrosis regression. First is a longitudinal study of patients with advanced chronic liver disease caused by an aetiology where an intervention may change the natural history of the disease, such as alcohol cessation, obesity surgery, or commencing highly effective anti-viral medications (e.g. in patient with chronic hepatitis B or C virus infection). It would require at least two separate parallel assessments of histology and MRI measures before and after intervention with an adequate time interval to show meaningful change, a subject of much debate at present [329]. The

second potential study could use a liscensed anti-fibrotic or disease modifying medication that was shown to cause fibrosis reversal on serial biopsies, but none are currently available.

6.3.3 HCC

In chapter 4, non-contrast mDIXON sequences detected liver lesions that were subsequently diagnosed as hepatocellular carcinomas. Diffusion weighted imaging (DWI), a method deriving its image contrast from differences in the motion of water molecules between tissues, is known to be able to sensitively detect HCCs [330-332]. Current international guidelines recommend the use of intravenous contrast to diagnose HCCs [245, 333]. All patients diagnosed with HCCs at a multi-disciplinary team meetings could be invited to participate in a study which compares clinical scans with contrast to contrast-free MR sequences (liver T_1, mDIXON, DWI) to ascertain the most specific non-contrast sequences for HCC screening. The most sensitive MRI sequences could then be compared to standard of care screening with ultrasound to detect HCCs in patients with liver cirrhosis.

6.3.4 Small bowel permeability

Diffusion weighted imaging (DWI) was not available on our 3T Philips scanner at the time of the study. DWI is a well-tolerated, non-time-consuming and accurate tool for detecting and assessing inflammation in small bowel Crohn's disease that does not require intravenous gadolinium administration [313, 314]. MRI using magnetization transfer (MT) is another promising technique that allows image contrast to be generated based on the interactions between the protons in free water and those of large immobilized macromolecules, such as collagen [334]. MT has been shown to be a sensitive marker of bowel fibrosis and inflammation in animal models of Crohn's disease [334, 335] and more recently in humans with Crohn's [336, 337]. The diagnostic accuracy of MT is not yet fully elucidated and the protocol was not available at our unit at the time of this study.

Both non-contrast techniques should be compared to the developed MR protocols described in this work to evaluate the best *invivo* biomarker of bacterial translocation with prognostic importance in a patient study. It is worth stressing that the work to date has demonstrated a correlation of MR

measures with increased small bowel permeability, as defined by LMR, but that bacteria and their products are much larger molecules. All available techniques should be applied to a patient population in whom it is believed bacterial translocation is important to outcomes (e.g. cirrhosis or Crohn's disease). This will enable the best available biomarker to be taken forward to diagnostic, prognostic and therapeutic studies.

6.4 Conclusion

This thesis provides data that suggests a non-contrast MRI scan may uniquely be able to simultaneously evaluate multiple measures of prognostic importance in patients with chronic liver disease including liver fibrosis, portal pressure, the development of a hyperdynamic circulation, small bowel permeability and hepatocellular carcinoma surveillance. These findings need to be validated, optimised and shown to evaluate efficacy of interventions in order to lead to clinical adoption. MRI has the potential to be a key non-invasive tool to evaluate the efficacy of interventions in chronic liver disease and stratify patients according to the potential clinical outcomes.

7. References

1. Williams, R., et al., *Addressing liver disease in the UK: a blueprint for attaining excellence in health care and reducing premature mortality from lifestyle issues of excess consumption of alcohol, obesity, and viral hepatitis.* The Lancet, 2014. **384**(9958): p. 1953-1997.
2. Williams, R., et al., *Implementation of the Lancet Standing Commission on Liver Disease in the UK.* Lancet, 2015. **386**(10008): p. 2098-2111.
3. Vernon, G., A. Baranova, and Z.M. Younossi, *Systematic review: the epidemiology and natural history of non-alcoholic fatty liver disease and non-alcoholic steatohepatitis in adults.* Aliment Pharmacol Ther, 2011. **34**(3): p. 274-85.
4. Ratib, S., et al., *1 and 5 year survival estimates for people with cirrhosis of the liver in England, 1998-2009: a large population study.* J Hepatol, 2014. **60**(2): p. 282-9.
5. Care., N.H.S.R., *Liver disease: the NHS atlas of variation in healthcare for people with liver disease.* 2013.
6. England, P.H. *Liver Disease Profiles*. 2016; Available from: http://fingertips.phe.org.uk/profile/liver-disease.
7. Bhala, N., G. Aithal, and J. Ferguson, *How to tackle rising rates of liver disease in the UK.* Bmj, 2013. **346**: p. f807.
8. Bhathal, P.S. and H.J. Grossman, *Reduction of the increased portal vascular resistance of the isolated perfused cirrhotic rat liver by vasodilators.* J Hepatol, 1985. **1**(4): p. 325-37.
9. Garcia-Pagan, J.C., J. Gracia-Sancho, and J. Bosch, *Functional aspects on the pathophysiology of portal hypertension in cirrhosis.* Journal of Hepatology, 2012. **57**(2): p. 458-461.
10. Desmet, V.J. and T. Roskams, *Cirrhosis reversal: a duel between dogma and myth.* J Hepatol, 2004. **40**(5): p. 860-7.

11. Iwakiri, Y., V. Shah, and D.C. Rockey, *Vascular pathobiology in chronic liver disease and cirrhosis – Current status and future directions.* Journal of Hepatology, 2014. **61**(4): p. 912-924.
12. Ribatti, D. and E. Crivellato, *"Sprouting angiogenesis", a reappraisal.* Dev Biol, 2012. **372**(2): p. 157-65.
13. Dill, M.T., et al., *Disruption of Notch1 induces vascular remodeling, intussusceptive angiogenesis, and angiosarcomas in livers of mice.* Gastroenterology, 2012. **142**(4): p. 967-977.e2.
14. Arroyo, V. and J. Colmenero, *Ascites and hepatorenal syndrome in cirrhosis: pathophysiological basis of therapy and current management.* Journal of Hepatology, 2003. **38**: p. 69-89.
15. Moller, S. and F. Bendtsen, *The pathophysiology of arterial vasodilatation and hyperdynamic circulation in cirrhosis.* Liver Int, 2018. **38**(4): p. 570-580.
16. Moller, S., et al., *Determinants of the hyperdynamic circulation and central hypovolaemia in cirrhosis.* Gut, 2011. **60**(9): p. 1254-9.
17. Bernardi, M., et al., *Mechanisms of decompensation and organ failure in cirrhosis: From peripheral arterial vasodilation to systemic inflammation hypothesis.* J Hepatol, 2015. **63**(5): p. 1272-84.
18. McAvoy, N.C., et al., *Differential visceral blood flow in the hyperdynamic circulation of patients with liver cirrhosis.* Aliment Pharmacol Ther, 2016. **43**(9): p. 947-54.
19. Moller, S. and J.H. Henriksen, *Cardiovascular complications of cirrhosis.* Gut, 2008. **57**(2): p. 268-78.
20. Rabie, R.N., et al., *The use of E/A ratio as a predictor of outcome in cirrhotic patients treated with transjugular intrahepatic portosystemic shunt.* Am J Gastroenterol, 2009. **104**(10): p. 2458-66.
21. Carvalheiro, F., et al., *Diastolic Dysfunction in Liver Cirrhosis: Prognostic Predictor in Liver Transplantation?* Transplant Proc, 2016. **48**(1): p. 128-31.
22. Gines, P. and R.W. Schrier, *Renal failure in cirrhosis.* N Engl J Med, 2009. **361**(13): p. 1279-90.

23. Stadlbauer, V., et al., *Relationship between activation of the sympathetic nervous system and renal blood flow autoregulation in cirrhosis.* Gastroenterology, 2008. **134**(1): p. 111-9.

24. Krag, A., et al., *Low cardiac output predicts development of hepatorenal syndrome and survival in patients with cirrhosis and ascites.* Gut, 2010. **59**(1): p. 105-10.

25. Machicao, V.I., M. Balakrishnan, and M.B. Fallon, *Pulmonary complications in chronic liver disease.* Hepatology, 2014. **59**(4): p. 1627-37.

26. de Franchis, R., *Evolving consensus in portal hypertension. Report of the Baveno IV consensus workshop on methodology of diagnosis and therapy in portal hypertension.* J Hepatol, 2005. **43**(1): p. 167-76.

27. Fleming, K.M., et al., *All-cause mortality in people with cirrhosis compared with the general population: a population-based cohort study.* Liver Int, 2012. **32**(1): p. 79-84.

28. Fleming, K.M., et al., *The rate of decompensation and clinical progression of disease in people with cirrhosis: a cohort study.* Aliment Pharmacol Ther, 2010. **32**(11-12): p. 1343-50.

29. D'Amico, G., G. Garcia-Tsao, and L. Pagliaro, *Natural history and prognostic indicators of survival in cirrhosis: a systematic review of 118 studies.* J Hepatol, 2006. **44**(1): p. 217-31.

30. Pugh, R.N., et al., *Transection of the oesophagus for bleeding oesophageal varices.* Br J Surg, 1973. **60**(8): p. 646-9.

31. Christensen, E., et al., *Prognostic value of Child-Turcotte criteria in medically treated cirrhosis.* Hepatology, 1984. **4**(3): p. 430-5.

32. Malinchoc, M., et al., *A model to predict poor survival in patients undergoing transjugular intrahepatic portosystemic shunts.* Hepatology, 2000. **31**(4): p. 864-71.

33. Yoo, H.Y., D. Edwin, and P.J. Thuluvath, *Relationship of the model for end-stage liver disease (MELD) scale to hepatic encephalopathy, as defined by*

electroencephalography and neuropsychometric testing, and ascites. Am J Gastroenterol, 2003. **98**(6): p. 1395-9.

34. Huo, T.I., et al., *Limitation of the model for end-stage liver disease for outcome prediction in patients with cirrhosis-related complications.* Clin Transplant, 2006. **20**(2): p. 188-94.
35. Kamath, P.S., et al., *A model to predict survival in patients with end-stage liver disease.* Hepatology, 2001. **33**(2): p. 464-70.
36. Ekstedt, M., et al., *Fibrosis stage is the strongest predictor for disease-specific mortality in NAFLD after up to 33 years of follow-up.* Hepatology, 2015. **61**(5): p. 1547-54.
37. Ripoll, C., et al., *Hepatic venous pressure gradient predicts clinical decompensation in patients with compensated cirrhosis.* Gastroenterology, 2007. **133**(2): p. 481-8.
38. Parkes, J., et al., *Enhanced liver fibrosis test can predict clinical outcomes in patients with chronic liver disease.* Gut, 2010. **59**(9): p. 1245-51.
39. Naveau, S., et al., *Diagnostic and prognostic values of noninvasive biomarkers of fibrosis in patients with alcoholic liver disease.* Hepatology, 2009. **49**(1): p. 97-105.
40. Vergniol, J., et al., *Noninvasive tests for fibrosis and liver stiffness predict 5-year outcomes of patients with chronic hepatitis C.* Gastroenterology, 2011. **140**(7): p. 1970-9, 1979 e1-3.
41. Robic, M.A., et al., *Liver stiffness accurately predicts portal hypertension related complications in patients with chronic liver disease: a prospective study.* J Hepatol, 2011. **55**(5): p. 1017-24.
42. Angulo, P., et al., *Simple noninvasive systems predict long-term outcomes of patients with nonalcoholic fatty liver disease.* Gastroenterology, 2013. **145**(4): p. 782-9.e4.
43. Asrani, S.K., et al., *Role of magnetic resonance elastography in compensated and decompensated liver disease.* J Hepatol, 2014. **60**(5): p. 934-9.

44. Pavlides, M., et al., *Multiparametric magnetic resonance imaging predicts clinical outcomes in patients with chronic liver disease.* Journal of Hepatology, 2016. **64**(2): p. 308-315.

45. Bradley, C.R., et al., *Multi organ assessment of Compensated Cirrhosis Patients using quantitative Magnetic Resonance Imaging.* J Hepatol, 2018.

46. Castera, L., M. Pinzani, and J. Bosch, *Non invasive evaluation of portal hypertension using transient elastography.* J Hepatol, 2012. **56**(3): p. 696-703.

47. Castera, L. and M. Pinzani, *Biopsy and non-invasive methods for the diagnosis of liver fibrosis: does it take two to tango?* Gut, 2010. **59**(7): p. 861-6.

48. Torok, N.J., et al., *Strategies and endpoints of antifibrotic drug trials: Summary and recommendations from the AASLD Emerging Trends Conference, Chicago, June 2014.* Hepatology, 2015. **62**(2): p. 627-34.

49. Hallion, L. and C.A. Francois-Frank, *Research experiments carried out in the aid of a novel volumetric apparatus on the vaso-motor innervation of the intestine. .* Arch Physiol Norm Pathol., 1896. **8**: p. 493-508.

50. Myers, J.D. and W.J. Taylor, *An estimation of portal venous pressure by occlusive catheterization of a hepatic venule. .* J Clin Invest.

1951, 1951. **30**: p. 662-63.

51. Silva-Junior, G., et al., *The prognostic value of hepatic venous pressure gradient in patients with cirrhosis is highly dependent on the accuracy of the technique.* Hepatology, 2015. **62**(5): p. 1584-92.

52. Ripoll, C., et al., *Influence of hepatic venous pressure gradient on the prediction of survival of patients with cirrhosis in the MELD Era.* Hepatology, 2005. **42**(4): p. 793-801.

53. Garcia-Tsao, G., et al., *Portal pressure, presence of gastroesophageal varices and variceal bleeding.* Hepatology, 1985. **5**(3): p. 419-24.

54. Gluud, C., J.H. Henriksen, and G. Nielsen, *Prognostic indicators in alcoholic cirrhotic men.* Hepatology, 1988. **8**(2): p. 222-7.

55. Merkel, C., et al., *Prognostic usefulness of hepatic vein catheterization in patients with cirrhosis and esophageal varices.* Gastroenterology, 1992. **102**(3): p. 973-9.

56. Moitinho, E., et al., *Prognostic value of early measurements of portal pressure in acute variceal bleeding.* Gastroenterology, 1999. **117**(3): p. 626-31.

57. Merkel, C., et al., *The hemodynamic response to medical treatment of portal hypertension as a predictor of clinical effectiveness in the primary prophylaxis of variceal bleeding in cirrhosis.* Hepatology, 2000. **32**(5): p. 930-4.

58. Villanueva, C., et al., *Somatostatin treatment and risk stratification by continuous portal pressure monitoring during acute variceal bleeding.* Gastroenterology, 2001. **121**(1): p. 110-7.

59. Monescillo, A., et al., *Influence of portal hypertension and its early decompression by TIPS placement on the outcome of variceal bleeding.* Hepatology, 2004. **40**(4): p. 793-801.

60. Groszmann, R.J., et al., *Beta-blockers to prevent gastroesophageal varices in patients with cirrhosis.* N Engl J Med, 2005. **353**(21): p. 2254-61.

61. Rincon, D., et al., *Prognostic value of hepatic venous pressure gradient for in-hospital mortality of patients with severe acute alcoholic hepatitis.* Aliment Pharmacol Ther, 2007. **25**(7): p. 841-8.

62. Abraldes, J.G., et al., *Hepatic venous pressure gradient and prognosis in patients with acute variceal bleeding treated with pharmacologic and endoscopic therapy.* J Hepatol, 2008. **48**(2): p. 229-36.

63. Ripoll, C., et al., *Hepatic venous pressure gradient predicts development of hepatocellular carcinoma independently of severity of cirrhosis.* J Hepatol, 2009. **50**(5): p. 923-8.

64. Berzigotti, A., et al., *Prognostic value of a single HVPG measurement and Doppler-ultrasound evaluation in patients with cirrhosis and portal hypertension.* J Gastroenterol, 2011. **46**(5): p. 687-95.

65. Zipprich, A., et al., *Prognostic indicators of survival in patients with compensated and decompensated cirrhosis.* Liver Int, 2012. **32**(9): p. 1407-14.

66. Harrison, P., et al., *Assessment and management of cirrhosis in people older than 16 years: summary of NICE guidance.* BMJ, 2016. **354**.

67. NICE., *Clinical Guideline 50: Cirrhosis in over 16s: Assessment and management.* . 2016.

68. de Franchis, R., *Expanding consensus in portal hypertension: Report of the Baveno VI Consensus Workshop: Stratifying risk and individualizing care for portal hypertension.* J Hepatol, 2015. **63**(3): p. 743-52.

69. Garcia-Tsao, G., et al., *Portal hypertensive bleeding in cirrhosis: Risk stratification, diagnosis, and management: 2016 practice guidance by the American Association for the study of liver diseases.* Hepatology, 2017. **65**(1): p. 310-335.

70. Garcia-Tsao, G. and J. Bosch, *Management of varices and variceal hemorrhage in cirrhosis.* NEJM, 2010. **362**(9): p. 823-832.

71. Merli, M., et al., *Incidence and natural history of small esophageal varices in cirrhotic patients.* J Hepatol, 2003. **38**(3): p. 266-72.

72. Stokkeland, K., et al., *Improved prognosis for patients hospitalized with esophageal varices in Sweden 1969-2002.* Hepatology, 2006. **43**(3): p. 500-5.

73. Tripathi, D., et al., *UK guidelines on the management of variceal haemorrhage in cirrhotic patients.* Gut, 2015. **64**(11): p. 1680-704.

74. Berzigotti, A., et al., *Elastography, spleen size, and platelet count identify portal hypertension in patients with compensated cirrhosis.* Gastroenterology, 2013. **144**(1): p. 102-111.e1.

75. Augustin, S., et al., *Detection of early portal hypertension with routine data and liver stiffness in patients with asymptomatic liver disease: a prospective study.* J Hepatol, 2014. **60**(3): p. 561-9.

76. Abraldes, J.G., et al., *Noninvasive tools and risk of clinically significant portal hypertension and varices in compensated cirrhosis: The "Anticipate" study.* Hepatology, 2016. **64**(6): p. 2173-2184.

77. Maurice, J.B., et al., *Validation of the Baveno VI criteria to identify low risk cirrhotic patients not requiring endoscopic surveillance for varices.* J Hepatol, 2016. **65**(5): p. 899-905.

78. Augustin, S., et al., *Expanding the Baveno VI criteria for the screening of varices in patients with compensated advanced chronic liver disease.* Hepatology, 2017. **66**(6): p. 1980-1988.

79. Szakacs, Z., et al., *Baveno Criteria Safely Identify Patients With Compensated Advanced Chronic Liver Disease Who Can Avoid Variceal Screening Endoscopy: A Diagnostic Test Accuracy Meta-Analysis.* Front Physiol, 2019. **10**: p. 1028.

80. Colecchia, A., et al., *A combined model based on spleen stiffness measurement and Baveno VI criteria to rule out high-risk varices in advanced chronic liver disease.* J Hepatol, 2018. **69**(2): p. 308-317.

81. Berzigotti, A., *Non-invasive evaluation of portal hypertension using ultrasound elastography.* J Hepatol, 2017. **67**(2): p. 399-411.

82. Kim, B.K., et al., *A liver stiffness measurement-based, noninvasive prediction model for high-risk esophageal varices in B-viral liver cirrhosis.* Am J Gastroenterol, 2010. **105**(6): p. 1382-90.

83. Perazzo, H., et al., *Points to be considered when using transient elastography for diagnosis of portal hypertension according to the Baveno's VI consensus.* J Hepatol, 2015. **63**(4): p. 1048-9.

84. Jangouk, P., et al., *Validating, deconstructing and refining Baveno criteria for ruling out high-risk varices in patients with compensated cirrhosis.* Liver Int, 2017. **37**(8): p. 1177-1183.

85. Llop, E., et al., *Validation of noninvasive methods to predict the presence of gastroesophageal varices in a cohort of patients with compensated advanced chronic liver disease.* J Gastroenterol Hepatol, 2017. **32**(11): p. 1867-1872.

86. Silva, M.J., et al., *Baveno VI Recommendation on Avoidance of Screening Endoscopy in Cirrhotic Patients: Are We There Yet?* GE Port J Gastroenterol, 2017. **24**(2): p. 79-83.

87. Sousa, M., et al., *The Baveno VI criteria for predicting esophageal varices: validation in real life practice.* Rev Esp Enferm Dig, 2017. **109**(10): p. 704-707.

88. Bae, J., et al., *Validation of the Baveno VI and the expanded Baveno VI criteria to identify patients who could avoid screening endoscopy.* Liver Int, 2018.

89. Bellan, M., et al., *Gas6 as a predictor of esophageal varices in patients affected by hepatitis C virus related-chronic liver disease.* Biomark Med, 2018. **12**(1): p. 27-34.

90. Matsui, N., et al., *Magnetic resonance elastography increases usefulness and safety of non-invasive screening for esophageal varices.* J Gastroenterol Hepatol, 2018. **33**(12): p. 2022-2028.

91. Petta, S., et al., *Non-invasive prediction of esophageal varices by stiffness and platelet in non-alcoholic fatty liver disease cirrhosis.* J Hepatol, 2018. **69**(4): p. 878-885.

92. Stanislas, D., A., et al., *Liver transient elastography combined to platelet count (Baveno VI) predict high esophageal varices in Balck African patient with compensated Hepatitis B related cirrhosis.* Opn J. Gastroenterol., 2018. **8**(192).

93. Lee, H.A., et al., *Prediction of the varices needing treatment with non-invasive tests in patients with compensated advanced chronic liver disease.* Liver Int, 2019. **39**(6): p. 1071-1079.

94. Moctezuma-Velazquez, C., et al., *Non-Invasive Prediction of High-Risk Varices in Patients with Primary Biliary Cholangitis and Primary Sclerosing Cholangitis.* Am J Gastroenterol, 2019. **114**(3): p. 446-452.

95. Thabut, D., et al., *Validation of Baveno VI Criteria for Screening and Surveillance of Esophageal Varices in Patients With Compensated Cirrhosis and a Sustained Response to Antiviral Therapy.* Gastroenterology, 2019. **156**(4): p. 997-1009.e5.

96. Tosetti, G., et al., *Evaluation of three "beyond Baveno VI" criteria to safely spare endoscopies in compensated advanced chronic liver disease.* Dig Liver Dis, 2019. **51**(8): p. 1135-1140.

97. Gluud, L.L., et al., *Banding ligation versus beta-blockers as primary prophylaxis in esophageal varices: systematic review of randomized trials.* Am J Gastroenterol, 2007. **102**(12): p. 2842-8; quiz 2841, 2849.

98. Tripathi, D. and P.C. Hayes, *Beta-blockers in portal hypertension: new developments and controversies.* Liver Int, 2014. **34**(5): p. 655-67.

99. Feu, F., et al., *Relation between portal pressure response to pharmacotherapy and risk of recurrent variceal haemorrhage in patients with cirrhosis.* Lancet, 1995. **346**(8982): p. 1056-1059.

100. Augustin, S., et al., *Long-term follow-up of hemodynamic responders to pharmacological therapy after variceal bleeding.* Hepatology, 2012. **56**(2): p. 706-14.

101. Thalheimer, U., J. Bosch, and A.K. Burroughs, *How to prevent varices from bleeding: shades of grey--the case for nonselective beta blockers.* Gastroenterology, 2007. **133**(6): p. 2029-36.

102. Reiberger, T., et al., *Non-selective betablocker therapy decreases intestinal permeability and serum levels of LBP and IL-6 in patients with cirrhosis.* J Hepatol, 2013. **58**(5): p. 911-21.

103. Senzolo, M., et al., *beta-Blockers protect against spontaneous bacterial peritonitis in cirrhotic patients: a meta-analysis.* Liver Int, 2009. **29**(8): p. 1189-93.

104. Perez-Paramo, M., et al., *Effect of propranolol on the factors promoting bacterial translocation in cirrhotic rats with ascites.* Hepatology, 2000. **31**: p. 43-48.

105. Bang, U.C., et al., *Effect of propranolol on survival in patients with decompensated cirrhosis: a nationwide study based Danish patient registers.* Liver Int, 2016. **36**(9): p. 1304-12.

106. Villanueva, C., et al., *beta blockers to prevent decompensation of cirrhosis in patients with clinically significant portal hypertension (PREDESCI): a randomised, double-blind, placebo-controlled, multicentre trial.* Lancet, 2019. **393**(10181): p. 1597-1608.

107. Sinagra, E., et al., *Systematic review with meta-analysis: the haemodynamic effects of carvedilol compared with propranolol for portal hypertension in cirrhosis.* Aliment Pharmacol Ther, 2014. **39**(6): p. 557-68.

108. Krag, A., et al., *Betablockers induce cardiac chronotropic incompetence.* J Hepatol, 2012. **56**(1): p. 298-9.

109. Gomez, E.V., et al., *Arterial blood pressure is closely related to ascites development in compensated HCV-related cirrhosis.* PLoS One, 2014. **9**(4): p. e95736.

110. Sersté T, M.C., Francoz C, et al., *Deleterious effects of beta-blockers on survival in patients with cirrhosis and refractory ascites.* Hepatology, 2010. **52**: p. 1017-22.

111. Sersté, T., et al., *Beta-blockers cause paracentesis-induced circulatory dysfunction in patients with cirrhosis and refractory ascites: A cross-over study.* Journal of Hepatology, 2011. **55**(4): p. 794-799.

112. Mandorfer, M., et al., *Nonselective beta blockers increase risk for hepatorenal syndrome and death in patients with cirrhosis and spontaneous bacterial peritonitis.* Gastroenterology, 2014. **146**(7): p. 1680-90.e1.

113. Thomas, S., et al., *The use of beta-blockers is associated with the occurrence of acute kidney injury in severe alcoholic hepatitis.* Liver International, 2015. **35**(8): p. 1974-1982.

114. Krag, A., et al., *The window hypothesis: haemodynamic and non-haemodynamic effects of beta-blockers improve survival of patients with cirrhosis during a window in the disease.* Gut, 2012. **61**(7): p. 967-9.

115. Reiberger, T. and M. Mandorfer, *Beta adrenergic blockade and decompensated cirrhosis.* J Hepatol, 2017. **66**(4): p. 849-859.

116. Kerbert, A.J., et al., *Hemodynamic response to primary prophylactic therapy with nonselective beta-blockers is related to a reduction of first variceal bleeding risk in liver cirrhosis: a meta-analysis.* Eur J Gastroenterol Hepatol, 2017. **29**(4): p. 380-387.

117. Villanueva, C., et al., *A randomized trial to assess whether portal pressure guided therapy to prevent variceal rebleeding improves survival in cirrhosis.* Hepatology, 2017. **65**(5): p. 1693-1707.

118. Qi, X., et al., *Emerging non-invasive approaches for diagnosis and monitoring of portal hypertension.* Lancet Gastroenterol Hepatol, 2018. **3**(10): p. 708-719.

119. Hametner, S., et al., *The VITRO Score (Von Willebrand Factor Antigen/Thrombocyte Ratio) as a New Marker for Clinically Significant Portal Hypertension in Comparison to Other Non-Invasive Parameters of Fibrosis Including ELF Test.* PLoS One, 2016. **11**(2): p. e0149230.

120. Sandahl, T.D., et al., *The macrophage activation marker sCD163 combined with markers of the Enhanced Liver Fibrosis (ELF) score predicts clinically significant portal hypertension in patients with cirrhosis.* Aliment Pharmacol Ther, 2016. **43**(11): p. 1222-31.

121. Pind, M.L., et al., *Indocyanine green retention test (ICG-r15) as a noninvasive predictor of portal hypertension in patients with different severity of cirrhosis.* Eur J Gastroenterol Hepatol, 2016. **28**(8): p. 948-54.

122. Leeming, D.J., et al., *Pro-C5, a marker of true type V collagen formation and fibrillation, correlates with portal hypertension in patients with alcoholic cirrhosis.* Scand J Gastroenterol, 2015. **50**(5): p. 584-92.

123. Bruha, R., et al., *Osteopontin: A non-invasive parameter of portal hypertension and prognostic marker of cirrhosis.* World J Gastroenterol, 2016. **22**(12): p. 3441-50.

124. Kim, M.Y., et al., *Damping index of Doppler hepatic vein waveform to assess the severity of portal hypertension and response to propranolol in liver cirrhosis: a prospective nonrandomized study.* Liver Int, 2007. **27**(8): p. 1103-10.

125. Bolognesi, M., et al., *Noninvasive grading of the severity of portal hypertension in cirrhotic patients by echo-color-Doppler.* Ultrasound Med Biol, 2001. **27**(7): p. 901-7.

126. Lee, C.M., et al., *Diagnosis of Clinically Significant Portal Hypertension in Patients with Cirrhosis: Splenic Arterial Resistive Index versus Liver Stiffness Measurement.* Ultrasound Med Biol, 2016. **42**(6): p. 1312-20.

127. Eisenbrey, J.R., et al., *Chronic liver disease: noninvasive subharmonic aided pressure estimation of hepatic venous pressure gradient.* Radiology, 2013. **268**(2): p. 581-8.

128. Attia, D., et al., *Evaluation of Liver and Spleen Stiffness with Acoustic Radiation Force Impulse Quantification Elastography for Diagnosing Clinically Significant Portal Hypertension.* Ultraschall Med, 2015. **36**(6): p. 603-10.

129. Deng, H., et al., *Supersonic shear imaging for the diagnosis of liver fibrosis and portal hypertension in liver diseases: a meta-analysis.* Expert Rev Gastroenterol Hepatol, 2018. **12**(1): p. 91-98.

130. Procopet, B., et al., *Real-time shear-wave elastography: applicability, reliability and accuracy for clinically significant portal hypertension.* J Hepatol, 2015. **62**(5): p. 1068-75.

131. Qi, X., et al., *Virtual Hepatic Venous Pressure Gradient with CT Angiography (CHESS 1601): A Prospective Multicenter Study for the Noninvasive Diagnosis of Portal Hypertension.* Radiology, 2019. **290**(2): p. 370-377.

132. Liu, F., et al., *Development and validation of a radiomics signature for clinically significant portal hypertension in cirrhosis (CHESS1701): a prospective multicenter study.* EBioMedicine, 2018. **36**: p. 151-158.

133. Gouya, H., et al., *Portal hypertension in patients with cirrhosis: indirect assessment of hepatic venous pressure gradient by measuring azygos flow with 2D-cine phase-contrast magnetic resonance imaging.* Eur Radiol, 2016. **26**(7): p. 1981-90.

134. Palaniyappan, N., et al., *Non-invasive assessment of portal hypertension using quantitative magnetic resonance imaging.* J Hepatol, 2016. **65**(6): p. 1131-1139.

135. Chouhan, M.D., et al., *Caval Subtraction 2D Phase-Contrast MRI to Measure Total Liver and Hepatic Arterial Blood Flow: Proof-of-Principle, Correlation With Portal*

Hypertension Severity and Validation in Patients With Chronic Liver Disease. Invest Radiol, 2017. **52**(3): p. 170-176.

136. Hoad, C.L., et al., *A study of T(1) relaxation time as a measure of liver fibrosis and the influence of confounding histological factors.* NMR Biomed, 2015. **28**(6): p. 706-14.
137. Banerjee, R., et al., *Multiparametric magnetic resonance for the non-invasive diagnosis of liver disease.* J Hepatol, 2014. **60**(1): p. 69-77.
138. Chow, A.M., et al., *Measurement of liver T(1) and T(2) relaxation times in an experimental mouse model of liver fibrosis.* J Magn Reson Imaging, 2012. **36**(1): p. 152-8.
139. Guimaraes, A.R., et al., *T2 relaxation time is related to liver fibrosis severity.* Quant Imaging Med Surg, 2016. **6**(2): p. 103-14.
140. Roulot, D., et al., *Transient elastography as a screening tool for liver fibrosis and cirrhosis in a community-based population aged over 45 years.* Gut, 2011. **60**(7): p. 977-84.
141. Sandrin, L., et al., *Transient elastography: a new noninvasive method for assessment of hepatic fibrosis.* Ultrasound Med Biol, 2003. **29**(12): p. 1705-13.
142. Castera, L., X. Forns, and A. Alberti, *Non-invasive evaluation of liver fibrosis using transient elastography.* Journal of Hepatology, 2008. **48**(5): p. 835-847.
143. Groszmann, R.J. and S. Wongcharatrawee, *The hepatic venous pressure gradient: anything worth doing should be done right.* Hepatology, 2004. **39**(2): p. 280-2.
144. Zipprich, A., et al., *Comparison of balloon vs. straight catheter for the measurement of portal hypertension.* Aliment Pharmacol Ther, 2010. **32**(11-12): p. 1351-6.
145. Maleux, G., et al., *Prospective study comparing different indirect methods to measure portal pressure.* J Vasc Interv Radiol, 2011. **22**(11): p. 1553-8.
146. Keiding, S. and H. Vilstrup, *Intrahepatic heterogeneity of hepatic venous pressure gradient in human cirrhosis.* Scand J Gastroenterol, 2002. **37**(8): p. 960-4.

147. Armonis, A., D. Patch, and A. Burroughs, *Hepatic venous pressure measurement: an old test as a new prognostic marker in cirrhosis?* Hepatology, 1997. **25**(1): p. 245-8.

148. Poynard, T., et al., *Liver biopsy analysis has a low level of performance for diagnosis of intermediate stages of fibrosis.* Clin Gastroenterol Hepatol, 2012. **10**(6): p. 657-63 e7.

149. Scott, R. and I.N. Guha, *Non-invasive monitoring of liver fibrosis.* Br Med Bull, 2014. **112**(1): p. 97-106.

150. Agrawal, S., et al., *Visual morphometry and three non-invasive markers in the evaluation of liver fibrosis in chronic liver disease.* Scand J Gastroenterol, 2017. **52**(1): p. 107-115.

151. Henninger, B., et al., *Evaluation of MR imaging with T1 and T2* mapping for the determination of hepatic iron overload.* Eur Radiol, 2012. **22**(11): p. 2478-86.

152. St Pierre, T.G., P.R. Clark, and W. Chua-Anusorn, *Single spin-echo proton transverse relaxometry of iron-loaded liver.* NMR Biomed, 2004. **17**(7): p. 446-58.

153. Wood, J.C., et al., *MRI R2 and R2* mapping accurately estimates hepatic iron concentration in transfusion-dependent thalassemia and sickle cell disease patients.* Blood, 2005. **106**(4): p. 1460-5.

154. de Bazelaire, C.M., et al., *MR imaging relaxation times of abdominal and pelvic tissues measured in vivo at 3.0 T: preliminary results.* Radiology, 2004. **230**(3): p. 652-9.

155. Zhao, F., et al., *MR T1rho as an imaging biomarker for monitoring liver injury progression and regression: an experimental study in rats with carbon tetrachloride intoxication.* Eur Radiol, 2012. **22**(8): p. 1709-16.

156. Stanisz, G.J., et al., *MR properties of excised neural tissue following experimentally induced inflammation.* Magn Reson Med, 2004. **51**(3): p. 473-9.

157. Heye, T., et al., *MR relaxometry of the liver: significant elevation of T1 relaxation time in patients with liver cirrhosis.* Eur Radiol, 2012. **22**(6): p. 1224-32.

158. Mozes, F.E., et al., *Influence of fat on liver T1 measurements using modified Look-Locker inversion recovery (MOLLI) methods at 3T.* J Magn Reson Imaging, 2016. **44**(1): p. 105-11.

159. Reeder, S.B., H.C.H. Hu, and C.B. Sirlin, *Proton density fat-fraction: A standardized mr-based biomarker of tissue fat concentration.* Journal of Magnetic Resonance Imaging, 2012. **36**(5): p. 1011-1014.

160. Francis, S.T., R. Bowtell, and P.A. Gowland, *Modeling and optimization of Look-Locker spin labeling for measuring perfusion and transit time changes in activation studies taking into account arterial blood volume.* Magn Reson Med, 2008. **59**(2): p. 316-25.

161. Reynaert, H., et al., *Hepatic stellate cells: role in microcirculation and pathophysiology of portal hypertension.* Gut, 2002. **50**(4): p. 571-81.

162. Perello, A., et al., *Wedged hepatic venous pressure adequately reflects portal pressure in hepatitis C virus-related cirrhosis.* Hepatology, 1999. **30**(6): p. 1393-7.

163. D'Amico, G., et al., *Hepatic vein pressure gradient reduction and prevention of variceal bleeding in cirrhosis: a systematic review.* Gastroenterology, 2006. **131**(5): p. 1611-24.

164. Shi, K.Q., et al., *Transient elastography: a meta-analysis of diagnostic accuracy in evaluation of portal hypertension in chronic liver disease.* Liver Int, 2013. **33**(1): p. 62-71.

165. Vizzutti, F., et al., *Liver stiffness measurement predicts severe portal hypertension in patients with HCV-related cirrhosis.* Hepatology, 2007. **45**(5): p. 1290-7.

166. *EASL-ALEH Clinical Practice Guidelines: Non-invasive tests for evaluation of liver disease severity and prognosis.* J Hepatol, 2015. **63**(1): p. 237-64.

167. Castera, L., et al., *Pitfalls of liver stiffness measurement: a 5-year prospective study of 13,369 examinations.* Hepatology, 2010. **51**(3): p. 828-35.

168. Colecchia, A., et al., *Measurement of spleen stiffness to evaluate portal hypertension and the presence of esophageal varices in patients with HCV-related cirrhosis.* Gastroenterology, 2012. **143**(3): p. 646-654.

169. Ronot, M., et al., *Assessment of portal hypertension and high-risk oesophageal varices with liver and spleen three-dimensional multifrequency MR elastography in liver cirrhosis.* Eur Radiol, 2014. **24**(6): p. 1394-402.

170. McDonald, N., et al., *Assessment of Haemodynamic Response to Nonselective Beta-Blockers in Portal Hypertension by Phase-Contrast Magnetic Resonance Angiography.* Biomed Res Int, 2017. **2017**: p. 9281450.

171. Bossuyt, P.M., et al., *Towards complete and accurate reporting of studies of diagnostic accuracy: the STARD initiative.* BMJ, 2003. **326**(7379): p. 41-4.

172. McCorry, R.B., et al., *Development and evaluation of a nurse-led transient elastography service for the staging of hepatic fibrosis in patients with suspected chronic liver disease.* Qjm, 2012. **105**(8): p. 749-54.

173. Buchanan, C., et al., *Intradialytic Cardiac Magnetic Resonance Imaging to Assess Cardiovascular Responses in a Short-Term Trial of Hemodiafiltration and Hemodialysis.* J Am Soc Nephrol, 2017. **28**(4): p. 1269-1277.

174. E., T., *Evaluating liver fibrosis in the presence of elevated iron using MR relaxometry.* 2014.

175. St Pierre, T.G., et al., *Noninvasive measurement and imaging of liver iron concentrations using proton magnetic resonance.* Blood, 2005. **105**(2): p. 855-61.

176. Bulte, J.W., et al., *Hepatic hemosiderosis in non-human primates: quantification of liver iron using different field strengths.* Magn Reson Med, 1997. **37**(4): p. 530-6.

177. Ghugre, N.R., et al., *Multi-field behavior of Relaxivity in an Iron-rich environment.*, in *Proc Intl Soc Mag Reson Med.* . 2008.

178. Ghugre, N.R., et al., *Mechanisms of tissue-iron relaxivity: nuclear magnetic resonance studies of human liver biopsy specimens.* Magn Reson Med, 2005. **54**(5): p. 1185-93.

179. Zhang, X., et al., *In vivo blood T(1) measurements at 1.5 T, 3 T, and 7 T.* Magn Reson Med, 2013. **70**(4): p. 1082-6.

180. Bradley, C., et al., *Short-term changes observed in multiparametric liver MRI following therapy with direct-acting antivirals in chronic hepatitis C virus patients.* Eur Radiol, 2019. **29**(6): p. 3100-3107.

181. Yzet, T., et al., *Hepatic vascular flow measurements by phase contrast MRI and doppler echography: a comparative and reproducibility study.* J Magn Reson Imaging, 2010. **31**(3): p. 579-88.

182. Cox, E.F., et al., *Temporal assessment of pancreatic blood flow and perfusion following secretin stimulation using noninvasive MRI.* J Magn Reson Imaging, 2015. **42**(5): p. 1233-40.

183. Chang, K.J., et al., *3.0-T MR imaging of the abdomen: comparison with 1.5 T.* Radiographics, 2008. **28**(7): p. 1983-98.

184. Calvaruso, V., et al., *Computer-assisted image analysis of liver collagen: relationship to Ishak scoring and hepatic venous pressure gradient.* Hepatology, 2009. **49**(4): p. 1236-44.

185. Levick, C., et al., *Non-invasive assessment of portal hypertension by multi-parametric magnetic resonance imaging of the spleen: A proof of concept study.* PLoS One, 2019. **14**(8): p. e0221066.

186. Cadranel, J.F., P. Rufat, and F. Degos, *Practices of liver biopsy in France: results of a prospective nationwide survey. For the Group of Epidemiology of the French Association for the Study of the Liver (AFEF).* Hepatology, 2000. **32**(3): p. 477-81.

187. Bedossa, P., D. Dargere, and V. Paradis, *Sampling variability of liver fibrosis in chronic hepatitis C.* Hepatology, 2003. **38**(6): p. 1449-57.

188. Ratziu, V., et al., *Sampling variability of liver biopsy in nonalcoholic fatty liver disease.* Gastroenterology, 2005. **128**(7): p. 1898-906.

189. Gibson, P.R., et al., *Splenomegaly--an insensitive sign of portal hypertension.* Aust N Z J Med, 1990. **20**(6): p. 771-4.

190. Takuma, Y., et al., *Portal Hypertension in Patients with Liver Cirrhosis: Diagnostic Accuracy of Spleen Stiffness.* Radiology, 2016. **279**(2): p. 609-19.

191. Elkrief, L., et al., *Prospective comparison of spleen and liver stiffness by using shear-wave and transient elastography for detection of portal hypertension in cirrhosis.* Radiology, 2015. **275**(2): p. 589-98.

192. Talwalkar, J.A., et al., *Feasibility of in vivo MR elastographic splenic stiffness measurements in the assessment of portal hypertension.* AJR Am J Roentgenol, 2009. **193**(1): p. 122-7.

193. Zwiebel, W.J., et al., *Splanchnic blood flow in patients with cirrhosis and portal hypertension: investigation with duplex Doppler US.* Radiology, 1995. **194**(3): p. 807-12.

194. Berzigotti, A., et al., *Noninvasive prediction of clinically significant portal hypertension and esophageal varices in patients with compensated liver cirrhosis.* Am J Gastroenterol, 2008. **103**(5): p. 1159-67.

195. Bosch, J. and R.J. Groszmann, *Measurement of azygos venous blood flow by a continuous thermal dilution technique: an index of blood flow through gastroesophageal collaterals in cirrhosis.* Hepatology, 1984. **4**(3): p. 424-9.

196. Bosch, J., et al., *Measurement of azygos venous blood flow in the evaluation of portal hypertension in patients with cirrhosis. Clinical and haemodynamic correlations in 100 patients.* J Hepatol, 1985. **1**(2): p. 125-39.

197. Lomas, D.J., et al., *Non-invasive measurement of azygos venous blood flow using magnetic resonance.* J Hepatol, 1995. **22**(4): p. 399-403.

198. Debatin, J.F., et al., *Azygos blood flow: phase contrast quantitation in volunteers and patients with portal hypertension pre- and postintrahepatic shunt placement.* Hepatology, 1996. **24**(5): p. 1109-15.

199. Collaborators, P.O.H., *Global prevalence and genotype distribution of hepatitis C virus infection in 2015: a modelling study.* Lancet Gastroenterol Hepatol, 2017. **2**(3): p. 161-176.

200. Afdhal, N., et al., *Ledipasvir and sofosbuvir for untreated HCV genotype 1 infection.* N Engl J Med, 2014. **370**(20): p. 1889-98.

201. Poordad, F., et al., *ABT-450/r-ombitasvir and dasabuvir with ribavirin for hepatitis C with cirrhosis.* N Engl J Med, 2014. **370**(21): p. 1973-82.

202. Lawitz, E., et al., *Simeprevir plus sofosbuvir, with or without ribavirin, to treat chronic infection with hepatitis C virus genotype 1 in non-responders to pegylated interferon and ribavirin and treatment-naive patients: the COSMOS randomised study.* Lancet, 2014. **384**(9956): p. 1756-65.

203. Foster, G.R., et al., *Impact of direct acting antiviral therapy in patients with chronic hepatitis C and decompensated cirrhosis.* Journal of Hepatology, 2016. **64**(6): p. 1224-1231.

204. Charlton, M., et al., *Ledipasvir and Sofosbuvir Plus Ribavirin for Treatment of HCV Infection in Patients With Advanced Liver Disease.* Gastroenterology, 2015. **149**(3): p. 649-59.

205. Innes, H.A., et al., *Toward a more complete understanding of the association between a hepatitis C sustained viral response and cause-specific outcomes.* Hepatology, 2015. **62**(2): p. 355-64.

206. Nahon, P., et al., *Eradication of Hepatitis C Virus Infection in Patients With Cirrhosis Reduces Risk of Liver and Non-Liver Complications.* Gastroenterology, 2017. **152**(1): p. 142-156 e2.

207. Morgan, T.R., et al., *Outcome of sustained virological responders with histologically advanced chronic hepatitis C.* Hepatology, 2010. **52**(3): p. 833-44.

208. D'Ambrosio, R., et al., *A morphometric and immunohistochemical study to assess the benefit of a sustained virological response in hepatitis C virus patients with cirrhosis.* Hepatology, 2012. **56**(2): p. 532-43.

209. Pol, S., et al., *Reversibility of hepatitis C virus-related cirrhosis.* Hum Pathol, 2004. **35**(1): p. 107-12.

210. Mallet, V., et al., *Brief communication: the relationship of regression of cirrhosis to outcome in chronic hepatitis C.* Ann Intern Med, 2008. **149**(6): p. 399-403.

211. George, S.L., et al., *Clinical, virologic, histologic, and biochemical outcomes after successful HCV therapy: a 5-year follow-up of 150 patients.* Hepatology, 2009. **49**(3): p. 729-38.

212. Poynard, T., et al., *Impact of pegylated interferon alfa-2b and ribavirin on liver fibrosis in patients with chronic hepatitis C.* Gastroenterology, 2002. **122**(5): p. 1303-13.

213. Koretz, R.L., et al., *Is widespread screening for hepatitis C justified?* BMJ, 2015. **350**: p. g7809.

214. Burroughs, A.K., et al., *Assessment of therapeutic benefit of antiviral therapy in chronic hepatitis C: is hepatic venous pressure gradient a better end point?* Gut, 2002. **50**(3): p. 425-7.

215. Rincon, D., et al., *Antiviral therapy decreases hepatic venous pressure gradient in patients with chronic hepatitis C and advanced fibrosis.* Am J Gastroenterol, 2006. **101**(10): p. 2269-74.

216. Roberts, S., et al., *Effect of sustained viral response on hepatic venous pressure gradient in hepatitis C-related cirrhosis.* Clin Gastroenterol Hepatol, 2007. **5**(8): p. 932-7.

217. Lens, S., et al., *Effects of All-oral Anti-viral Therapy on HVPG and Systemic Hemodynamics in Patients with Hepatitis C Virus-associated Cirrhosis.* Gastroenterology, 2017.

218. Pons, M., et al., *Rapid liver and spleen stiffness improvement in compensated advanced chronic liver disease patients treated with oral antivirals.* Therap Adv Gastroenterol, 2017. **10**(8): p. 619-629.

219. D'Ambrosio, R., et al., *The diagnostic accuracy of Fibroscan for cirrhosis is influenced by liver morphometry in HCV patients with a sustained virological response.* J Hepatol, 2013. **59**(2): p. 251-6.

220. Pons, M., et al., *Non-invasive prediction of liver-related events in patients with HCV-associated compensated advanced chronic liver disease after oral antivirals.* J Hepatol, 2020. **72**(3): p. 472-480.

221. Cheung, M.C., et al., *Outcomes after successful direct-acting antiviral therapy for patients with chronic hepatitis C and decompensated cirrhosis.* J Hepatol, 2016. **65**(4): p. 741-7.

222. Neuberger, J., et al., *Selection of patients for liver transplantation and allocation of donated livers in the UK.* Gut, 2008. **57**(2): p. 252-7.

223. *EASL Recommendations on Treatment of Hepatitis C 2018.* J Hepatol, 2018. **69**(2): p. 461-511.

224. Martinot-Peignoux, M., et al., *Twelve weeks posttreatment follow-up is as relevant as 24 weeks to determine the sustained virologic response in patients with hepatitis C virus receiving pegylated interferon and ribavirin.* Hepatology, 2010. **51**(4): p. 1122-6.

225. Swain, M.G., et al., *A sustained virologic response is durable in patients with chronic hepatitis C treated with peginterferon alfa-2a and ribavirin.* Gastroenterology, 2010. **139**(5): p. 1593-601.

226. Sterling, R.K., et al., *Development of a simple noninvasive index to predict significant fibrosis in patients with HIV/HCV coinfection.* Hepatology, 2006. **43**(6): p. 1317-25.

227. Wai, C.T., et al., *A simple noninvasive index can predict both significant fibrosis and cirrhosis in patients with chronic hepatitis C.* Hepatology, 2003. **38**(2): p. 518-26.

228. Gurcan, N.I., et al., *Liver Apparent Diffusion Coefficient Changes during Telaprevir-Based Therapy for Chronic Hepatitis C.* Balkan Med J, 2016. **33**(6): p. 602-606.

229. Aube, C., et al., *Diagnosis and measurement of liver fibrosis by MRI in bile duct ligated rats.* Dig Dis Sci, 2007. **52**(10): p. 2601-9.

230. Anderson, S.W., et al., *Effect of disease progression on liver apparent diffusion coefficient and T2 values in a murine model of hepatic fibrosis at 11.7 Tesla MRI.* J Magn Reson Imaging, 2012. **35**(1): p. 140-6.

231. Schwabl, P., et al., *Interferon-free regimens improve portal hypertension and histological necroinflammation in HIV/HCV patients with advanced liver disease.* Aliment Pharmacol Ther, 2017. **45**(1): p. 139-149.

232. Mauro, E., et al., *Portal pressure and liver stiffness measurements in the prediction of fibrosis regression after sustained virological response in recurrent hepatitis C.* Hepatology, 2018. **67**(5): p. 1683-1694.

233. Bachofner, J.A., et al., *Direct antiviral agent treatment of chronic hepatitis C results in rapid regression of transient elastography and fibrosis markers fibrosis-4 score and aspartate aminotransferase-platelet ratio index.* Liver Int, 2017. **37**(3): p. 369-376.

234. Knop, V., et al., *Regression of fibrosis and portal hypertension in HCV-associated cirrhosis and sustained virologic response after interferon-free antiviral therapy.* J Viral Hepat, 2016. **23**(12): p. 994-1002.

235. Poynard, T., et al., *Slow regression of liver fibrosis presumed by repeated biomarkers after virological cure in patients with chronic hepatitis C.* J Hepatol, 2013. **59**(4): p. 675-83.

236. Reiberger, T., et al., *A prospective evaluation of pulmonary, systemic and hepatic haemodynamics in HIV-HCV-coinfected patients before and after antiviral therapy with pegylated interferon and ribavirin.* Antivir Ther, 2012. **17**(7): p. 1327-34.

237. Afdhal, N., et al., *Effect of Viral Suppression on Hepatic Venous Pressure Gradient in Hepatitis C With Cirrhosis and Portal Hypertension.* J Viral Hepat, 2017.

238. Mandorfer, M., et al., *Sustained virologic response to interferon-free therapies ameliorates HCV-induced portal hypertension.* J Hepatol, 2016. **65**(4): p. 692-9.

239. Morishima, C., et al., *Reduction in Hepatic Inflammation Is Associated With Less Fibrosis Progression and Fewer Clinical Outcomes in Advanced Hepatitis C.* Am J Gastroenterol, 2012. **107**(9): p. 1388-98.

240. Ronot, M., et al., *Liver fibrosis in chronic hepatitis C virus infection: differentiating minimal from intermediate fibrosis with perfusion CT.* Radiology, 2010. **256**(1): p. 135-42.

241. D'Ambrosio, R., et al., *Serological Tests Do Not Predict Residual Fibrosis in Hepatitis C Cirrhotics with a Sustained Virological Response to Interferon.* PLoS One, 2016. **11**(6): p. e0155967.

242. Shiffman, M.L., et al., *Long term changes in liver histology following treatment of chronic hepatitis C virus.* Ann Hepatol, 2014. **13**(4): p. 340-9.

243. Waziry, R., et al., *Hepatocellular carcinoma risk following direct-acting antiviral HCV therapy: A systematic review, meta-analyses, and meta-regression.* J Hepatol, 2017.

244. Kanwal, F., et al., *Risk of Hepatocellular Cancer in HCV Patients Treated with Direct Acting Antiviral Agents.* Gastroenterology, 2017.

245. *EASL-EORTC clinical practice guidelines: management of hepatocellular carcinoma.* J Hepatol, 2012. **56**(4): p. 908-43.

246. *Hepatitis C guidance: AASLD-IDSA recommendations for testing, managing, and treating adults infected with hepatitis C virus.* Hepatology, 2015. **62**(3): p. 932-54.

247. Singal, A., et al., *Meta-analysis: surveillance with ultrasound for early-stage hepatocellular carcinoma in patients with cirrhosis.* Aliment Pharmacol Ther, 2009. **30**(1): p. 37-47.

248. Bruix, J., M. Reig, and M. Sherman, *Evidence-Based Diagnosis, Staging, and Treatment of Patients With Hepatocellular Carcinoma.* Gastroenterology, 2016. **150**(4): p. 835-53.

249. Reig, M., et al., *Unexpected high rate of early tumor recurrence in patients with HCV-related HCC undergoing interferon-free therapy.* J Hepatol, 2016. **65**(4): p. 719-26.

250. DeMeo, M.T., et al., *Intestinal permeation and gastrointestinal disease.* J Clin Gastroenterol, 2002. **34**(4): p. 385-96.

251. Camilleri, M., et al., *Intestinal barrier function in health and gastrointestinal disease.* Neurogastroenterol Motil, 2012. **24**(6): p. 503-12.

252. Berg, R.D. and A.W. Garlington, *Translocation of certain indigenous bacteria from the gastrointestinal tract to the mesenteric lymph nodes and other organs in a gnotobiotic mouse model.* Infect Immun, 1979. **23**(2): p. 403-11.

253. Ghoshal, U.C., et al., *The gut microbiota and irritable bowel syndrome: friend or foe?* Int J Inflam, 2012. **2012**: p. 151085.

254. Powell, D.W., *Barrier function of epithelia.* Am J Physiol, 1981. **241**(4): p. G275-88.

255. Koh, I.H., et al., *Where is the site of bacterial translocation--small or large bowel?* Transplant Proc, 1996. **28**(5): p. 2661.

256. MacFie, J., et al., *Gut origin of sepsis: a prospective study investigating associations between bacterial translocation, gastric microflora, and septic morbidity.* Gut, 1999. **45**(2): p. 223-8.

257. Marshall, J.C., et al., *The microbiology of multiple organ failure. The proximal gastrointestinal tract as an occult reservoir of pathogens.* Arch Surg, 1988. **123**(3): p. 309-15.

258. Wiest, R., M. Lawson, and M. Geuking, *Pathological bacterial translocation in liver cirrhosis.* J Hepatol, 2014. **60**(1): p. 197-209.

259. Arvaniti, V., et al., *Infections in patients with cirrhosis increase mortality four-fold and should be used in determining prognosis.* Gastroenterology, 2010. **139**(4): p. 1246-56, 1256 e1-5.

260. Schmidt, M., et al., *Decreasing mortality among patients hospitalized with cirrhosis in the United States from 2002 through 2010.* Gastroenterology, 2015. **148**: p. 967-977.

261. Moreau R, et al., *Acute-on-Chronic Liver Failure Is a Distinct Syndrome That Develops in Patients With Acute Decompensation of Cirrhosis.* Gastroenterology, 2013. **144**: p. 1426-1437.

262. Vergis, N., et al., *In Patients With Severe Alcoholic Hepatitis, Prednisolone Increases Susceptibility to Infection and Infection-Related Mortality, and Is*

Associated With High Circulating Levels of Bacterial DNA. Gastroenterology, 2017. **152**(5): p. 1068-1077 e4.

263. Cirera I, B.T., Navasa M, Vila J, Grande L, Taura P, et al., *Bacterial translocation of enteric organisms in patients with cirrhosis.* J Hepatol, 2001. **34**: p. 32–37.
264. Scarpellini, E., et al., *Intestinal permeability in cirrhotic patients with and without spontaneous bacterial peritonitis: is the ring closed?* Am J Gastroenterol, 2010. **105**(2): p. 323-7.
265. Astaldi, G. and E. Strosselli, *Peroral biopsy of the intestinal mucosa in hepatic cirrhosis.* Am J Dig Dis, 1960. **5**: p. 603–612.
266. Misra V, M.S., Dwivedi M, Gupta S., *Histomorphometric study of portal hypertensive enteropathy.* Am J Clin Pathol, 1997. **108**: p. 652–657.
267. Norman DA, A.J., Seelig Jr LL, Gomez-Sanchez C, Krejs GJ., *Water and electrolyte movement and mucosal morphology in the jejunum of patients with portal hypertension.* Gastroenterology 1980. **79**: p. 707–715.
268. Guingrich, J.A. and J.E. Kuhlman, *Colonic Wall Thickening in Patients with Cirrhosis: CT Findings and Clinical Implications.* AJR, 1999. **172**: p. 919-924.
269. Chesta, J., et al., *Bacterial overgrowth in small intestine in patients with liver cirrhosis.* Rev Med Chil, 1991. **119**: p. 626–632.
270. Bauer, T.M., et al., *Small intestinal bacterial overgrowth in patients with cirrhosis: prevalence and relation with spontaneous bacterial peritonitis.* Am J Gastroenterol, 2001. **96**: p. 2962–2967.
271. Bauer, T.M., et al., *Small intestinal bacterial overgrowth in human cirrhosis is associated with systemic endotoxemia.* Am J Gastroenterol, 2002. **97**: p. 2364–2370.
272. Bode, J.C., et al., *Jejunal microflora in patients with chronic alcohol abuse.* Hepatogastroenterology, 1984. **31**: p. 30–34.
273. Pardo, A., et al., *Effect of cisapride on intestinal bacterial overgrowth and bacterial translocation in cirrhosis.* Hepatology, 2000. **31**: p. 858–863.

274. Morencos, F.C., et al., *Small bowel bacterial overgrowth in patients with alcoholic cirrhosis.* Dig Dis Sci, 1995. **40**: p. 1252–1256.

275. Yang, C.Y., C.S. Chang, and G.H. Chen, *Small-intestinal bacterial overgrowth in patients with liver cirrhosis, diagnosed with glucose H2 or CH4 breath tests.* Scand J Gastroenterol 1998. **33**: p. 867–871.

276. Pande, C., A. Kumar, and S.K. Sarin, *Small-intestinal bacterial overgrowth in cirrhosis is related to the severity of liver disease.* Aliment Pharmacol Ther, 2009. **29**(12): p. 1273-81.

277. Chang, C.S., et al., *Small intestinal bacterial overgrowth versus antimicrobial capacity in patients with spontaneous bacterial peritonitis.* Scand J Gastroenterol, 2001. **36**: p. 92–96.

278. Jun, D.W., et al., *Association between small intestinal bacterial overgrowth and peripheral bacterial DNA in cirrhotic patients.* Dig Dis Sci 2010(55): p. 1465–1471.

279. Guarner, C., et al., *Intestinal bacterial overgrowth and bacterial translocation in cirrhotic rats with ascites.* J Hepatol 1997. **26**: p. 1372–1378.

280. Chang, C.S., et al., *Small intestine dysmotility and bacterial overgrowth in cirrhotic patients with spontaneous bacterial peritonitis* Hepatology, 1998. **28**: p. 1187–1190.

281. Chesta, J., C. Defilippi, and C. Defilippi, *Abnormalities in proximal small bowel motility in patients with cirrhosis. .* Hepatology, 1993. **17**: p. 828–832.

282. Sadik, R., et al., *Etiology of portal hypertension may influence gastrointestinal transit time.* Scand J Gastroenterol, 2003. **38**: p. 1039–1044.

283. Stewart, J.J., et al., *Intestinal myoelectrical activity and transit time in chronic portal hypertension. .* Am J Physiol, 1992. **263**: p. G474–G479.

284. Thalheimer, U., et al., *Infection, coagulation, and variceal bleeding in cirrhosis.* Gut, 2005. **54**(4): p. 556-63.

285. Bischoff, S.C., et al., *Intestinal permeability - a new target for disease prevention and therapy.* Bmc Gastroenterology, 2014. **14**.

286. Bjarnason, I., A. MacPherson, and D. Hollander, *Intestinal permeability: An overview.* Gastroenterology, 1995. **108**(5): p. 1566-1581.

287. Camilleri, M., et al., *Understanding measurements of intestinal permeability in healthy humans with urine lactulose and mannitol excretion.* Neurogastroenterol Motil, 2010. **22**(1): p. e15-26.

288. Smecuol, E., et al., *Acute gastrointestinal permeability responses to different non-steroidal anti-inflammatory drugs.* Gut, 2001. **49**(5): p. 650-5.

289. Kelly, C.P., et al., *Larazotide acetate in patients with coeliac disease undergoing a gluten challenge: a randomised placebo-controlled study.* Aliment Pharmacol Ther, 2013. **37**(2): p. 252-62.

290. Smith, H.E., et al., *Multiple micronutrient supplementation transiently ameliorates environmental enteropathy in Malawian children aged 12-35 months in a randomized controlled clinical trial.* J Nutr, 2014. **144**(12): p. 2059-65.

291. Gunnarsdottir, S.A., et al., *Small intestinal motility disturbances and bacterial overgrowth in patients with liver cirrhosis and portal hypertension.* Am J Gastroenterol, 2003. **98**(6): p. 1362-70.

292. Peeters, M., et al., *Test conditions greatly influence permeation of water soluble molecules through the intestinal mucosa: Need for standardisation.* Gut, 1994. **35**(10): p. 1404-1408.

293. Blomquist, L., et al., *Evaluation of the lactulose/mannitol and 51Cr-ethylenediaminetetraacetic acid/14C-mannitol methods for intestinal permeability.* Scand J Gastroenterol, 1997. **32**(8): p. 805-12.

294. Chang, J., et al., *Impaired Intestinal Permeability Contributes to Ongoing Bowel Symptoms in Patients With Inflammatory Bowel Disease and Mucosal Healing.* Gastroenterology, 2017. **153**(3): p. 723-731 e1.

295. Rasmussen, D.N., et al., *Confocal Laser Endomicroscopy in Inflammatory Bowel Disease--A Systematic Review.* J Crohns Colitis, 2015. **9**(12): p. 1152-9.

296. Wold, P.B., et al., *Assessment of small bowel Crohn disease: noninvasive peroral CT enterography compared with other imaging methods and endoscopy--feasibility study.* Radiology, 2003. **229**(1): p. 275-81.

297. Bodily, K.D., et al., *Crohn Disease: Mural Attenuation and Thickness at Contrast-enhanced CT Enterography—Correlation with Endoscopic and Histologic Findings of Inflammation.* Radiology, 2006. **238**(2): p. 505-516.

298. Booya, F., et al., *Active Crohn disease: CT findings and interobserver agreement for enteric phase CT enterography.* Radiology, 2006. **241**(3): p. 787-95.

299. Rimola, J., et al., *Magnetic resonance imaging for evaluation of Crohn's disease: validation of parameters of severity and quantitative index of activity.* Inflamm Bowel Dis, 2011. **17**(8): p. 1759-68.

300. Hollander, D., et al., *Increased intestinal permeability in patients with Crohn's disease and their relatives. A possible etiologic factor.* Ann Intern Med, 1986. **105**(6): p. 883-5.

301. Suenaert, P., et al., *Anti-tumor necrosis factor treatment restores the gut barrier in Crohn's disease.* Am J Gastroenterol, 2002. **97**(8): p. 2000-4.

302. Irvine, E.J. and J.K. Marshall, *Increased intestinal permeability precedes the onset of Crohn's disease in a subject with familial risk.* Gastroenterology, 2000. **119**(6): p. 1740-4.

303. Ordas, I., et al., *Accuracy of magnetic resonance enterography in assessing response to therapy and mucosal healing in patients with Crohn's disease.* Gastroenterology, 2014. **146**(2): p. 374-82.e1.

304. Administration, T.U.S.F.a.D., *FDA Drug Safety Communication: FDA evaluating the risk of brain deposits with repeated use of gadolinium-based contrast agents for magnetic resonance imaging (MRI)*, FDA, Editor. 2015.

305. Church, P.C., et al., *Systematic review with meta-analysis: magnetic resonance enterography signs for the detection of inflammation and intestinal damage in Crohn's disease.* Aliment Pharmacol Ther, 2015. **41**: p. 153-166.

306. Vanuytsel, T., et al., *Psychological stress and corticotropin-releasing hormone increase intestinal permeability in humans by a mast cell-dependent mechanism.* Gut, 2014. **63**(8): p. 1293-1299.

307. Hoad, C.L., E.F. Cox, and P.A. Gowland, *Quantification of T(2) in the abdomen at 3.0 T using a T(2)-prepared balanced turbo field echo sequence.* Magn Reson Med, 2010. **63**(2): p. 356-64.

308. Menys, A., et al., *Global small bowel motility: assessment with dynamic MR imaging.* Radiology, 2013. **269**(2): p. 443-50.

309. Plumb, A.A., et al., *Magnetic resonance imaging-quantified small bowel motility is a sensitive marker of response to medical therapy in Crohn's disease.* Aliment Pharmacol Ther, 2015. **42**(3): p. 343-55.

310. Kovesi, P.D. *MATLAB and Octave Functions for Computer Vision and Image Processing 2000* [cited November 2017; Available from: http://www.peterkovesi.com/matlabfns/#edgelink.

311. Kubica, P., et al., *Modern approach for determination of lactulose, mannitol and sucrose in human urine using HPLC-MS/MS for the studies of intestinal and upper digestive tract permeability.* J Chromatogr B Analyt Technol Biomed Life Sci, 2012. **907**: p. 34-40.

312. Cronin, C., G., et al., *Normal small bowel wall characteristics on MR enterography.* European Journal of Radiology, 2010 **75** p. 207-211.

313. Hordonneau, C., et al., *Diffusion-Weighted Magnetic Resonance Imaging in Ileocolonic Crohn's Disease: Validation of Quantitative Index of Activity.* Am J Gastroenterol, 2014. **109** p. 89-98.

314. Buisson, A., et al., *Diffusion-weighted magnetic resonance imaging for detecting and assessing ileal inflammation in Crohn's disease.* Aliment Pharmacol Ther, 2013. **37**(5): p. 537-45.

315. Hawkey, C.J., et al., *Less small-bowel injury with lumiracoxib compared with naproxen plus omeprazole.* Clin Gastroenterol Hepatol, 2008. **6**(5): p. 536-44.

316. Bjarnason, I., et al., *Mechanisms of Damage to the Gastrointestinal Tract From Nonsteroidal Anti-Inflammatory Drugs.* Gastroenterology, 2018. **154**(3): p. 500-514.

317. Rimola, J., et al., *Magnetic resonance for assessment of disease activity and severity in ileocolonic Crohn's disease.* Gut, 2009. **58**(8): p. 1113-20.

318. Grover, M., et al., *(13) C mannitol as a novel biomarker for measurement of intestinal permeability.* Neurogastroenterol Motil, 2016. **28**(7): p. 1114-9.

319. Lepper, P.M., et al., *Association of lipopolysaccharide-binding protein and coronary artery disease in men.* J Am Coll Cardiol, 2007. **50**(1): p. 25-31.

320. Kaser, A., et al., *Endotoxin and its binding proteins in chronic liver disease: the effect of transjugular intrahepatic portosystemic shunting.* Liver, 2002. **22**(5): p. 380-7.

321. Strutz, F., et al., *Relationship of antibodies to endotoxin core to mortality in medical patients with sepsis syndrome.* Intensive Care Med, 1999. **25**(5): p. 435-44.

322. Bennett-Guerrero, E., et al., *Endotoxin-neutralizing capacity of serum from cardiac surgical patients.* J Cardiothorac Vasc Anesth, 2001. **15**(4): p. 451-4.

323. Relja, B., et al., *Intestinal-FABP and liver-FABP: Novel markers for severe abdominal injury.* Acad Emerg Med, 2010. **17**(7): p. 729-35.

324. Thuijls, G., et al., *Non-invasive markers for early diagnosis and determination of the severity of necrotizing enterocolitis.* Ann Surg, 2010. **251**(6): p. 1174-80.

325. Reisinger, K.W., et al., *Noninvasive measurement of intestinal epithelial damage at time of refeeding can predict clinical outcome after necrotizing enterocolitis.* Pediatr Res, 2013. **73**(2): p. 209-13.

326. Monbaliu, D., et al., *Liver fatty acid-binding protein: an early and sensitive plasma marker of hepatocellular damage and a reliable predictor of graft viability after liver transplantation from non-heart-beating donors.* Transplant Proc, 2005. **37**(1): p. 413-6.

327. Vreugdenhil, A.C., et al., *Additional value of serum I-FABP levels for evaluating celiac disease activity in children.* Scand J Gastroenterol, 2011. **46**(12): p. 1435-41.

328. Adriaanse, M.P., et al., *Serum I-FABP as marker for enterocyte damage in coeliac disease and its relation to villous atrophy and circulating autoantibodies.* Aliment Pharmacol Ther, 2013. **37**(4): p. 482-90.

329. Rinella, M.E., et al., *Report on the AASLD/EASL joint workshop on clinical trial endpoints in NAFLD.* Journal of Hepatology, 2019.

330. Woo, S., et al., *Intravoxel incoherent motion diffusion-weighted MR imaging of hepatocellular carcinoma: correlation with enhancement degree and histologic grade.* Radiology, 2014. **270**(3): p. 758-67.

331. Nasu, K., et al., *Diffusion-weighted imaging of surgically resected hepatocellular carcinoma: imaging characteristics and relationship among signal intensity, apparent diffusion coefficient, and histopathologic grade.* AJR Am J Roentgenol, 2009. **193**(2): p. 438-44.

332. Park, M.S., et al., *Hepatocellular carcinoma: detection with diffusion-weighted versus contrast-enhanced magnetic resonance imaging in pretransplant patients.* Hepatology, 2012. **56**(1): p. 140-8.

333. Heimbach, J.K., et al., *AASLD guidelines for the treatment of hepatocellular carcinoma.* Hepatology, 2018. **67**(1): p. 358-380.

334. Adler, J., et al., *Magnetization transfer helps detect intestinal fibrosis in an animal model of Crohn disease.* Radiology, 2011. **259**(1): p. 127-35.

335. Dillman, J.R., et al., *Comparison of noncontrast MRI magnetization transfer and T2 -Weighted signal intensity ratios for detection of bowel wall fibrosis in a Crohn's disease animal model.* J Magn Reson Imaging, 2015. **42**(3): p. 801-10.

336. Coimbra, A., et al., *A Multicenter Study to Validate Magnetic Resonance Enterography Against Histological Assessments of Stenotic Disease in Patients with Crohn's Disease.* Gastroenterology. **152**(5): p. S768-S769.

337. Pazahr, S., et al., *Magnetization transfer for the assessment of bowel fibrosis in patients with Crohn's disease: initial experience.* MAGMA, 2013. **26**(3): p. 291-301.